Vol. 69 • No. 1

January 2026

Microwave Journal

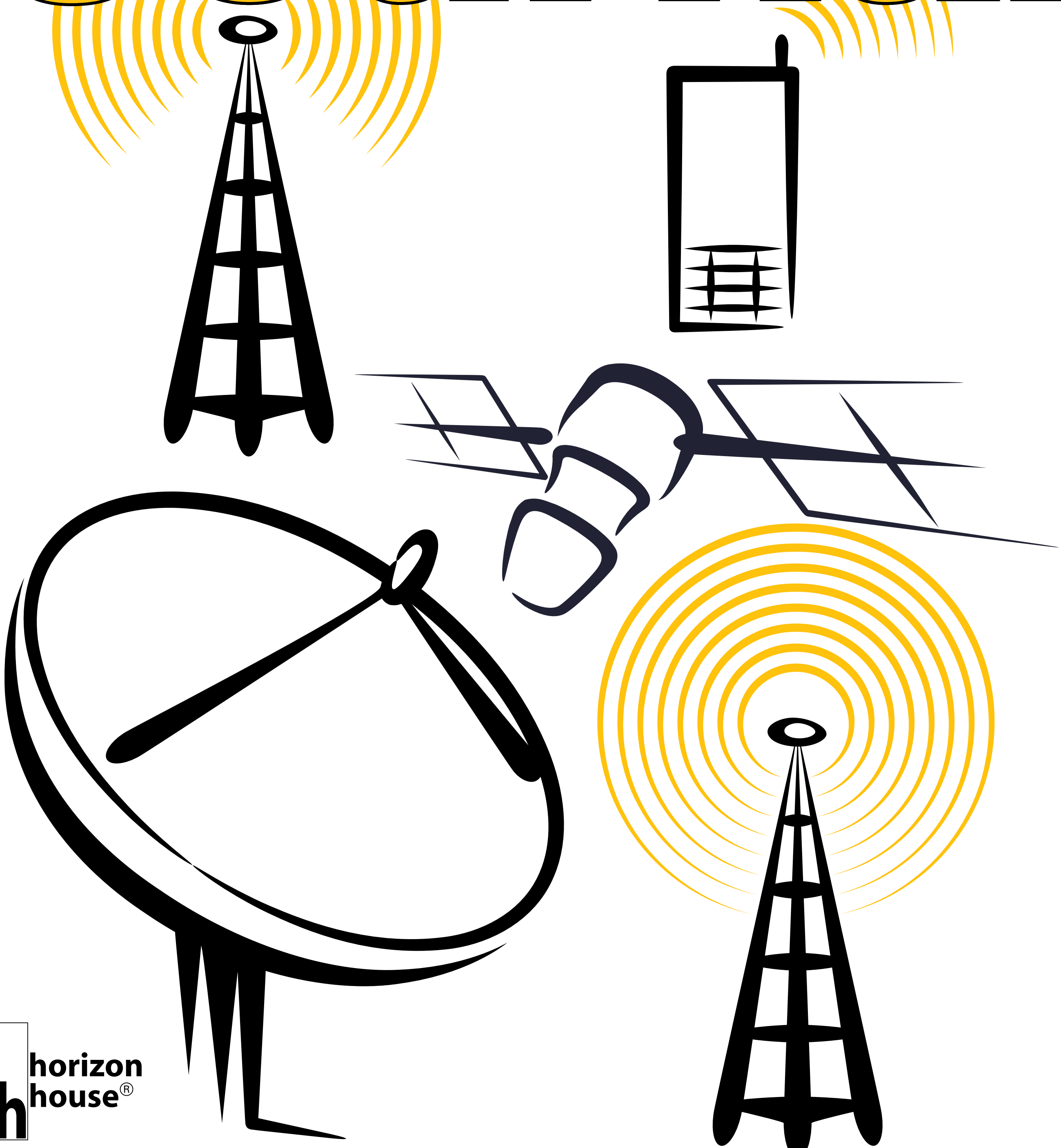

horizon house®

Founded in 1958

mwjournal.com

DC TO 50 GHz

MMIC Amplifiers

300+ Models Designed in House

- Wide selection of GaAs HBT and E-pHEMT designs
- Noise figure as low as 0.38 dB
- OIP3 up to +50 dBm
- Industry-leading phase noise performance
- In-house packaging assembly
- Surface mount and bare die formats
- Upscreening available

LEARN MORE

Options for Every Requirement

CATV (75Ω)

Supporting DOCSIS® 3.1 and 4.0 requirements

Dual Matched

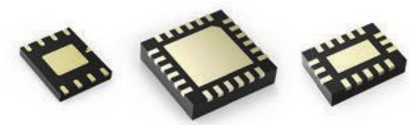

Save space in balanced and push-pull configurations

Hi-Rel

Rugged ceramic package meets MIL requirements for harsh operating conditions

High Linearity

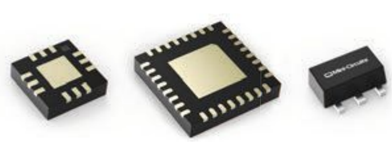

High dynamic range over wide bandwidths up to 45 GHz

Low Noise

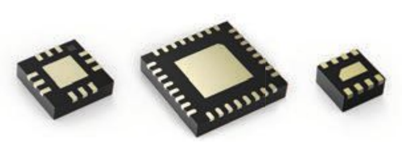

NF as low as 0.38 dB for sensitive receiver applications

Low Additive Phase Noise

As low as -173 dBc/Hz @ 10 kHz offset

RF Transistors

<1 dB NF with footprints as small as 1.18 x 1.42mm

Variable Gain

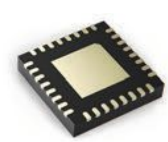

Up to 31.5 dB digital gain control

Wideband Gain Blocks

Flat gain for broadband and multi-band use

Mini-Circuits®

We Don’t Just Claim Best-in-Class. We Deliver It

Our amplifiers and surface-mount filters set the standard for RF performance. Designed, tested, and proven in mission-critical environments. US-manufactured.

High Q SMT Filters 1-10 GHz
The best performance at this size in the industry

- High selectivity with low insertion loss
- For lowpass, highpass, bandpass, notch, and diplexer applications
- Custom solutions available, including multiplexers & switched filter banks

High Power SAW Filters from 20 MHz up to 1.5 GHz
Input power options up to +35 dBm CW

- Narrow, wide, and fractional bandwidths
- Ultra-flat group delay and excellent spurious rejection
- Semi-standard and custom solutions

Ultra-Low Phase Noise & High Linearity Amplifiers

- Ultra-low phase noise (-182 dBc at 100 kHz)
- Ultra high linearity (IP2 to +100 dBm, IP3 to +61dBm)
- Widest selection of MIL space-qualifiable products
- Modified standards at no extra charge

SPECTRUM CONTROL ™

The appearance of U.S. Department of Defense (DoD) visual information does not imply or constitute DoD endorsement.


Radiall
PHASED
ARRAY
CONNECTORS
OPTIMIZED RF CONNECTIVITY FOR MODERN ELECTRONICS
Engineered to outperform 3-piece SMP and SMPM designs, Radiall's IMP connectors use a single-piece, spring-loaded interface that sharply reduces insertion loss. With fewer contact points—and one-third to one-half the loss of multi-piece solutions—IMP delivers unwavering signal integrity up to 40 GHz, even in the tightest spaces.

Microwave Journal
January 2026
Vol. 69 • No. 1
Radar & Antennas
mwjournal.com

CONTENTS

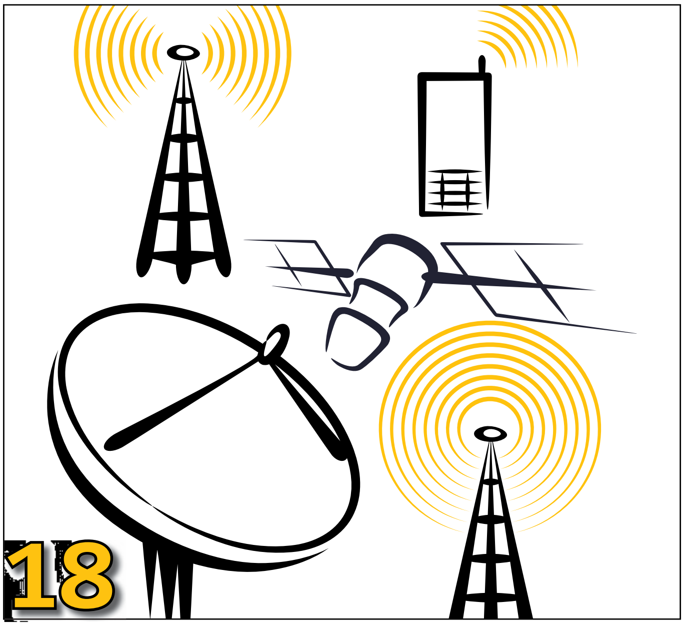

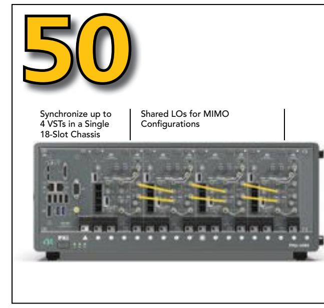

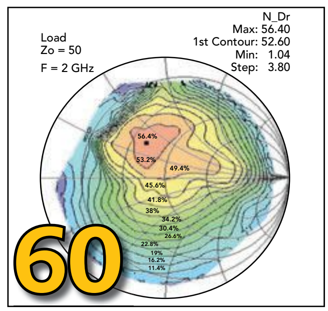

ACCESS NOW!
digital.microwavejournal.com

eXclusive Digital Content ›››

69 YEARS OF PUBLISHING EXCELLENCE

apidRF

World's 1st AI Driven RFIC DESIGN PLATFORM

A PUSH-BUTTON GDS TAPE-OUT READY SOLUTION

END APPLICATIONS CUSTOMERS

PERFORMANCE-DRIVEN FOCUS
EXPANDED DESIGN CHOICES
ENHANCED SECURITY AND CONFIDENTIALITY
REDUCED DEPENDENCE ON IC VENDORS
SIGNIFICANT COST SAVINGS

SEMICONDUCTOR COMPANIES

HUGE DESIGN COST REDUCTION
TAILORED TO CUSTOMER NEEDS
100X, 1000X FASTER
SUCCESSFUL RATE INCREASE

apidRF

TRULY ENABLES A "DIRECT INTERACTION" MODEL FOR THE RFIC INDUSTRY ACROSS EVERY SECTOR.

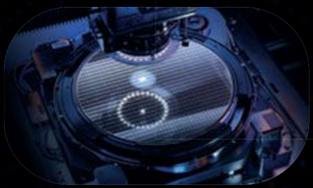

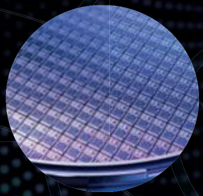

FOUNDRIES

HIGHER REVENUE GREATER DESIGN VOLUME
EXPANDED CUSTOMER BASE LOWERING DESIGN ENTRY BARRIERS
ACCELERATED PRODUCT ITERATION

SIMPLE 3 STEPS

- LOGIN WWW.RAPIDRF.AI
- ENTER DESIGN TARGET
- PRESS "GENERATE"

A TAPE-OUT-READY GDS FILE WILL BE GENERATED AND **AVAILABLE FOR DOWNLOAD.**

Microwave Journal

CONTENTS

mwjournal.com

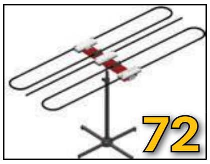

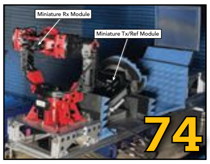

Product Features

Tech Briefs

Departments

Microwave Journal (USPS 396-250) (ISSN 0192-6225) is published monthly by Horizon House Publications Inc., 685 Canton St., Norwood, MA 02062. Periodicals postage paid at Norwood, MA 02062 and additional mailing offices.

POSTMASTER: Send address corrections to mwj@e-circ.net.com. Subscription information: (978) 671-0446. This journal is issued without charge upon written request to qualified persons working in the RF & microwave industry. Other subscriptions are: domestic, $130.00 per year, two-year subscriptions, $200.00; foreign, $225.00 per year, two-year subscriptions, $400.00; back issues (if available) and single copies, $20.00 domestic and $30.00 foreign. Claims for missing issues must be filed within 90 days of date of issue for complimentary replacement.

STAFF

Group Director: Carl Sheffres
Associate Publisher: Michael Hallman
Media Director: Patrick Hindle
Brand & Content Director: Jennifer DiMarco
Technical Editor: Del Pierson
Associate Technical Editor: Cliff Drubin
Editorial & Media Specialist: Kelley Roche
Associate Editor: Kaitlyn Joyner
Multimedia Staff Editor: Barbara Walsh
Electronic Marketing Manager: Chris Stanfa
Senior Digital Content Specialist: Lauren Tully
Digital Content Specialist: Vincent Carrabino
Director of Production & Distribution: Edward Kiessling
Art Director: Janice Levenson
Graphic Designer: Ann Pierce

EUROPE
Office Manager: Nina Plesu

CORPORATE STAFF
CEO: William M. Bazzy
President: Ivar Bazzy
Vice President: Jared Bazzy

EXECUTIVE EDITORIAL OFFICE
685 Canton Street, Norwood, MA 02062
Tel: (781) 769-9750
FAX: (781) 769-5037
e-mail: mwj@mwjournal.com

EUROPEAN EDITORIAL OFFICE
16 Sussex Street, London SW1V 4RW, England
Tel: Editorial: +44 207 596 8730 Sales: +44 207 596 8740
FAX: +44 207 596 8749

SUBSCRIPTION SERVICES
Send subscription inquiries and address changes to:
Tel: (978) 671-0446
e-mail: mwj@e-circ.net

www.mwjournal.com

Printed in the USA

Microwave Journal ONLINE .COM

Online Panel

February 18

Chiplets and 3D Heterogenous Integration

This panel of experts will discuss the challenges of advanced packaging technologies such as Chiplets and 3D Heterogenous Integration including integration, stacking, signal integrity and thermal concerns. The group will discuss simulation, testing and performance advantages of these approaches.

WHITE PAPERS

Coilcraft

The Fundamentals of RF Inductors

Executive Interview

Maryam Rofougaran, CEO and Founder of Movandi, discusses Movandi's recent innovations in mmWave 5G technology and expansion into Oman.

Join Us Online

Follow us @Pathindle @MWJEditor

Join us at the RF and Microwave Community

Become a fan at facebook.com/microwavejournal

Microwave Journal podcasts include the RF/microwave update series, Frequency Matters, plus interviews with industry experts and executives.

Catch *Frequency Matters,* the industry update from *Microwave Journal,* microwavejournal.com/FrequencyMatters

Visit us @ mwjournal.com

PWR SERIES

Power Sensors

Turn Your PC into a High-Performance Power Meter

LEARN MORE

- Dynamic range options spanning -60 to +20 dBm
- CW, true RMS, peak and average measurement capability
- Sample rates up to 80 million samples per second
- 50 and 75Ω models
- Software package supports automated measurement with statistical analysis and time domain plots
- No external calibration required

Model #	Control Interface	Measurement Type	Freq. Range (MHz)	Input Power Range (dBm)	Measurement Speed (ms)
PWR-40PW-RC	USB & Ethernet	Peak & Avg.	500-40000	-20 to 20	5.00E-05
PWR-18PWHS-RC	USB & Ethernet	Peak & Avg.	50-18000	-60 to 20	1.30E-05
PWR-18RMS-RC	USB & Ethernet	RMS	50-18000	-60 to 20	0.5
PWR-9PWHS-RC	USB & Ethernet	Peak & Avg.	50-9000	-60 to 20	0.000013
PWR-9RMS-RC	USB & Ethernet	RMS	50-9000	-60 to 20	0.5
PWR-8P-RC	USB & Ethernet	Peak & Avg.	10-8000	-60 to 20	0.002
PWR-8FS	USB	CW	1-8000	-30 to 20	10
PWR-8GHS	USB	CW	1-8000	-30 to 20	30
PWR-8GHS-RC	USB & Ethernet	CW	1-8000	-30 to 20	30
PWR-8PW-RC	USB & Ethernet	Peak & Avg.	10-8000	-60 to 20	0.00005

MARK YOUR CALENDAR

STAY CONNECTED TO COMING EVENTS

JANUARY

18-21
IEEE Radio & Wireless Week
Los Angeles, Calif.
www.radiowirelessweek.org

FEBRUARY

7-9
IEEE IMFW
Hong Kong, China
www.imfw-ieee.org

24-26
DesignCon
Santa Clara, Calif.
www.designcon.com

MARCH

2-5
MWC Barcelona
Fira Gran Via, Barcelona
www.mwcbarcelona.com

9-11
German Microwave Conference
Karlsruhe, Germany
www.gemic2026.kit.edu

23-26
Satellite x GovMilSpace
Washington DC
www.SATShow.com

24-26
EMV
Cologne, Germany
https://emv.mesago.com

APRIL

19-24
EUCAP
Dublin, Ireland
www.eucap2026.org

20-21
IEEE WAMICON
Clearwater, Fla.
www.ieeewamicon.org

Register online at mwjournal.com

ONLINE PANEL SERIES

2/18
Chiplets and 3D Heterogenous Integration

Call for Papers Deadlines

1/16
Annual Microwave Power Symposium (IMPI)

2/9
International Conference on Microwave Acoustics & Mechanics (IC-MAM)

FOR DETAILS VISIT MWJOURNAL.COM/EVENTS

The Digitisation of Direct RF

Mike Roberts
Slipstream Engineering, Shipley, U.K.

Modern communication, sensing, radar and electronic warfare (EW) systems increasingly require the ability to process wide instantaneous bandwidths (IBW) and support highly agile, multi-band operation. These demands are driving rapid advancement in high speed data converter technology, with analogue-to-digital converters (ADCs) and digital-to-analogue converters (DACs) pushing to higher sampling rates and wider input bandwidths. At the same time, semiconductor manufacturers are extending the RF input bandwidths of these converters into the microwave range and beyond, allowing radio signals to be digitised at or near their carrier frequencies. Systems that exploit these capabilities are referred to as Direct RF architectures.

In a traditional heterodyne radio receiver, the RF signal is translated to a lower intermediate frequency (IF) using mixers and local oscillators, then it is filtered and digitised. In contrast, a Direct RF approach digitises the incoming RF signal directly, potentially eliminating most of the analogue signal processing chain. The analogue frequency translation that typically occurs in mixers is replaced by digital downconversion (DDC) within the ADC or digital up-converter (DUC) contained within the DAC.

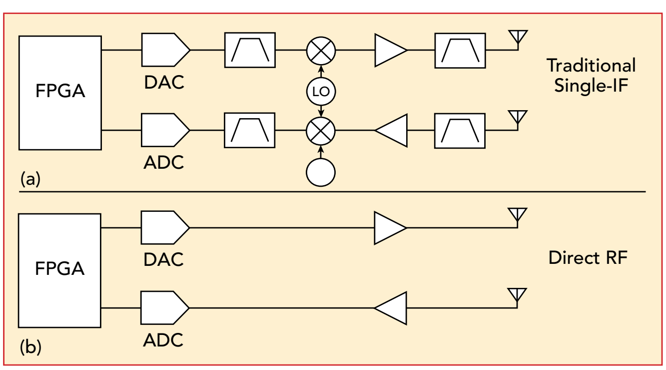

Fig. 1 **(a) Single-IF vs. (b) Direct RF system.**

The key motivation behind Direct RF is system simplification and software-driven adaptability. With fewer analogue stages, the radio becomes more compact, easier to calibrate and more repeatable from unit to unit. Digital processing provides reconfigurability with centre frequency, bandwidth, filtering and channelisation being determined through software/firmware rather than fixed analogue hardware.

Direct RF does not, however, eliminate all RF hardware considerations. Challenges arise from multiple sources, such as sampling-based spurious artefacts, clock distribution, dynamic range limitations of ADCs and transmit power amplifier (PA) efficiency. Practical RF filtering and front-end matching networks remain essential. Therefore, while Direct RF reduces analogue complexity and alleviates some classical RF engineering problems, it creates new system behaviour that requires careful analysis and design.

The following sections provide a detailed overview of Direct RF system operation, current converter technology, advantages and trade-offs and future expected developments in RF front-end architectures.

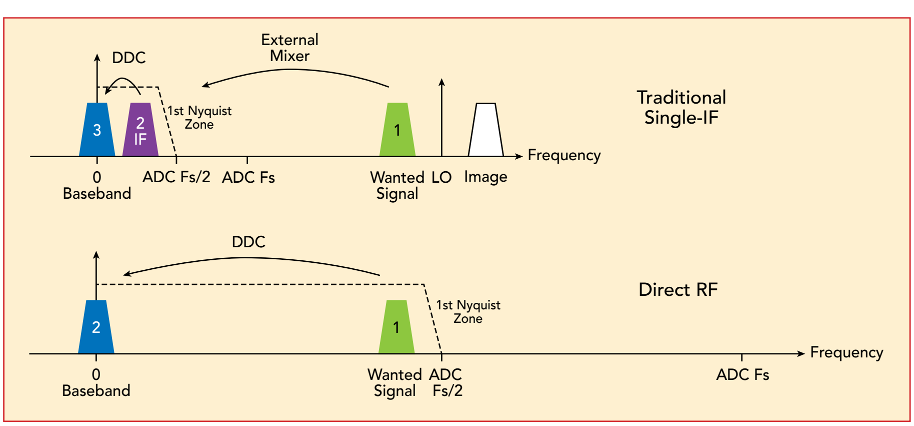

Fig. 2 **Receiver example of a single-IF vs. a Direct RF system mixing process.**

PRINCIPLES OF DIRECT RF SAMPLING

Conventional Versus Direct RF Architectures

Figure 1 illustrates a simplified comparison of a single-IF heterodyne system and a Direct RF system. ***Figure 2*** provides an associated receiver frequency plan for these two cases. In a traditional heterodyne system, the input signal at RF

Fig. 3 5 GSPS ADC with a 100 MHz wide wanted signal.

is mixed to an IF frequency located well within the analogue bandwidth of the ADC. The ADC sampling rate is typically selected to be at least 2.5x the signal bandwidth to support digital processing without aliasing. The mixer and LO define where the signal resides in the spectrum prior to digitisation.

In a Direct RF system, the analogue mixing stage is removed entirely. The RF signal is sampled directly, and digital frequency translation (DDC in the case of a receiver) moves the signal to baseband. The sampling rate must therefore be greater than 2.5x the carrier frequency of the RF signal, rather than only exceeding the signal bandwidth. For example, to digitise a 200 MHz wide signal at 3 GHz, a sampling rate of at least around 7.5 GSPS is required, with higher values preferred to avoid in-band spurious folding.

Analog Devices provides a frequency folding tool, which is useful for visualising spurious sampling products.[1] The main spurious products of concern are HD2 and HD3. These products are generated by the second and third harmonic of the input signal mixing with the sample clock in the converter. ***Figure 3*** shows an example of a 5 GSPS sample rate ADC with 100 MHz IBW signal for 200 MHz, 1000 MHz and 1662.5 MHz input frequencies, with plots produced from an AD frequency folding tool.[1] In the 200 MHz input signal case, the harmonics of the input signal can be seen to lie within the first Nyquist zone. As the input frequency is increased to 1 GHz, the third harmonic product is folded around Fs/2 into the first Nyquist zone (labelled HD3). As the input frequency is increased further, the second harmonic folds around Fs/2 and appears in-band as HD2. The pink areas show the input frequencies at which in-band spurious products will appear. In this case, where the input signal IBW is significantly less than the sample rate, there are many input frequencies available with no in-band sampling product-based spurious (up to third order). The matter of sample rate choice and associated maximum IBW will be discussed later in this article.

Notably, the ratio of signal bandwidth to sampling frequency determines spur-free frequency regions. If the signal bandwidth is narrow relative to the sampling frequency, there are many spur-free centre frequency options. If the signal bandwidth increases, spur-free regions diminish rapidly, as discussed later in this article.

Current State of High Speed Data Converters

Direct RF operation has become feasible due to advances in high speed mixed-signal ICs, multi-core sampling architectures and integrated DSP blocks. Some representative high performance platforms are highlighted in ***Table 1***.

There are multiple suppliers who use these devices in higher-level modules and systems, such as Mercury Systems, Avnet, Annapolis,

TABLE 1

SUMMARY OF A SELECTION OF DIRECT RF DATA CONVERTER DEVICES IN THE PUBLIC DOMAIN

Manufacturer	Product Line	ADC Sample Rates	DAC Sample Rates	Resolution ADC/DAC	Analogue Input Bandwidth ADC/DAC	Number of Channels ADC/DAC	Integrated FPGA
Analog Devices	MxFE AD9082	6 GSPS	12 GSPS	12 bit / 16 bit	8 GHz / 8 GHz	2/4	NO
AMD (Xilinx)	RFSoC Gen 3	5 GSPS	9.85 GSPS	14 bit / 14 bit	6 GHz / 6 GHz	8/8	YES
Analog Devices	Apollo MxFE AD9084/AD9088	20 GSPS	28 GSPS	12 bit / 16 bit	18 GHz / 18 GHz	4/4	NO
AMD (Xilinx)	Versal RF (VR1652 example shown)	32 GSPS	16 GSPS	14 bit / 14 bit	18 GHz / 18 GHz	4/8	YES
Altera (Intel)	Direct RF (Stratix 10 example shown)	64 GSPS	64 GSPS	10 bit /10 bit	36 GHz / 36 GHz	8/8	YES
Texas Instruments	AFE7900 Series (AFE7958 shown)	3 GSPS	12 GSPS	-	12 GHz / 12 GHz	6/4	NO
Texas Instruments	AFE8100 Series (AFE8192 shown)	6 GSPS	12 GSPS	-	7.2 GHz / 7.2 GHz	16/16	NO

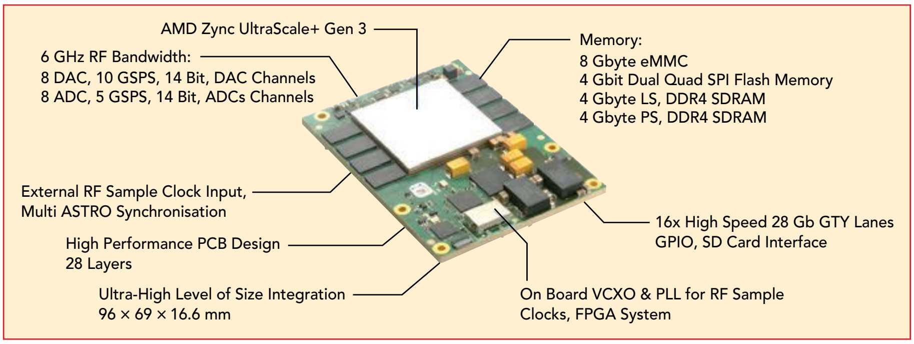

Fig. 4 Slipstream Design's ASTRO RFSoC SOM.

Slipstream, Enclustra and Trenz.

Example Deployment: Slipstream Design's ASTRO RFSoC SOM

Slipstream Design's ASTRO RF system-on-module (SOM) utilises the AMD Gen3 RFSoC, which integrates the Direct RF converters with a powerful on-board Zynq FPGA and quad ARM processors. The SOM integrates 8 x 5 GSPS 14 bit ADCs and 8 x 10 GSPS 14 bit DACs onto a compact 94 x 69 mm module. ***Figure 4*** shows the module that features on-board sample clock support. This type of module demonstrates how Direct RF capability can now be delivered in compact embedded form factors, suitable for airborne, unmanned and distributed RF sensing applications.

ADVANTAGES OF THE DIRECT RF APPROACH

Reconfigurability Through Software

Digital LO (numerically controlled oscillator (NCO)) tuning and baseband filter reconfiguration allow agile multi-band operation without changing analogue hardware. This is particularly beneficial in adaptive radar, EW, multi-mission radios and dynamic spectrum systems.

Reduction in Analogue Hardware

Eliminating mixers, LO distribution networks and IF filters reduces size and weight, minimises temperature and aging-related variation and improves unit-to-unit reproducibility.

Simplified Calibration

Digital calibration loops and numerically defined signal chains offer deterministic phase and gain characteristics. Unlike analogue networks, there is no tuning required during manufacture or deployment.

Ease of Channelisation

Wideband receive data can be digitally channelised into multiple sub-bands efficiently, using polyphase filter banks or FFT-based channelisers.

CHALLENGES IN DEPLOYING DIRECT RF SYSTEMS

Although Direct RF has many benefits, there still exist challenges that require a combination of software, firmware and RF hardware capabili-

ties and skill sets to overcome. For example, some challenges include:

Spur-Free Operating Window Versus Bandwidth

Continuing the receiver example from earlier, as illustrated in ***Figure 5***, increasing the input IBW from 100 to 400 MHz dramatically reduces the number of spur-free centre frequency regions when using a 5 GSPS ADC. The designer is left with only one or two usable input frequency windows, depending on which Nyquist zone they choose. This means that the system designer who wanted a flexible input frequency range would need to consider either an external mixer or increasing the sample rate of the data converters to widen the spur-free zone and restore flexibility of centre frequency, as demonstrated in ***Figure 6***. However, increasing the sample rate comes with trade-offs:

- Higher sampling rates increase converter and FPGA power consumption.
- Multi-core interleaving introduces additional calibration requirements to suppress interleaving spurs.
- Higher clock rates increase clock jitter demands.

Increasing sample rates remains one of the central engineering trade-offs in Direct RF systems.

Out-of-Band Interference and ADC Saturation

A key dynamic range metric is the difference between IIP3 and noise figure.[2] For a high performing ADC such as the AD9082, a greater than 10 dB difference between IIP3 (35.8 dBm) and noise figure (25 dB) is achieved. It is possible to achieve slightly better results with a high performing heterodyne solution using, for example, a mixer like the Marki Microwave MT3-0113HCQG-2. With high performing solutions, it is possible to achieve a 19 dB difference between IIP3 and noise figure

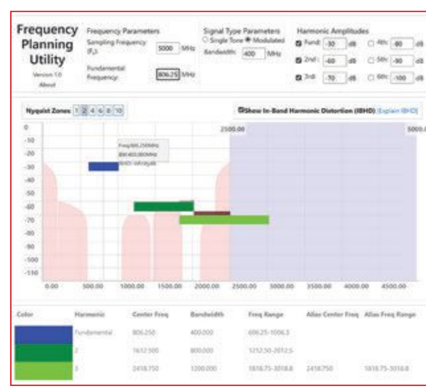

Fig. 5 A 400 MHz IBW signal with a 5 GSPS sample rate.

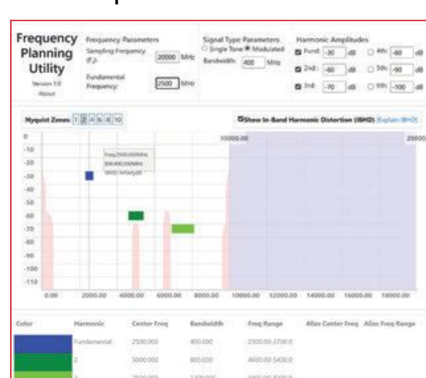

Fig. 6 A 400 MHz IBW signal with a 20 GSPS sample rate.

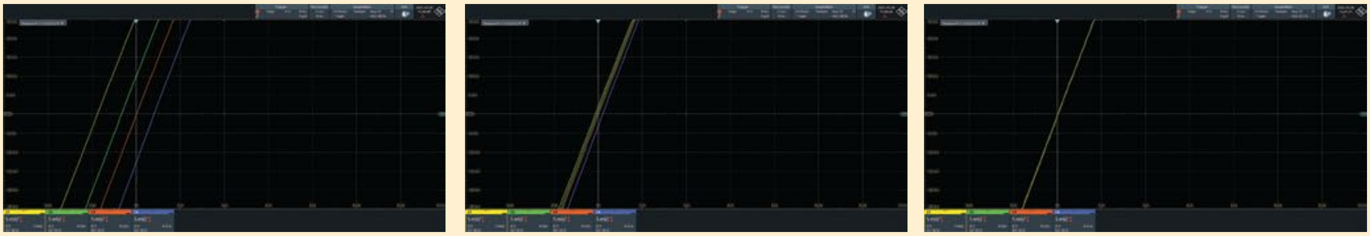
(a) (b) (c)

Fig. 7 Synchronisation of an ASTRO RFSoC with (a) DAC outputs before synchronisation, (b) MTS and (c) with equalisation filters.

(29 dBm IIP3 and 10 dB NF). That said, the performance differential of pure dynamic range is not hugely significant.

For receivers, the significant metric is the maximum input signal. Typically, most Direct RF ADCs will have a full-scale input power of around +5 dBm. Without appropriate filtering, high-power out-of-band interferers can result in this level being exceeded anywhere in the band of operation, resulting in saturation of the ADC and temporary failure of the entire receiver band. Providing narrowband and low loss, tunable filtering that can track the RF input signal in Direct RF applications is challenging, particularly in a small form factor, and is the subject of much current research.

This is where heterodyne solutions have an advantage, as they can leverage the fixed-frequency IF filter to reject out-of-band signals. Because the IF filter is fixed in frequency, it can be highly optimised for the bandwidth of operation. Although the mixer will generate spurs as a result of high level out-of-band interferers, it will not cease to function, as is the case with ADC saturation. It is also typical to see systems with switchable IF filters in heterodyne solutions to accommodate different signal bandwidths.

Transmit PA Efficiency

An often overlooked challenge in the context of Direct RF (transmit side) is the ability to generate the high RF signal levels suitable for transmission in practical systems in a power-efficient manner over a wide RF bandwidth. Although Direct RF DACs can flexibly generate a wide range of output frequencies, typically, PAs have poor power-added efficiency (PAE) when operating in backed-off modes and over wide frequency ranges. The Analog Devices ADPA1113 2 to 6 GHz 40 W GaN PA, for example, has a peak PAE of around 30 percent over this bandwidth. A narrowband (< 200 MHz) PA in this frequency range would be expected to have a peak efficiency of greater than 65 percent. This demonstrates the need for reconfigurable and digitally adaptable PA technology. Adaptive PA architectures, including load-modulated balanced amplifiers (LMBA) and wideband Doherty structures, are likely to become critical in future Direct RF systems.

Channel Synchronisation Across Many Converters

Another key challenge with high sample rate Direct RF data converters is the requirement for multiple sample clocks to be synchronised. This challenge exists where more than one ADC or DAC is required to operate in a coherent manner. An example of this is a phased array application where many elements must operate coherently with each other to form a beam. In a traditional heterodyne system, this is less problematic because the local oscillator can be distributed to every element, and notwithstanding practical

routing problems, this automatically provides coherence across all elements. Since the heterodyne approach uses much lower sample rate ADCs, synchronisation of these clocks is far less of a challenge.

With the high sample rates of Direct RF converters and the associated digital circuitry (such as FIFOs) that sit between the point of sampling and the resulting data stream, synchronisation across multiple Direct RF converters is a key technical challenge. Typically, achieving synchronisation across multiple converters requires a combination of using vendor-supplied synchronisation schemes, custom clock distribution hardware and custom-implemented digital equalisation filtering. This requires a range of different engineering disciplines, from RF to software and firmware, to implement. ***Figure 7*** shows measured data of four different Slipstream Design ASTRO DAC channels. Figure 7a shows the DAC outputs prior to synchronisation, Figure 7b shows the data with the AMD Multi-Tile Synchronisation (MTS) applied and Figure 7c shows the result with custom digitally applied equalisation filters to remove the effects of RF tracking and cables following a calibration process. Figure 7 shows measured improvements demonstrating progressive synchronisation refinement.

FUTURE CIRCUITRY TO SUPPORT DIRECT RF

The trend of Direct RF converters is likely to continue with IBW and RF input frequency continuing to increase. Although such devices promise extreme flexibility and software reconfigurability, they will not eliminate the need for RF components between the antenna and the data converters.

At the most basic level, typical interfaces to data converters are differential, requiring a balun. The wideband nature of Direct RF converters is driving a move towards single-ended interfaces using wideband on-chip differential amplifiers.

It is expected that in many applications, including wideband systems operating in relatively harsh electromagnetic environments, systems will continue to use a single stage of external frequency conversion (mixer + LO) to bring the required IBW down to a fixed location in the data converters' Nyquist zone. This approach is likely to provide the most robust solution for rejecting out-of-band interferers and managing spurs. Until low loss narrowband tunable filters become a reality, this will likely remain a relatively common architecture, with the high sample rate of the data converters enabling the high signal IBW. External frequency converters also serve to extend the frequency range of the data converters, making them difficult to obsolete. It is expected that, where an external mixer cannot be used, switched filter banks will remain critically important to manage harmonics and spurs. The design of such functionality requires a high level of RF engineering skill.

It is expected that reconfigurable and adaptable PAs, such as LMBAs,

RF-LAMBDA

MADE IN USA

THE LEADER OF RF BROADBAND SOLUTIONS

EMC Broadband RF Power Amplifier

High Power Solid State

HUNDREDS IN STOCK

FAST SHIPPING

FREQUENCY UP TO 90GHZ

POWER UP TO 2KW CW

BENCHTOP AND RACKMOUNT

REMC06G18GG 6-18GHZ 400W

- AUTOMATIC BUILT IN SELF CALIBRATION AND BIAS ADJUSTMENT.
- OVER TEMPERATURE, CURRENT, INPUT POWER PROTECTION.
- VSWR MEASUREMENT AND OPEN CIRCUIT PROTECTION.
- USER FRIENDLY CONTROL INTERFACE.
- REMOTE ETHERNET CONTROL AND FIRMWARE UPDATE.
- HIGH POWER EFFICIENCY AND LIGHTWEIGHT.

RAMP42G47GA 42-47GHZ 8W

REMC02G06GE 2-6GHZ 500W

REMC18G40GQ 18-40GHZ 200W CW

RAMP18G40GB-U 18-40G 20W

RAMP05M80GC 0.5-80GHZ

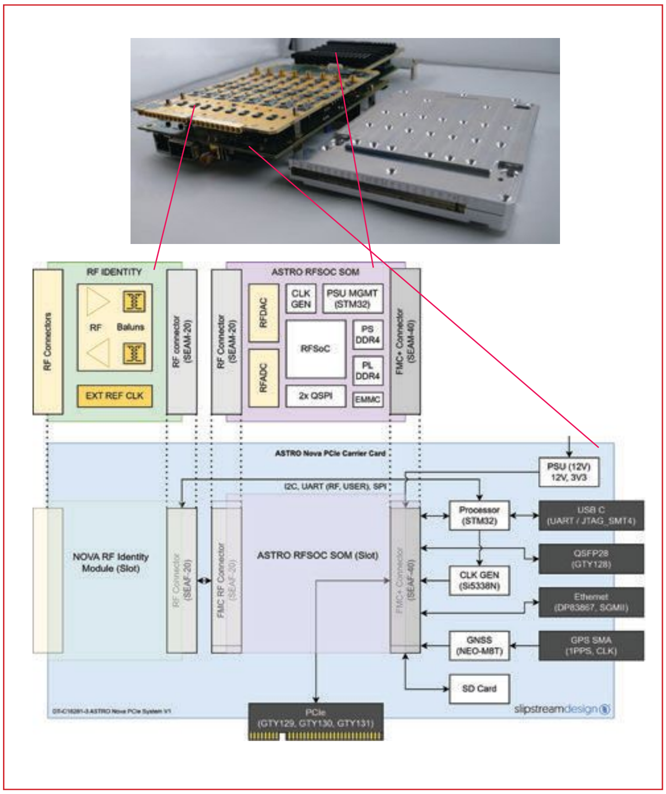

Fig. 8 **ASTRO Nova (PCIe) concept.**

will be essential RF hardware in future Direct RF systems, allowing the flexibility of these systems to be reflected in practical implementations.

The digital techniques and RF hardware associated with high sample rate multiple converter synchronisation and clocking will be a key technology and engineering discipline for the successful uptake of Direct RF, particularly in systems that require many coherent elements.

RF PERSONALITY MODULES

Reflecting on the continued need for application-specific RF circuitry that sits between the converters and the antenna, Slipstream Design has adopted a modular approach, pairing high speed converter modules with RF personality modules. These personality modules allow the same converter core to be adapted to different missions or frequency requirements without redesign of the underlying digital platform. ***Figure 8*** shows ASTRO Nova (PCIe), which features the 8-channel ASTRO RFSoC SOM (8 DAC/8 ADC) module fitted to a PCIe carrier with an RF personality card that sits between the converters and the RF ports.

CONCLUSION

Direct RF technology has evolved from a research concept into deployment-ready system architectures, driven by innovations in high speed converters and integrated digital processing. The advantages, including reduced analogue complexity, software-driven reconfigurability, compact implementation and manufacturing repeatability, are substantial and increasingly attractive across radar, EW, satcom and multi-band communications.

However, system designers must be aware of the non-ideal factors, including the relationship between IBW and sampling rate, spur management, limitations in ADC full-scale handling of out-of-band interferers, PA efficiency constraints and synchronisation across multichannel systems. These challenges do not limit the applicability of Direct RF, but they do shape the necessary RF front-end architectures that accompany it.

Future Direct RF systems are likely to pair high speed converters with adaptive filtering, reconfigurable up-/down-conversion modules and digitally configurable PA architectures. The result will be radio systems that combine the flexibility of software-defined waveforms with the practical RF performance needed in real operational environments.

In summary, modern radio systems demand a combination of RF, digital design, firmware, system architecture, thermal and packaging expertise. While more of the signal chain has shifted into the digital domain, the RF challenges have not disappeared; they have simply changed in nature! ■

References

1. Frequency Folding Tool, Analog.com, 2025, Web: https://tools.analog.com/en/toolbox/FreqFolding/.
2. W. Taylor, "Considering GSPS ADCs in RF Systems," *Analog.com* and *Analog Devices, Inc.*, November, 2021, Web: https://www.analog.com/en/resources/technical-articles/considering-gsps-adcs-in-rf-systems.html?utm_source=chatgpt.com.


EXODUS
Best in Class
RF Amplifier SSPA's
POWER
REVEALED
AMP20184
0.8-2.5 GHz, 500W
AMP20130
80-1000 MHz, 1300W
RF & Microwave
Amplifiers
10KHz-75GHz
AMP20192
1.0-2.0 GHz, 10KW
AMP20191
2.0-4.0 GHz, 10KW
AMP20182
4.0-8.0 GHz, 10KW
AMP20178
6.0-18.0 GHz, 400W
AMP20160
1.0-6.0 GHz, 750W
EXODUS ADVANCED
COMMUNICATIONS
3674 E. Sunset Rd, #100
Las Vegas, NV 89120
Tel: 702-534-6564
www.exoduscomm.com

Leonardo: Cingolani Presents "Michelangelo – the Security Dome"

Leonardo recently unveiled "Michelangelo Dome" at the Officine Farneto in Rome, introducing a new, advanced integrated defense system designed to counter emerging threats in an increasingly complex global landscape.

The project, developed to protect critical infrastructure, sensitive urban areas, territories and assets of national and European interest, through a modular, open, scalable and multi-domain solution, forms part of Leonardo's broader strategy to consolidate its position as a leading player in the field of Global Security.

Michelangelo Dome is not a standalone system, but a comprehensive architecture that brings together next-generation land, naval, air and space sensors, cyber-defense platforms, command-and-control systems, AI and coordinated effectors. The platform creates a dynamic security dome capable of detecting, tracking and neutralizing threats even in the event of large-scale, coordinated attacks, across all operational domains: aerial and missile threats including hypersonic missiles and drone swarms, surface and subsurface attacks at sea and hostile ground forces.

Thanks to advanced data fusion from multiple sensors and the use of predictive algorithms, Michelangelo can anticipate hostile activity, optimize operational responses and automatically coordinate the most effective countermeasures.

With Michelangelo, Leonardo strengthens its role as a European benchmark in multi-domain security and contributes to the goals of strategic autonomy, technological resilience and greater integration of European and NATO defense capabilities. The initiative aligns with wider continental cooperation programs and aims to further enhance Italy's industrial excellence.

Next-Generation Jammer: Turning Point in Airborne Supremacy

As the Next Generation Jammer (NGJ) moves through low-rate production (LRP) and prepares to transition to full-rate production (FRP), the time has come to tell the story of a system conceived to rewrite airborne electronic warfare.

Born to replace the aging AN/ALQ-99, NGJ is not a single upgrade — it is a family of purpose-built pods designed to dominate the electromagnetic spectrum. Engineered for carriage on the EA-18G Growler and adaptable to other host platforms, NGJ was created to defeat modern, resilient threats: frequency-hopping radars, networked datalinks and the distributed sensor webs that define today's contested environments.

The NGJ family — mid-band (MB), low-band (LB) and high-band (HB) — is designed to work as a layered triad, providing end-to-end spectrum coverage. With MB maturing first and now in production, and LB and HB advancing through development and test, the program is transitioning from demonstration to sustained operational capability.

The path to NGJ's maturity was not straightforward. Early development demanded breakthroughs in active electronically scanned arrays, compact high-power transmit/receive chains and advanced thermal control so an aircraft could execute a true high-power electronic attack without compromising flight performance. Engineers also built a modular processing backbone so the system could learn and be reprogrammed in months — not years — as threats evolved.

Programmatic friction accompanied technical complexity. A formal protest once paused development, prompting a deliberate re-examination of evaluation methods, technical risk assessments and upgrade paths. Those corrective steps sharpened requirements, intensified testing regimens and hardened the resulting architectures for sustained operational use.

EA-18G (Source: U.S. Navy)

What elevates NGJ above previous generations is its software-first design. At its core, NGJ is a reconfigurable, open-architecture system that treats the electromagnetic spectrum as a dynamic battlespace: new waveforms, exploitation algorithms and cooperative tactics can be inserted rapidly. Mission crews can tailor effects in real time and share an electronic order of battle across platforms, turning jamming from blunt suppression into a precise, mission-level instrument that protects strike packages, suppresses integrated air defenses and preserves freedom of action for allied forces.

Early results validate the concept. NGJ-MB is entering operational service aboard Growlers, and orders from the U.S. Navy and allied air forces reflect growing operational demand. As NGJ advances from LRP to FRP, deployments of incrementally upgraded pod sets will expand, and the system's software ecosystem will continue to evolve.

Hydra MAX Sets the Standard for Next-Gen Military Satcom

ALL.SPACE announced the successful completion of testing under the U.S. Army's Next Generation Tactical Terminal (NGTT) program.

For More Information Visit mwjournal.com for more defense news.

Source: All.Space Networks Ltd.

ALL.SPACE's Hydra MAX terminal has been validated as a first-of-its-kind solution capable of delivering seamless and simultaneous connectivity across LEO, MEO and GEO satellite networks while on-the-move (OTM).

The NGTT program was established to address a long-standing challenge in beyond-line-of-sight communications: maintaining uninterrupted, high-throughput connectivity during maneuver operations. ALL.SPACE was selected to deliver a production-ready, multi-orbit terminal meeting Technology Readiness Level 6 (TRL 6) — bridging the tactical edge to the cloud and ensuring mission-critical applications remain accessible, even in contested environments.

As part of the NGTT initiative, ALL.SPACE — with support from Telesat Government Solutions and Viasat — successfully demonstrated simultaneous multi-beam OTM LEO/GEO and LEO/MEO operation of the Hydra MAX terminal using off-road land mobility profiles at Aberdeen Proving Ground.

The testing and demonstrations sustained high data rates and high-resolution video while both stationary and in motion. Despite challenging off-road conditions and rapid azimuth and elevation changes, the terminal maintained its LEO three beam lock — highlighting exceptional robustness, agility and performance.

ALL.SPACE's Hydra terminals use digital beamforming with monopulse tracking to deliver up to 4x faster responsiveness than traditional methods, ensuring precise, high speed connectivity across wide scan angles even under intense motion, vibration and dynamic conditions.

In a defining moment for ALL.SPACE, Hydra MAX has now been formally recognized by the U.S. Army as achieving TRL 6 — marking a significant transition from a prototype to an operationally validated system. This designation confirms the Hydra MAX has been proven in a relevant military environment, demonstrating readiness for near-production deployment and integration into broader defense and Joint Force networks.

Purpose-built to align with the Department of Defense's Joint All-Domain Command and Control (JADC2) objectives, Hydra MAX supports MOSA, enabling rapid integration with future constellations, including Telesat Lightspeed once Hydra MAX is certified for the network.


Reactel, Inc.
Reacting First to All Your Filter Needs.
Filter Solutions For Mission Critical Applications
High Performance, Rugged Packaging, Small Size and Weight
Great things can come in small packages. Reactel filters are ideally suited for the demanding environments that unmanned vehicles encounter.
Many manufacturers rely on Reactel to provide units which are:
High performance - Lightweight - Low profile
Contact a Reactel engineer with your filter or multiplexer requirements. We can create a unit which will be the perfect fit for your applications.
REACTEL, INC.
RF & Microwave Filters - Multiplexers - Multifunction Assemblies
REACTEL, INC.
REACTEL, INC.
REACTEL, INC.
8031 Cessna Avenue • Gaithersburg, Maryland 20879 • (301) 519-3660 • reactel@reactel.com • reactel.com
Intertek
RoHS
MADE IN MD
Since 1979

DC TO 86 GHz

Filter Technologies

For Every Application

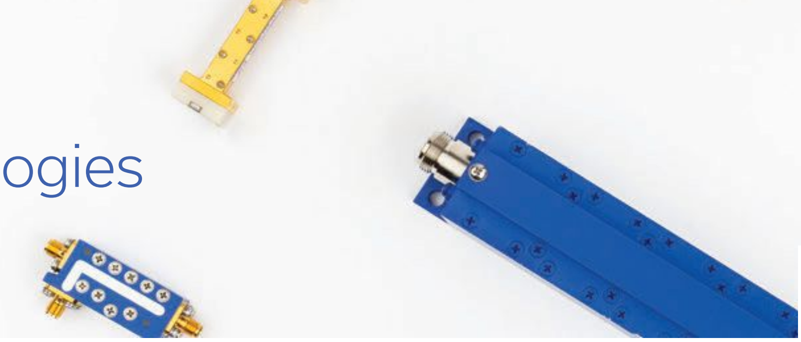

LEARN MORE

CAVITY

- Passbands to 43.5 GHz
- Stopbands to 57 GHz
- Bandwidths as narrow as 1%
- 100+ dB rejection

CERAMIC RESONATOR

- Fractional bandwidths from 0.5 to 40%
- Excellent power handling, up to 20W
- High Q in miniature SMT package

LUMPED L-C

- Wide catalog selection
- Several package options including aqueous washable
- Variety of filter topologies

LTCC

- Tiny size, as small as 0202
- Industry's widest selection of mmWave LTCC filters
- Proprietary designs with stopband rejection up to 100 dB

MICROSTRIP

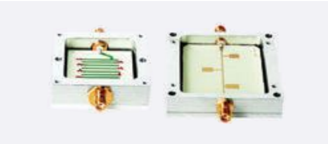

- Connectorized designs with 4 to 40% fractional bandwidth
- Power handling up to 10W
- Flat group delay

MMIC REFLECTIONLESS

- Patented topology absorbs and internally terminates stopband signals
- Perfect for pairing with amplifiers, mixers, multipliers, ADC/DACs & more

RECTANGULAR WAVEGUIDE

- WR-12, WR-15 and WR-28 interfaces
- Passbands up to 87 GHz
- High stopband rejection, 40 dB

SUSPENDED SUBSTRATE

- Ultra-wide passbands up to 26 GHz
- Wide stopbands up to 40 GHz
- High Q

THIN FILM ON ALUMINA

- Passbands from DC to 40 GHz
- High rejection with wide passband
- Miniature SMT package

Mini-Circuits®

Cliff Drubin, Associate Technical Editor

Automotive Radar Industry: China's Acceleration and the Next Wave of Sensing

Yole Group released its "Automotive Radar 2025" report alongside a new reverse engineering and costing report, "Automotive Radar Chipset Comparison 2025." These two reports provide a comprehensive view of the automotive radar industry, from system-level dynamics and market shifts to chip-level innovation and cost structures.

The report delivers a comprehensive analysis of the radar ecosystem, from technologies and semiconductor platforms to market trends and regulatory drivers. It explores how evolving architectures, integration strategies and regional dynamics are shaping next-generation ADAS and autonomous driving systems. The report also looks at the competitive landscape, key players, innovation pathways and future growth opportunities.

Without doubt, radar remains one of the fastest-growing sensing technologies in vehicles. In 2024, 166 million radar modules were shipped, up eight percent year-on-year. Despite slower growth than earlier years, radar integration continues to deepen across ADAS and autonomous driving platforms.

> Radar remains one of the fastest-growing vehicle sensor technologies.

However, ASPs remain under pressure, constraining revenue expansion despite volume gains. The industry is now centered on the 77 to 81 GHz band, as older 24 GHz systems are phased out.

According to Yole Group, 4D radar, capable of elevation estimation/measurement, represented about 40 percent of shipments in 2024 and is rapidly becoming the baseline for all new designs. Regulatory initiatives, including Euro NCAP, EU and NHTSA programs, are pushing OEMs toward broader radar coverage. By 2030, Yole Group's analysts expect five radars per vehicle to become the global standard, driven by safety requirements and OEM differentiation strategies.

Meanwhile, in-cabin radar is emerging to detect the status of occupants and monitor vital signs, supported by 60 GHz and UWB technologies, though mass adoption awaits finalized safety standards.

In addition to its annual market analysis, Yole Group has released "Automotive Radar Chipset Comparison 2025," a reverse engineering and costing study of two advanced radar devices from leading semiconductor players: TI' AWR2544 and Infineon Technologies' CTRX8191F. This comparison offers exclusive insight into the architecture, manufacturing cost and design strategy of two distinct approaches to automotive radar integration.

How Small Cell Innovation Can Accelerate 5G NTN Development

Small Cell Forum (SCF) published a report exploring how proven small cell design principles and open interfaces can help the ecosystem overcome some of the challenges facing emerging 5G non-terrestrial networks (NTNs), particularly regenerative LEO satellite systems. As these architectures move toward commercial relevance, the study sets out where terrestrial small cell experience can reduce complexity, improve interoperability and support efficient 5G NTN solutions.

The paper, "Small Cells and Non-Terrestrial Networks: Common Challenges and Common Solutions," explains that although terrestrial and space-based networks operate in very different environments, they share several engineering and operational constraints, including strict SWaP requirements. Compact and efficient radio designs, modular architectures and standardized interfaces are essential in both domains. SCF's existing body of work provides a set of components and frameworks that can be reused or adapted for 5G NTN satellite payloads and hybrid terrestrial–satellite deployments.

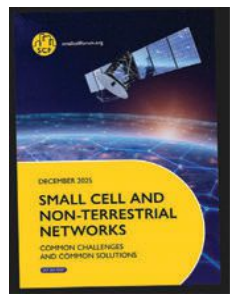

Source: SCF

The report summarizes key 5G NTN use cases including remote coverage extension, emergency communications, transportation and industrial applications. It outlines the main technical challenges for 5G NTN platforms, such as delay, Doppler and beam mobility and highlights the mitigation approaches available within current standards. It also reviews relevant 3GPP developments, pointing to areas where SCF's open interfaces, like FAPI and nFAPI, can support disaggregated multi-vendor interoperable 5G NTN solutions.

The paper identifies priority areas where SCF is now advancing specifications and deployment frameworks, including adding 5G NTN capabilities to upcoming FAPI releases and evolving shared infrastructure models for satellite integration. This work will give vendors and operators a clearer path to building 5G NTN systems that are interoperable and consistent with terrestrial networks.

Ericsson Mobility Report: Differentiated Connectivity Services Gaining Momentum

The Ericsson Mobility Report (EMR) – November 2025 reveals how the convergence of AI, cloud computing and mobile technologies are set to reshape data traffic patterns and connectivity demands.

For More Information Visit mwjournal.com for more commercial market news.

5G Standalone (SA) deployments have triggered a notable 2025 growth in the number of communications service providers (CSPs) offering differentiated connectivity commercial models based on 5G SA Network Slicing, where CSPs guarantee quality of service for customer use cases through the allocation of slices of the network. More than 90 CSPs have now launched/soft-launched 5G Standalone (5G SA) networks.

EMR researchers identified 118 cases, across 56 CSPs, where network slicing is used to provide differentiated connectivity services. Of the 118 cases, 65 have moved beyond proof-of-concept and into commercial services, across 33 CSPs. These are either subscription services or add-on packages for consumer or enterprise customers. 21 of the 65 commercial offerings were launched during 2025 alone.

The November 2025 EMR covers a new forecast timeframe, from 2025 through the end of 2031. The new reporting EMR period also covers the first expected deployments of commercial 6G. Based on previous mobile generation cycles' subscriptions uptake, EMR researchers expect the first commercial launches to be driven by leading service providers in front-runner markets such as the U.S., Japan, South Korea, China, India and some Gulf Cooperation Council countries.

Global 6G subscriptions are forecast to reach 180 million by the end of 2031, not including the early uptake of AI-enabled IoT devices. The subscription uptake number could increase significantly if 6G launches earlier than previous cycles indicate. Commercial 6G is expected to launch in Europe roughly a year later than in other regions, a delay greater than with 5G, primarily due to the comparatively later rollout of 5G SA.

As an ongoing major 5G use case, eMBB is forecast to top 6.4 billion 5G subscriptions by the end of 2031. Some 4.1 billion of these subscriptions are forecast to be 5G SA. In 2025 alone, 5G subscriptions are expected to top 2.9 billion by the end of the year, an increase of some 600 million subscriptions year-on-year.

5G networks are expected to manage 43 percent of all mobile data by the close of 2025 — up from 34 percent for the corresponding period last year. EMR experts forecast this to increase to 83 percent in 2031.

Fixed wireless access (FWA) broadband continues to grow as a 5G use case. The November 2025 EMR forecasts that about 1.4 billion people globally are expected to access FWA broadband by the end of 2031, 90 percent via 5G. EMR researchers have identified 159 providers that currently offer FWA services via 5G, approximately 65 percent of all FWA service providers. The number of service providers offering speed-based tariffs — a common monetization model for fixed broadband via fiber or cable — increased from 43 percent to 54 percent since the November 2024 EMR.

Ku/ Ka/ V/ E-Band Power Amplifier MMICs

Maximized performance for linear power applications

Ku/Ka-Band MMIC Die and Packaged MMICs

MMIC Die:

NPA1020-DE	12.5 - 14.5 GHz	15 W
NPA2020-DE	23.0 - 25.0 GHz	10 W
NPA2001-DE	26.5 - 29.5 GHz	35 W
NPA2002-DE	27.0 - 30.0 GHz	35 W
NPA2003-DE	27.5 - 31.0 GHz	35 W
NPA2004-DE	25.0 - 27.5 GHz	40 W
NPA2030-DE	27.5 - 31.0 GHz	20 W
NPA2040-DE	27.5 - 31.0 GHz	10 W

QFN Packaged MMICs:

NPQ2101-SM	27.5 - 31.0 GHz	5 W
NPQ2103-SM	27.5 - 31.0 GHz	8 W
NPQ2105-SM	27.5 - 31.0 GHz	12 W
NPQ2107-SM	27.5 - 31.0 GHz	17 W

Contact Nxbeam for Flange Packaged Options

V-Band MMICs

MMIC Die:

NPA4000-DE	47.0 - 52.0 GHz	1.5 W
NPA4010-DE	47.0 - 52.0 GHz	3.0 W

E-Band MMICs

MMIC Die:

NPA7000-DE	65.0 - 76.0 GHz	1.0 W

Around the **Circuit**

Barbara Walsh, Multimedia Staff Editor

MERGERS & ACQUISITIONS

Marki Microwave announced it has been acquired by **Industrial Growth Partners (IGP)**, a San Francisco-based private equity firm providing transformative capital for the industrial market. The partnership will enable Marki Microwave to accelerate investments in innovation, capacity and global expansion, supporting the company's long-term growth plans and deepening its commitment to customers worldwide. As part of the transaction, the Marki Microwave management team has invested alongside IGP, underscoring its confidence in the company's future and dedication to the business's strong growth trajectory.

Microwave Techniques, a manufacturer of high-power microwave components and RF solutions, announced the successful closing of its acquisition of **Symphony Microwave Technologies**, a design and manufacturing group specializing in high-power components and systems for industrial, medical, military, scientific and commercial applications. The acquisition creates an advanced manufacturer of high-power microwave technology and RF component solutions, with over 145 employees across facilities in Gorham, Maine; Nashua, N.H. and Hamburg, Germany. Terms of the transaction were not disclosed. The combined entity will sustain uninterrupted manufacturing for its complete range of existing products, including circulators, isolators, windows, loads, couplers, generators, systems and more.

COLLABORATIONS

Rohde & Schwarz has further deepened its collaboration with **Broadcom Inc.** to enable testing and validation of Wi-Fi 8 chipsets using the CMP180 radio communication tester. This alliance accelerates the path to market for OEMs and ODMs integrating Broadcom's upcoming Wi-Fi 8 chipsets in their products, ensuring conformity, performance and reliability. Wi-Fi 8, based on the IEEE 802.11bn specification, promises a significant leap forward in wireless connectivity. It is anticipated to bring higher throughput, lower latency, improved efficiency in congested spectrum environments and enhanced performance for extended reality, AI-assisted applications, real-time cloud gaming and ultra-high-definition content streaming.

ACHIEVEMENTS

Quantic PMI has earned the ISO 9001:2015 and AS9100D certifications for its quality management system for its Frederick, Md., and El Dorado Hills, Calif., facilities. This certification reinforces Quantic PMI's ability to meet stringent customer requirements and deliver consistent, RF and microwave components and integrated modules and subsystems. AS9100D was developed by the International Aerospace Quality Group and is the recognized standard for quality management in the aviation, space and defense industries. Fewer than 20,000 companies worldwide hold this certification. It builds on ISO 9001 by adding requirements for product safety, risk management, counterfeit parts prevention and traceability, making it one of the most rigorous quality standards in manufacturing today.

CONTRACTS

Sivers Semiconductors AB announced a mass-production purchase order agreement valued at approximately $3 million with **Tachyon Networks Inc.** for 28 GHz antenna modules. Sivers' antenna modules are central to Tachyon's innovative approach, enabling an affordable, disruptive solution that leverages Tachyon's extensive mmWave experience to extend high speed connectivity. The modules incorporate Sivers' TRB02801 beamforming transceiver, enabling mmWave fixed wireless access applications. Sivers' TRB02801 delivers a high performance 28 GHz RFIC for mmWave applications, supporting the full 24.25 to 29.5 GHz range with data rates up to 5 Gbit/s.

United Monolithic Semiconductors (UMS) announced that it has secured a four-year contract from the **Banque Publique d'Investissement** (BPI) aimed at accelerating the development of cutting-edge solutions for advanced 5G communication systems. This initiative will also engage in pathfinding activities in collaboration with prominent academic institutions and industrial laboratories. As the overall coordinator of the CAPTIVANT2 program, partially financed by BPI, UMS is dedicated to enhancing European technological sovereignty by tackling critical components within the RF link. This innovative program focuses on creating product solutions for both terrestrial 5G applications and space-based products, leveraging UMS' industry-leading technology platforms in GaN and GaAs.

PEOPLE

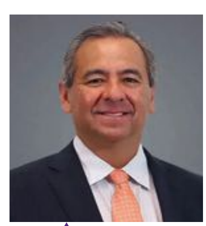

▲ *Manny Mora*

Kymeta announced the appointment of **Manny Mora** as president and CEO. This leadership transition marks a strategic acceleration of Kymeta's mission to deliver reliable, resilient connectivity for warfighters and mission-critical operators across the U.S. Department of Defense (DOD) and allied governments. Mora joins Kymeta following a 40-year career at General Dynamics Mission Systems, where he led space and intelligence systems and supported operational needs across the DOD, Intelligence Community, DHS and international partners.

For More Information For up-to-date news briefs, visit mwjournal.com

▲ *Tanios Elie BouRamia*

International Manufacturing Services, Inc. (IMS) has named **Tanios Elie BouRamia** as vice president of Sales & Marketing. BouRamia has over 15 years of experience driving global sales, marketing and product strategy across the electronics, automotive, medical device and industrial sectors. At IMS, he will lead initiatives to strengthen global channel partnerships, enhance customer engagement and expand market presence in high-reliability industries such as aerospace, defense and medical equipment.

▲ *Nick McKeown*

The Marconi Society has awarded the 2025 Marconi Prize, often called the "Nobel Prize for Communications" because it honors significant achievements in information communications technology, to **Professor Nick McKeown** for his fundamental contributions to high performance switches and routers and to software-defined networking and for transferring these contributions into widespread practice. McKeown, a British computer scientist raised in Bedford and Chelmsford, stands among influential technologists shaping the modern internet. His work spanning academia, industry and open-source ecosystems has redefined how networks are designed, operated and scaled globally.

▲ *Joseph Merenda*

Mini-Circuits announced the appointment of **Joseph Merenda** as the company's first Research & Development (R&D) Fellow, marking a milestone in the organization's long-term commitment to engineering excellence and technical innovation. The R&D Fellow role will be a cornerstone of Mini-Circuits' strategy to develop next-generation technologies, foster collaboration across engineering disciplines and deepen the company's technical leadership in the RF and microwave industry. A 40-year industry veteran, Merenda is widely recognized for his contributions to RF and microwave system design, product innovation and technical leadership. He has served in senior engineering roles across multiple organizations, authored numerous technical papers, webinars and filed several patents.

INVITED PAPER

Six Forces Redefining Connectivity in 2026

Stephen Douglas
Spirent Communications, Crawley, U.K.

Progress in telecom rarely moves in straight lines. It speeds forward, collides, pauses and then accelerates again, usually in places no one expects. In 2026, we are entering one of those acceleration points. Networks are becoming smarter, not just faster. The boundaries between terrestrial, satellite and cloud are fading. The way we design, test and secure these systems is being rewritten in real time.

Here are six shifts that will shape the upcoming years for engineers, network designers and technology leaders.

1 5G-ADVANCED BRINGS INTELLIGENCE TO THE NETWORK CORE

This year marks the true start of 5G-Advanced deployments. The new 3GPP Release 18 standard introduces capabilities that make networks context-aware and self-optimizing. We are moving beyond throughput toward intelligence.

Key updates include centimeter-level positioning accuracy via carrier-phase techniques, enhanced power-saving modes for both the radio and the device and support for extended-reality applications that require precise timing and synchronization. Release 18 also enables AI-assisted network management through standardized APIs, allowing the network to sense conditions and dynamically adapt traffic.

These enhancements are only possible through improvements at the RF layer. Advanced channel-state information, tighter phase coherence and distributed MIMO rely on highly accurate timing. Engineers now have to validate phase alignment within single-digit nanoseconds across massive antenna arrays. That introduces new demands for conformance and over-the-air testing.

The test challenge shifts from verifying maximum throughput to measuring how quickly a network detects a change and adjusts its configuration. In other words, it is not just about how fast the data moves, but how well the network can think on its feet.

2 AI SHIFTS FROM CLOUD TO EDGE

The next frontier for AI is no longer the data center. It is at the edge of the network, closer to where data is created and decisions must be made. As AI models grow larger and latency expectations shrink, centralizing everything in a hyperscale cluster no longer makes sense.

Processing large volumes of sensor and user data locally reduces latency, conserves bandwidth and strengthens data sovereignty, especially in industries such as healthcare, defense and finance. Local inference engines and on-premises GPU clusters are emerging as practical solutions to the physical limits of cloud computing.

For engineers, this shift introduces new design challenges. Distributed inference requires deterministic performance, precise timing and interference-free communication between many small edge nodes. Maintaining synchronization within tens of microseconds and ensuring clean RF conditions at every site are becoming just as important as the quality of the AI models themselves.

3 SATELLITES AND TERRESTRIAL NETWORKS CONVERGE

Satellite connectivity used to be the option of last resort. In 2026, it will become an enabler in mainstream communications. Also launched in 2026 is a new version of the 3GPP non-terrestrial networks (NTNs) standards that will enable direct text and limited voice communication from low Earth orbit (LEO) satellites when a terrestrial connection is out of reach.

This is a highly complex technical mission. In fact, the satellites move at nearly 7.5 kilometers per second, leading to a substantial Doppler effect and a 20 to 40 millisecond delay in propagation. To overcome this challenge, the LTE and 5G waveforms are being modified through advanced Doppler pre-compensation techniques.

Intersatellite handovers need to

take place within minutes due to orbit changes. This is a challenge that demands user equipment, baseband scheduling algorithms and predictively based beamforming techniques that use algorithms to predict satellite orbits. Another area undergoing improvements is antenna technology. Phased arrays are being adjusted to work across layers such as the L-, S- and Ka-Band.

Verification and validation of such networks remain a challenge. Traditional static channel emulators cannot simulate the fast-changing geometry of a LEO path. Currently, scientists are working to integrate orbit mechanics and fading simulations to model such a rapidly varying multipath channel. This will yield a new concept of coverage. Coverage will no longer be defined solely by tower radius, as it is at present.

4 ETHERNET RECLAIMS THE DATA CENTER

AI has redefined data center architecture. The large compute needs of model training and inference have made network infrastructure as important as processing infrastructure. InfiniBand held sway in high performance computing for years. However, Ethernet is back in the fray, thanks to breakthroughs such as remote direct memory access over converged Ethernet (RoCE v2) and new standards from the Ultra Ethernet Consortium.

Recent Ethernet fabrics have been approaching lossless performance with the addition of features such as explicit congestion notification (ECN), priority flow control (PFC) and novel congestion control algorithms designed to handle AI workloads. This enables large GPU clusters to communicate data with low latency while ensuring deterministic performance.

Hardware is also advancing. Efforts to migrate from 400-gigabit to 800-gigabit interfaces have been in full swing, with 1.6 terabit systems already in the planning stages of their 1.6 terabit designs employing pulse amplitude modulation 4.

Power density and cooling issues are emerging as bottlenecks. In fact, power densities of over 20 watts per 800-gigabit optical module are now forcing a rethink of cooling system designs.

Now, testing such fabrics is a mission-critical activity. A 1 percent packet loss margin could result in an overall AI cluster efficacy loss of over 30 percent. In essence, it is imperative to replicate traffic at a petabit scale while measuring latencies at a microsecond granularity and modeling an AI workload.

The data center network is becoming the computer," and Ethernet's rebound is merely a validation of open standards' ability to meet the scalability requirements of the industry when it is stretched to its limits.

5 GNSS INTERFERENCE BECOMES A CIVIL CONCERN

For several decades, Global Navigation Satellite System (GNSS) was considered a resilient and credible system. Now this is no longer the case. Affordable GNSS jammers and spoofers have been widely distributed around the globe, increasing GNSS interference issues in civil aviation, logistics and critical infrastructure. A single GNSS spoofing or jamming device can disrupt airport operations when located in close proximity to an airport runway.

Spoofing attacks have ranged from basic meaconing, which involves retransmitting legitimate signals after a pause, to complex pseudorange spoofing that tricks receivers into reporting incorrect positions. This has led to a resurgence of interest in resilient positioning, navigation and timing (PNT) techniques.

Future receivers will support multiple constellations, including GPS, Galileo, GLONASS and Beidou, with signals received on multiple frequencies, including L1, L2 and L5, to verify data through cross-consistency checks. Some of them will use encrypted military signals or authentication methods, such as Galileo's Open Service Navigation Message Authentication (OSNMA). Spoofed signals will

be detected using algorithms developed through AI.

To safely test such capabilities, precise tools are necessary. Laboratories are developing controlled radiated environments and hardware-in-the-loop simulation tools capable of mimicking spoofing and jamming in a manner compliant with regulatory spectra. Currently, designers must assess receivers' capabilities for detecting anomalies and restoring timing after spoofing attacks.

Regulators are aware of this reality. Standards of civil certification are being developed through initiatives such as the Resilient PNT Conformance Frameworks at the U.S. DOT. This trend indicates that a new field of innovation in RF technology is emerging in GNSS reliability, an aspect previously considered a given.

6 QUANTUM SECURITY MOVES INTO EARLY DEPLOYMENT

Quantum computing's threat to traditional encryption is no longer hypothetical. The development of a system that breaks large primes or elliptic-curve cryptography is not in sight, but preparatory work is underway. The U.S. NIST has selected various algorithms, such as CRYSTALS-Kyber and Dilithium, as defenses against quantum hacking, and a migration plan is being drawn up. This is slated to take a decade or more.

On a similar note, quantum key distribution (QKD) is also shifting its focus from lab demonstrations to field trials. This technology derives its strength from the quantum properties of photons, with any interception triggering a disturbance in their state. Initial systems are deployed according to the BB84 protocol in a metropolitan fiber-optic network at a rate of a few megabits per second over distances of 50 to 100 kilometers.

These systems present several unique challenges in terms of engineering. Photons are fragile particles, highly susceptible to loss and thermal noise that could easily destroy a quantum state. This is why ultra-low loss fiber, single-photon detectors or a cryogenic environment are often required. Quantum repeaters are also being developed as a means of increasing range, although coherence across repeater chains is a challenge.

Quantum systems require a different testing paradigm. Measurement alters the phenomenon of observation, so classical monitoring techniques are not possible in quantum systems. Quantum system builders have developed methods based on statistical analysis of error rates in quantum bits and on analysis of photon distributions. Others have developed hybrid systems combining post-quantum cryptography and QKD.

Quantum security is shifting from physics labs to network operations centers, ushering in a new era in our approach to trust and verification.

THE BIGGER PICTURE

All six of these trends share one theme: intelligence is moving closer to the physical layer. Whether it is 5G-Advanced adapting in real time, AI operating at the edge, photons or securing quantum links, the innovation is happening where computation meets signal.

For engineers, that is encouraging. The skills rooted in RF design, timing and measurement are becoming more valuable than ever. As networks evolve from passive transport to active participants in computation and security, precision and reliability at the signal level will decide how well the digital world functions.

The coming year will not simply deliver more bandwidth. It will redefine what it means for networks to sense, adapt and protect themselves. For those of us who have spent our careers at the intersection of hardware and protocol, it is both a technical challenge and an opportunity. The next generation of connectivity will not be built only in the cloud; it will be engineered at the physical layer, where every hertz and every nanosecond still matter. ■

INVITED PAPER

Direct RF Conversion and Devices Leveraging the Technology

Mike Barrick
Emerson, Fort Worth, Texas

RF semiconductor and sampling technologies are advancing rapidly. Combinations of these technologies have yielded high speed RF analog-to-digital converters (ADCs) and digital-to-analog converters (DACs) capable of direct conversion between digital and Ka-Band, decreasing the need for analog RF front-ends (RFFEs) and simplifying transceiver systems.

Use of these new converters in semiconductor devices, such as digital RF transceivers and RF system-on-chip (RFSoC) devices, has enabled decreases in size, weight and power that were previously not achievable and flexible, on-chip digital up-conversion (DUC), digital down-conversion (DDC) and filtering. A block diagram for a digital RF transceiver using direct conversion is shown in ***Figure 1***.

Digital RF transceivers and RFSoCs are being increasingly used in downstream devices, such as transmit/receive modules (TRMs), software-defined radios (SDRs) and commercial terrestrial and satellite communication (satcom). Since these devices now include mixed-signal RF and digital interfaces, traditional measurement approaches using vector network analyzers (VNAs) are no longer useful. A new approach for testing is needed.

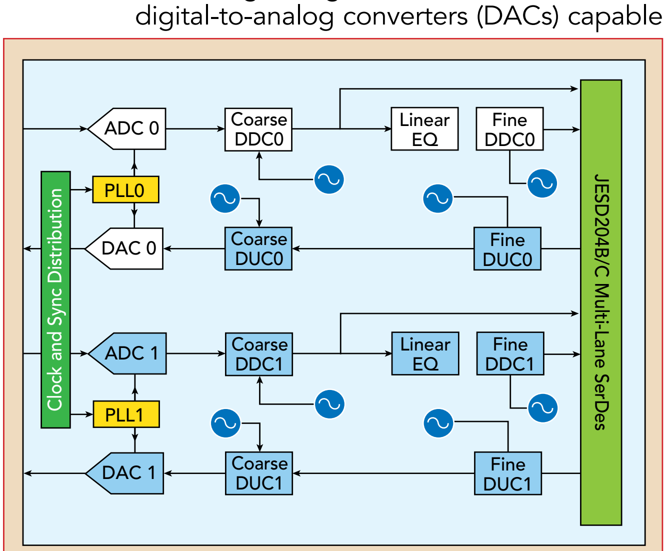

Fig. 1 Direct RF transceiver using direct conversion.

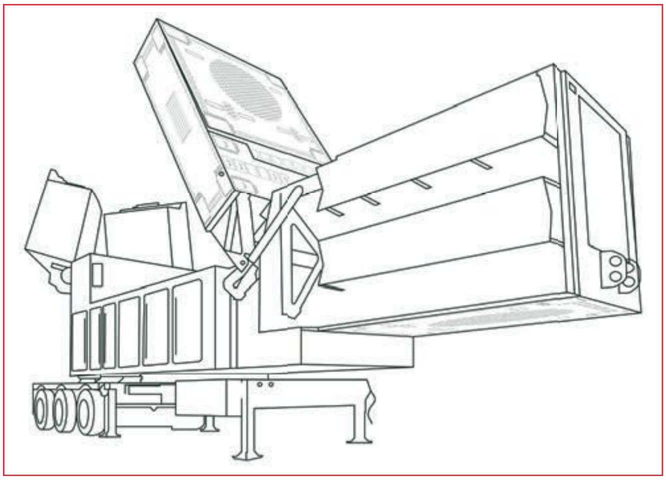

Fig. 2 AESA antenna with visible TRM antennas.

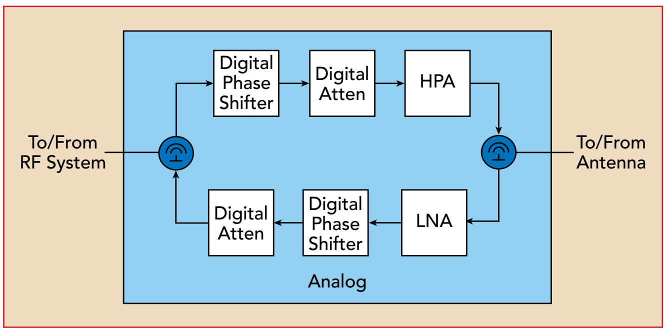

Fig. 3 Notional block diagram of an analog TRM.

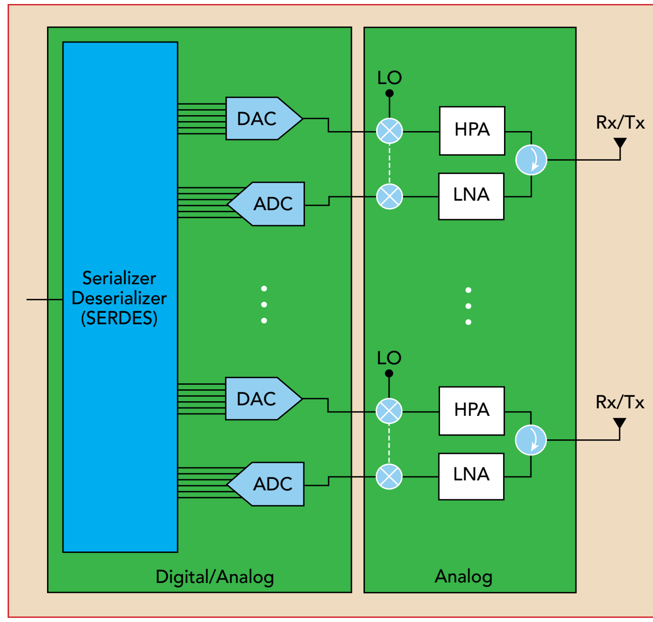

Fig. 4 Block diagram of a multichannel DTRM.

AESA AND TRM BACKGROUND

The first phased arrays in the early 1900s were mechanically scanned using switches. Today's active electronically scanned arrays (AESAs) use many solid-state TRMs or digital receiver exciters (DREXs), each connected to one or more antenna elements. ***Figure 2*** shows an example of a new generation AESA with phased array antenna elements visible on the face of the antenna.

Architecting of the AESA with TRMs/DREXs was made possible by advancements in RF semiconductor technology in the 1980s. Today, even newer technologies and device types are available for high-power transmit amplification and low noise receive amplification. Leveraging these advancements, the size, weight, power and cost (SWaP-C) of TRMs/DREXs have been reduced, and usage is building in commercial applications such as satcom.

TRMs and DREXs provide a range of functionality in an RF system, including high-power amplification (HPA) for the transmitter, low noise amplification (LNA) for the receiver, phase shifting to steer the AESA "beam," and circulators and switches to route signals. ***Figure 3*** shows a notional block diagram of an analog TRM.

Newer digital TRMs (DTRMs) transmit by receiving high speed serial (HSS) data from the RF system, applying serial to parallel conversion, converting to RF and amplifying to the required level using an HPA. Likewise, DTRMs receive by amplifying with an LNA, converting to digital, then applying parallel to HSS conversion. If the frequency is in the Ka-Band or below, this often leverages digital RF transceiver devices to handle RF to digital conversion as close to the antenna as possible, enabling additional signal processing functions in the DTRM, including DDC, DUC and filtering.

DTRMs often use multichannel digital RF transceivers with 16 or higher channels on a single semiconductor device. ***Figure 4*** shows a high-level block diagram of a multichannel DTRM with antennas.

AESAs configured with DTRMs offer additional advantages over analog TRMs, including increased flexibility and reduction in SWaP-C. However, the evolution to DTRMs also presents new challenges, including how to test multichannel DTRMs from "RF to Bits" in prototyping, development, characterization, hardware-in-the-loop (HIL) and production test phases.

WHAT IS REQUIRED TO TEST A TRM?

Analog TRMs have traditionally been tested using systems including VNAs, vector signal generators (VSGs) and vector signal analyzers (VSAs). Depending on the stage in the TRM test cycle, combinations of these instruments can be used to extract the desired measurement parameters.

Classical VNAs fundamentally provide small signal S-parameter measurements, such as gain, input match and output match, and enable calibration of the TRM using a range of transmit and receive gain and phase settings. In addition to CW measurements, some VNAs can also be useful for pulsed measurements, enabling measurement of semiconductor devices in the PA that are unable to operate at 100 percent duty cycle due to device heating.

The pairing of a VSG with a VSA (VST) provides additional measurement capability that is required for some stages of testing. These instruments enable the test engineer to excite the TRM with a modulated waveform and measure wideband signal parameters on the output. A range of potential measurements is enabled using these types of instruments, including noise figure

(NF), adjacent channel power (ACP), error vector magnitude (EVM), third-order intercept (TOI/IP3), spurious free dynamic range (SFDR), power-added efficiency (PAE), large signal parameters and others.

Multichannel TRMs present special challenges, as channel-to-channel isolation and relative characteristics between channels may be required. Multiport VNAs can be used to measure isolation between channels, per-channel gain and phase response. However, CW stimulus and measurement techniques used with multiport VNAs are fundamentally different from real-world modulated signals. Multichannel VSTs can simultaneously stimulate and measure all ports of the multichannel TRM using wideband, phase-aligned signals, enabling measurements in a configuration matching usage conditions. An example of a 4-channel, phase-aligned VST is shown in ***Figure 5***.

As described in the previous section, DTRMs no longer have an analog input/output for testing, so these traditional instruments are of limited utility. New solutions matching the mixed-signal nature of DTRMs are required, with the capability to make new measurements that are analogous to VNAs, VSGs and VSAs.

SDR BACKGROUND

SDRs are a more recent development than TRMs, having been initiated in the 1980s and accelerated by recent developments in RFSoCs. SDRs consist of a few fundamental building blocks, which could either be monolithic or distributed, including RFFE and digital I/Q baseband (Direct RF conversion), stream signal processing and host controller.

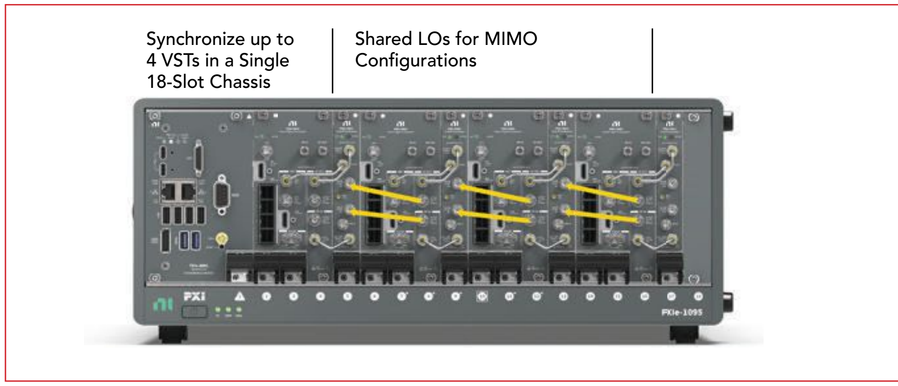

Fig. 5 **4-channel, phase-aligned VST.**

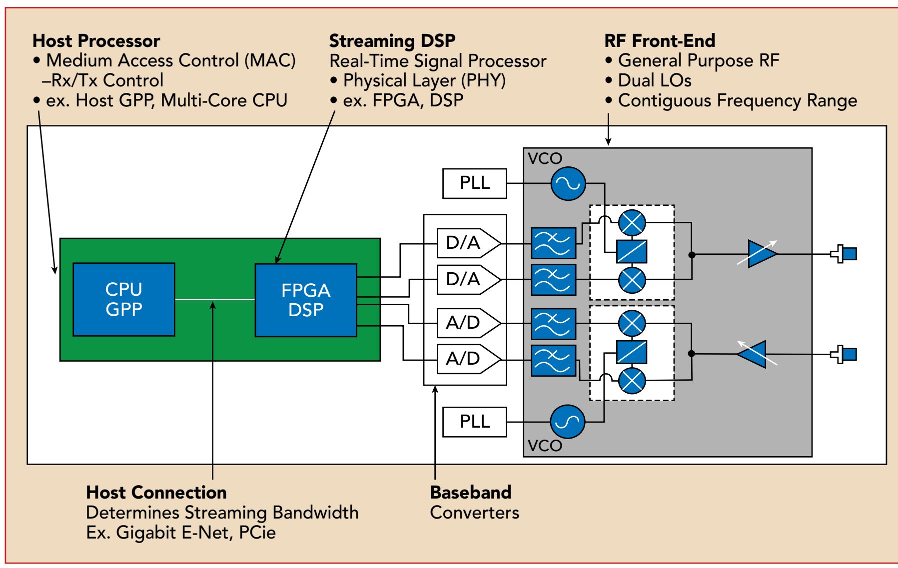

Fig. 6 **Generic SDR architecture.**


HIGH FREQUENCY Components
PPI
Passive Plus
RF & Microwave Components
HIGH QUALITY
RF/MICROWAVE PASSIVE COMPONENTS FOR HIGH FREQUENCY APPLICATIONS
Fundamental in radar systems and antennas, PPI components are indispensable for optimizing signal integrity, efficiency, and performance across high frequencies.
Broadband Capacitors
5 case sizes, 10nF & 100nF
up to 67 GHz
Broadband Resistors
1209 & 2010 sizes
up to 67 GHz
Broadband Conical Inductors
Flying Leads & SMT
up to 110 GHz
Reach out for Availability
www.passiveplus.com
+ (631) 425-0938
sales@passiveplus.com

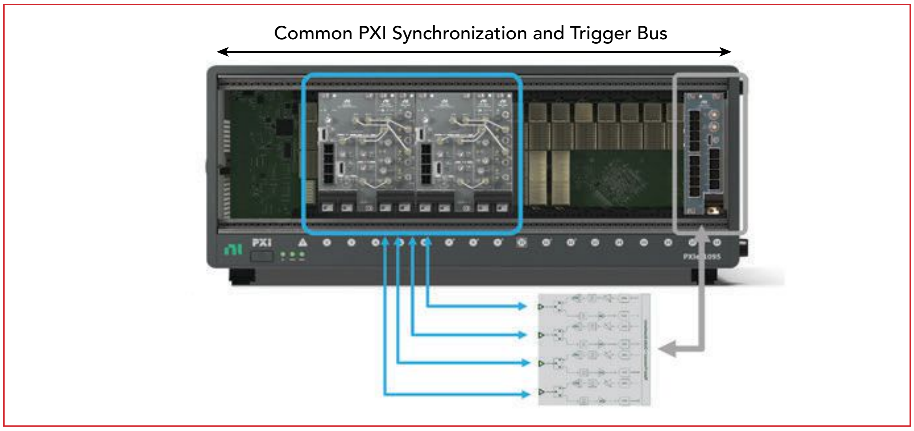

Fig. 7 **Single-box, 4-channel RF and HSS test system.**

A block diagram for a generic SDR is shown in ***Figure 6***.

Assuming that the board set for an SDR includes at least an integrated RFFE and digital I/Q baseband, DTRM and SDR test needs are very similar.

EVOLVED MIXED-SIGNAL TEST SYSTEM

The major change in the transition from analog TRMs to DTRMs is the replacement of one of the RF ports with an HSS bus. Likewise, SDRs have a similar configuration with both HSS and RF interfaces. A new means of emulating HSS signals with the test system is needed to meet measurement needs for these new mixed-signal devices.

A complete single-box test system providing four channels of RF transmit (Tx) and receive (Rx) capability, as well as four channels of HSS Tx and Rx capability, is shown in ***Figure 7***. Details of the test system components are provided in the following section.

EVOLVED MIXED-SIGNAL TEST SYSTEM COMPONENTS

Emulation of transmission and reception of HSS signals can be achieved using various approaches, most of them based on user-programmable FPGAs. Development boards from FPGA manufacturers are one option, but they can have short support lives and lack the ability to be synchronized with the test system. A modular commercial off-the-shelf (COTS) solution would be a superior solution, providing a user-programmable FPGA and flexible electrical or optical HSS interface as well as synchronization with the test system through the PXI backplane. An example of this solution is shown in ***Figure 8***.

Fig. 8 **NI PXIe-7903 Flex-RIO HSS module. Source: Based on Xilinx Virtex UltraScale+ VU11P FPGA with 48 multi-gigabit transceivers.**

HSS formats used for DTRMs and SDRs are not standardized, and can include various formats such as JESD-204C, 100 GbE, Vita 17.3 and Aurora. Each of these formats has user-selectable options, including the number of lanes, encoding and bit depth. Based on the multitude of HSS formats and the potential range of user-selected options for each format, semi-custom IP is typically needed for the FPGA, matching the implementation for the device(s) to be tested.

Modulated RF signal generation and analysis, and matching the frequency range and bandwidth to be tested, are needed on the RF side


330
320
310
300
290
280
270
260
250
240
230
030
040
GaN

of the device under test (DUT). Depending on the DUT configuration, either a single-channel or multichannel solution could be required. If the DUT is multichannel and simultaneous measurement capability is needed, a multichannel VST solution is necessary. However, if sequential measurements are acceptable, a single-channel VST with RF switching could be used. In either case, synchronization with the FPGA-based HSS solution is required. A modular VST solution is shown in ***Figure 9***, enabling synchronization with the test system through the PXI backplane, similar to the COTS FPGA solution.

In addition to HSS and RF I/O, DTRMs and SDRs typically require state control signals. These are usually provided over SPI, I^2C, MIPI or other interfaces. Ideally, these control signals would be synchronized with the test system so that the timing of HSS and RF could be tightly controlled.[1] A multichannel, SW-configurable solution to provide a large array of control signals is shown in ***Figure 10***. This includes synchronization with the test system through the PXI backplane, as in other examples.

Lastly, the DTRM or SDR needs power from the test system. In cases where high-power PAs utilizing GaN technology are used, power must be pulsed and measurements must be made during the "on" cycle of the device. In addition, DTRMs or SDRs may require multiple voltage rails with specific turn-on/off sequences. A power supply (source measure unit) capable of providing continuous or pulsed power in synchronization with the test system is shown in ***Figure 11***.

MIXED-SIGNAL MEASUREMENTS FOR DTRMS AND SDRS

While traditional VNA RF in/RF out measurements are no longer applicable for DTRMs and SDRs, analogous single or multichannel measurements with HSS in/RF out and RF in/HSS out are now possible, leveraging the system and components described in the previous sections.

Traditional VST-based Tx measurements can be emulated using a combination of HSS bit stream(s) into the SDR or DTRM, and measurement of RF output(s) from the device. Measurements on the resulting RF signal can be made, including generic time-domain and frequency-domain measurements as well as standards-based measurements like ACP and EVM. Two-

Fig. 9 **NI PXIe-5842 VST module.**

Fig. 10 **NI PXIe-6571 digital pattern instrument.**

Fig. 11 **NI PXIe-4139 source measure unit.**

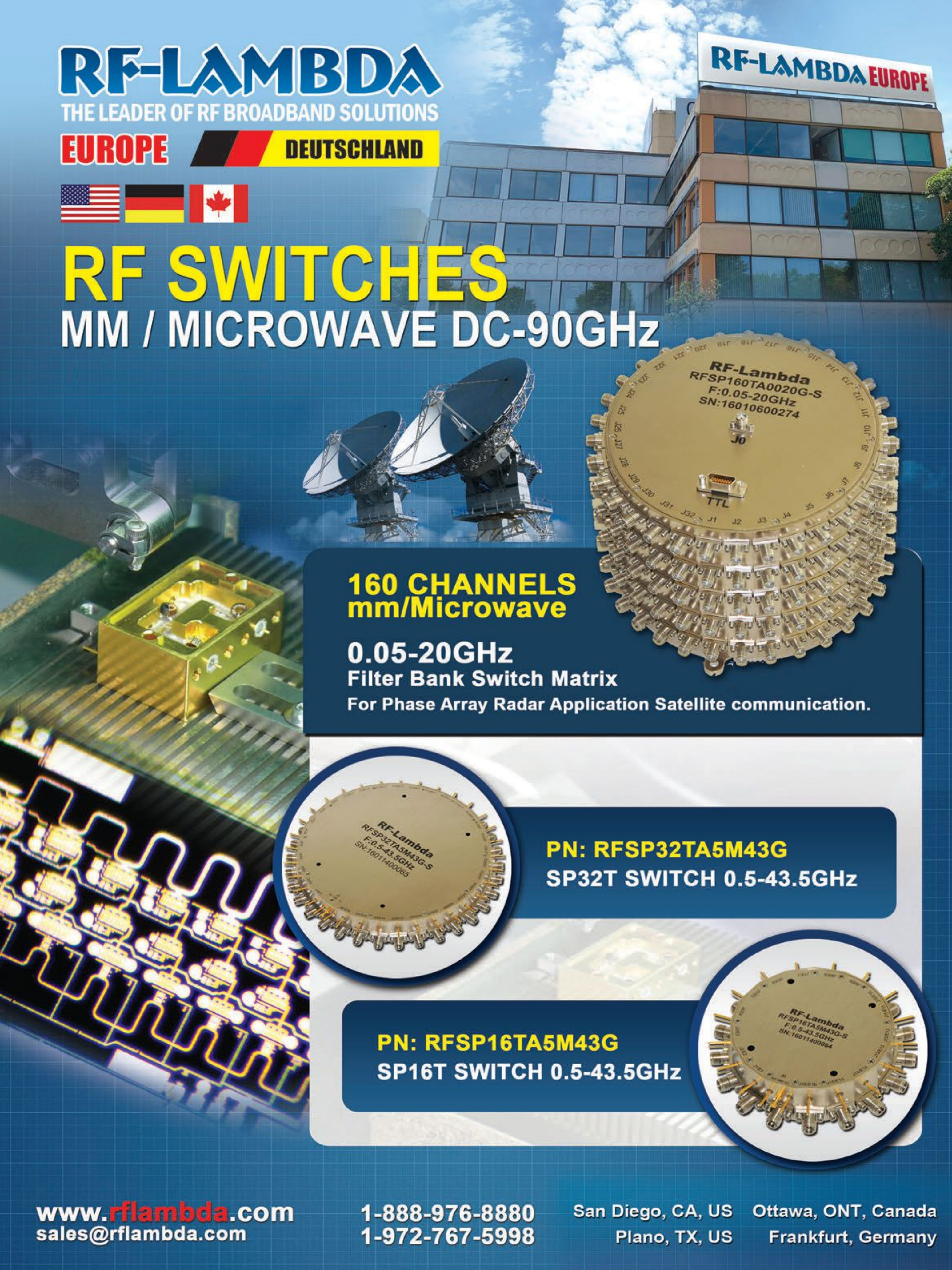

RF-LAMBDA
THE LEADER OF RF BROADBAND SOLUTIONS
EUROPE
DEUTSCHLAND
RF-LAMBDA EUROPE
RF SWITCHES
MM / MICROWAVE DC-90GHz
RF-Lambda
RFSP160TA0020G-S
F:0.05-20GHz
SN:16010600274
160 CHANNELS
mm/Microwave
0.05-20GHz
Filter Bank Switch Matrix
For Phase Array Radar Application Satellite communication.
PN: RFSP32TA5M43G
SP32T SWITCH 0.5-43.5GHz
PN: RFSP16TA5M43G
SP16T SWITCH 0.5-43.5GHz
www.rflambda.com
sales@rflambda.com
1-888-976-8880
1-972-767-5998
San Diego, CA, US
Plano, TX, US
Ottawa, ONT, Canada
Frankfurt, Germany

tone measurements like TOI can be emulated using dual tones encoded in the HSS stream. PAE can be measured for various types of input signals by measuring RF output power and input DC power and calculating the ratio of the two.

Likewise, analogous measurements to traditional Rx measurements, such as BER/BLER, can be constructed using modulated RF signals into the SDR or DTRM, and demodulated digital I/Q from the HSS stream. NF measurements can be measured using traditional Y-Factor techniques and monitoring the amplitude of the HSS digital I/Q stream.

Mixed-signal analogs to traditional VNA S-parameter measurements are challenging to construct, but some pre-work has been done in academia.[2] Standard VNA measurements use ratios of forward and reverse signals (A-incident and B-reflected waves) measured at calibrated reference planes. It is difficult to implement a similar approach with mixed-signal devices due to challenges, including a lack of a reference plane and suitable calibration standards on the digital side. Work continues to identify a suitable set of approaches.

CONCLUSION

DTRMs and SDRs require test solutions tailored for mixed-signal devices in development to production test stages. While measurements between these phases are similar, different phases have different requirements, such as accuracy, speed and other factors.

Test solutions for legacy analog TRMs have consisted of VNAs, VSGs and VSAs, but newer DTRMs require evolved capability to make mixed-signal measurements with HSS data streams and RF signals. Measurement requirements for SDRs require a similar mix of HSS and RF.

A solution has been proposed leveraging FPGA-based HSS, VST-based RF, power supply and control, all synchronized using PXI-based timing and synchronization with sub-nanosecond accuracy. This solution offers benefits including accuracy of traditional VSG and analysis, customized FPGA-based HSS interface matching the DUT configuration and the ability to leverage PXI-based timing and synchronization to provide fast changes in power, control, HSS and RF configuration to accelerate measurements of mixed-domain devices. ■

References

1. NI PXI Timing and Synchronization Design Advantages, NI.
2. D. C. Ribeiro, A. Prata, P. Miguel Cruz and N. Borges Carvalho, “D-Parameters: A Novel Framework for Characterization and Behavioral Modeling of Mixed-Signal Systems,” *IEEE Transactions on Microwave Theory and Techniques*, Vol. 63, No. 10, October 2015, pp. 3277–3287.
3. F. Verbeyst, P. Barmuta, M. Vanden Bossche and M. Rullmann, “Accurately Applying Wideband Modulated Signals to a DUT Using an Extended VSG-VSA Setup” *ARFTG*, June 2, 2023.

MiCable

NEW

0.4-8GHz HIGH POWER Directional & Dual-Directional Coupler

- High power handling : up to **600W**
- Low VSWR & insertion loss
- Excellent coupling, flatness and directivity which will significantly improve the signal acquisition accuracy

P/N	CW Power Max.(W)	Nominal Coupling (dB)	Main Line VSWR	Coupling VSWR	Insertion Loss*	Coupling	Flatness	Directivity Min.(dB)
			Max.(:1)		Max.(dB)			
0.4-8GHz Directional Coupler								
D3002H004080	120	30	1.3	1.3	0.8	30±1.0	±0.8	18
D4002H004080	120	40	1.3	1.3	0.8	40±1.0	±0.8	18
D3005H004080	250	30	1.4	1.4	0.7	30±0.9	±1.3	14
D4005H004080	250	40	1.4	1.4	0.7	40±1.0	±1.4	14
D3008H004080	400	30	1.4	1.4	0.7	30±0.9	±1.3	14
D4008H004080	400	40	1.4	1.4	0.7	40±1.0	±1.4	14
D3012H004080	600	30	1.4	1.4	0.7	30±0.9	±1.3	14
D4012H004080	600	40	1.4	1.4	0.7	40±1.0	±1.4	14
0.4-8GHz Dual-Directional Coupler								
D3002HB004080	120	30	1.3	1.3	0.8	30±1.0	±1.0	18
D4002HB004080	120	40	1.3	1.3	0.8	40±1.0	±1.0	18
D3005HB004080	250	30	1.4	1.4	0.7	30±0.9	±1.5	14
D4005HB004080	250	40	1.4	1.4	0.7	40±1.0	±1.6	14
D3008HB004080	400	30	1.4	1.4	0.7	30±0.9	±1.5	14
D4008HB004080	400	40	1.4	1.4	0.7	40±1.0	±1.6	14
D3012HB004080	600	30	1.4	1.4	0.7	30±0.9	±1.5	14
D4012HB004080	600	40	1.4	1.4	0.7	40±1.0	±1.6	14

*Theoretical I.L. Included

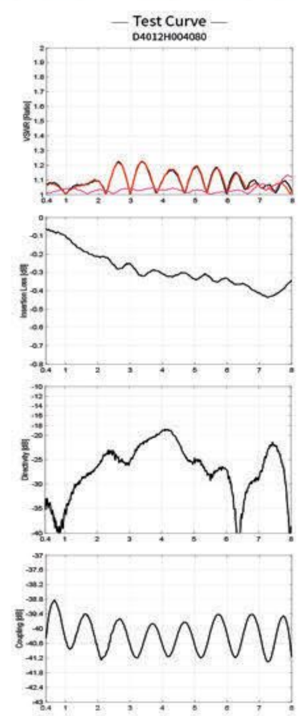

More Information-
Scan the QR Code

MIcable Inc.

www.micable.cn sales@micable.cn +86-591-87382856

Oscilloscope-Based Load-Pull Measurement System for Digitally Modulated Signals

A. Villagran-Gutierrez, J.R. Loo-Yau, E.A. Hernández-Domínguez and P. Moreno
Center for Research and Advanced Studies of the National Polytechnic Institute at Guadalajara (Cinvestav-Guadalajara)

J. Apolinar Reynoso-Hernández
Centro de Investigación Científica y de Educación Superior de Ensenada (CICESE), Ensenada, Baja California, México

An oscilloscope is used to capture the time-domain incident and reflected voltages at the ports of a device under test (DUT), enabling load-pull measurements with digitally modulated signals. This enables the extraction of load-pull contours for output power, gain, power-added efficiency (PAE), drain efficiency and adjacent channel power ratio (ACPR) without requiring prior tuner characterization or waveform corrections. It relies on the standard load-pull calibration while leveraging direct time-domain waveform measurements, eliminating the need for a comb generator as a phase reference. Power calibration still requires accounting for losses between the oscilloscope and the DUT's ports. The feasibility of this approach is validated through 2 GHz load-pull measurements on a GaAs FET using a 20 MHz LTE signal.

Although modern wireless system design relies on digitally modulated signals like LTE, RF and microwave power amplifiers (PAs) are typically designed using continuous wave (CW) test data. This results in suboptimal performance, as CW measurements fail to adequately describe PA linearity, with ACPR being a key figure of merit. A measurement system that characterizes transistors with modulated signals would greatly benefit PA design.

Modulated S-parameters lack sufficient detail for PA design.[1] To address this, load-pull measurements with multi-tone[2] or digitally modulated signals[3-6] provide more comprehensive data crucial for designing PAs. For example, Ghanipour et al.[7] demonstrate how the optimal matching impedance varies significantly between two-tone and digitally modulated signals, underscoring the value of modulated signal characterization. The vector component analyzer (VCA)[8] is a commercial approach for active device characterization with periodically modulated signals.

Microwave transistor characterization can be performed in the time domain, which has

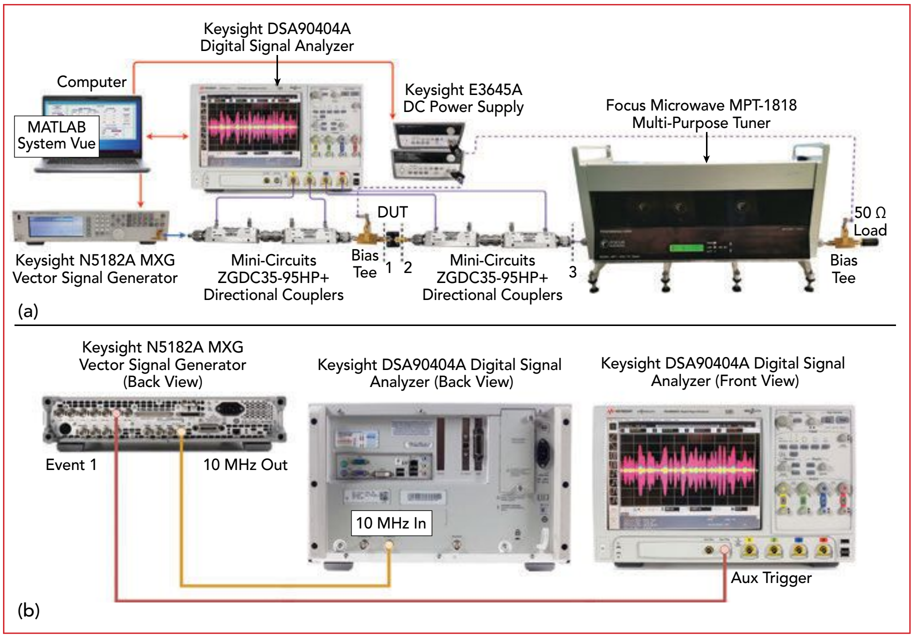

Fig. 1 Measurement setup (a); auxiliary trigger and 10 MHz reference signal connections (b).

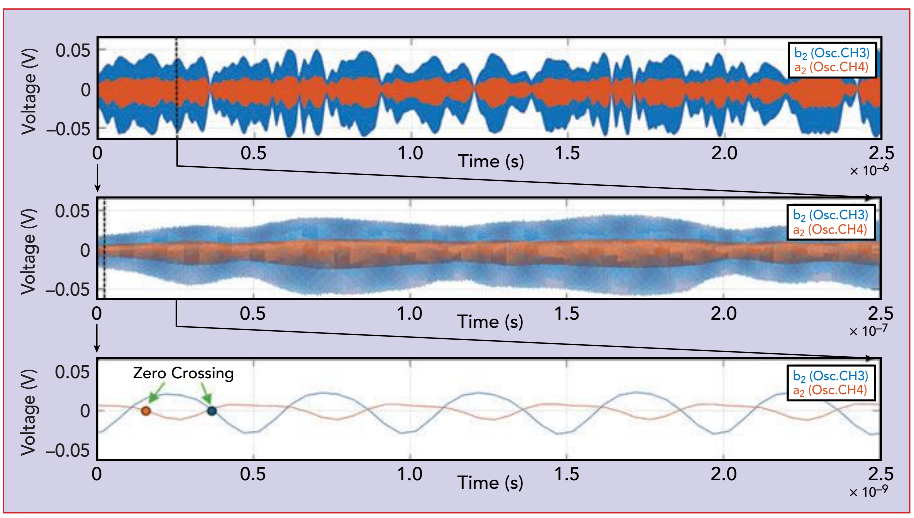

Fig. 2 Example phase calculation of the modulated signal for voltages at the output port.

been explored through various approaches. Time-domain load-pull techniques date back to using a microwave transistor analyzer (MTA) for waveform engineering.[9] Other time-domain load-pull methods employ a combination of vector network analyzers (VNAs) with oscilloscopes[10,11] or large signal network analyzers (LSNAs) for pulsed[12] and multi-tone[13] measurements or analyzing load lines.[14] Nonlinear vector network analyzers (NVNAs) have been used for reconstructing waveforms.[15] An alternative method uses an oscilloscope for low frequency load-pull to extract intrinsic current and voltage waveforms.[16]

Nonetheless, most measurement setups that work with the time domain tend to use CW signals because they simplify waveform reconstruction when using frequency-domain-based equipment, or because the objective is to analyze the load lines or perform waveform engineering. By contrast, this work uses time-domain waveforms measured with an oscilloscope to perform all the necessary calculations, enabling load-pull measurements without requiring an MTA, LSNA, NVNA or VNA.

The setup uses an oscilloscope and directional couplers to measure incident and reflected voltages at the DUT ports. A vector signal generator (VSG) generates the modulated signal, enabling the extraction of ACPR contours and traditional load-pull metrics such as output power (P_{out}), gain (G), PAE and drain efficiency (η_d). The system operates across a frequency range of 1.8 to 4.0 GHz, limited by the impedance tuner on the low end and the oscilloscope on the high end.

Frequency-domain measurement systems, such as the Maury Microwave MT2000,[4,5] LSNAs[17] or VNAs,[11,15] often rely on phase references for calibration, typically provided by comb generators. While oscilloscope-based systems offer an alternative, many calibration techniques focus on time-domain waveform corrections[18,19] and may require additional steps for phase alignment.[20,21] In contrast, this work simplifies the process by correcting reflection coefficients using a well-established load-pull calibration method,[22] avoiding the need for a comb generator.

MEASUREMENTS

The test setup employs an oscilloscope and four directional couplers to capture the time-domain waveforms of incident and reflected voltages at both ports of the DUT (see ***Figure 1***).[23] A VSG provides the modulated signal stimulus for the measurements. The DUT is biased with bias tees and DC power supplies, measuring V_{DS} and I_{DS} — parameters essential for calculating PAE and η_d. An impedance tuner is incorporated to adjust the load impedance for the load-pull measurements.

Custom MATLAB software controls the equipment and handles data acquisition via virtual instrument software architecture (VISA) commands. The voltage waveforms captured by the oscilloscope's four channels are transferred to the computer, where they are processed to calculate the calibrated load reflection coefficients (Γ_L) at the DUT's output port, along with P_{out}, G, η_d, PAE and ACPR. A Keysight SystemVue schematic is employed to configure the VSG to generate the modulated signal required for the measurements.

Reflection Coefficient Measurement

Γ_L is defined as the ratio of reflected to incident voltage at the output port. Its magnitude and phase are calculated separately to determine the uncorrected or raw Γ_L from the acquired data. First, the time-domain waveforms of the incident and reflected voltages are analyzed to compute the phase. Since both signals share the same carrier frequency (see ***Figure 2***), their phases are determined using zero crossings of the first period of each signal.[24] The raw Γ_L phase is then obtained by subtracting these values.

For improved accuracy, the oscilloscope's averaging function is enabled during this process, enhancing the precision of the phase measurements and the subsequent calculation of the raw Γ_L phase. The zero crossings are measured directly on the oscilloscope, then the oscilloscope's averaging function is turned off before calculating the magnitude of Γ_L. This is important because it has been observed that the oscilloscope's averaging alters the amplitude of the signal when measuring a modulated waveform. This is most likely because the averaging function of most oscilloscopes is intended for repetitive signals, benefiting mostly periodic signals, and the modulated signal used for this test is not repetitive within the measured time lapse of 25 µs. At this stage, the voltage waveforms from all four oscilloscope channels are measured, captured and transferred to the computer for further processing.

The magnitude of Γ_L is determined by computing the voltage's fast Fourier transform (FFT). Since the measurements are performed using a modulated signal, the average power within the signal's bandwidth for both the incident and reflected voltage spectra must be calculated. The magnitude of the raw Γ_L is then obtained by taking the ratio of the reflected spectrum to the incident spectrum.

Power Measurements

Conducting load-pull measurements requires determining the power at the DUT's input and output ports. These calculations rely on fundamental principles and equations from transmission line theory.[25] The incident (P_i^+) and reflected (P_i^-) powers are computed from the measured voltages using ***Equations 1*** and ***2***:

$$P_i^+ = \frac{1}{2}|a_i|^2 \quad (1)$$

$$P_i^- = \frac{1}{2}|b_i|^2 \quad (2)$$

Where:

- i=1,2 corresponds to the input and output ports.
- a_i and b_i represent the normalized incident and reflected voltages at port i, calculated by dividing the measured voltages by $\sqrt{Z_0}$, where Z_0 denotes the characteristic impedance.

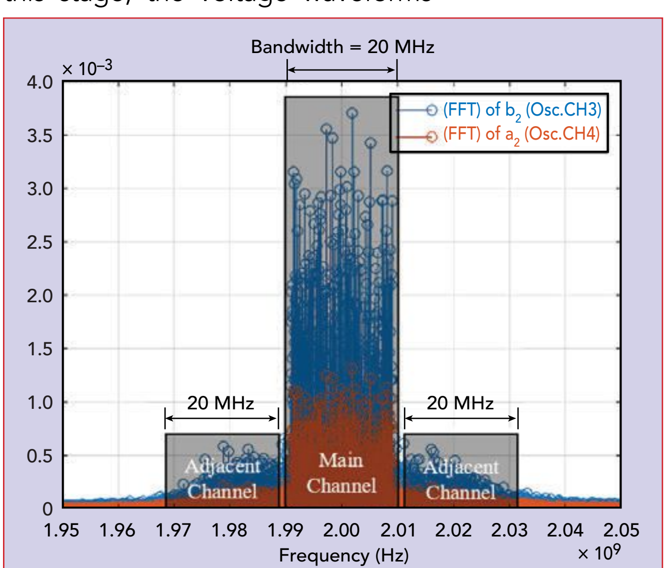

Fig. 3 Magnitude of the FFT of voltages from Figure 2 indicating the bandwidths of the main and adjacent channels.

First, the FFT of the measured voltages is calculated. Then, the power of each spectral component within the signal's bandwidth is determined using Equations 1 and 2. Finally, the total average power is computed by summing all the individual power spectral components.

Power measurements require calibration after determining the uncorrected incident and reflected average power at each port, as detailed in the following section. Once calibrated, the input power (P_{in}) and output power (P_{out}) are calculated using ***Equations 3*** and ***4***:

$$P_{in} = P_1^+ - P_1^- \quad (3)$$

$$P_{out} = P_2^+ - P_2^- \quad (4)$$

Where P_1^+ and P_1^- refer to the incident and reflected power at the input port and P_2^+ and P_2^- correspond to the incident and reflected power at the output port.

Efficiency Measurements

Drain efficiency (η_d) and PAE are calculated with ***Equations 5*** and ***6***:

$$\eta_d[\%] = \frac{P_{out}[W]}{V_{DS} \times I_{DS}} \times 100 \quad (5)$$

$$PAE[\%] = \frac{P_{out}[W] - P_{in}[W]}{V_{DS} \times I_{DS}} \times 100 \quad (6)$$

Where:

- V_{DS} and I_{DS} represent the bias drain-to-source voltage and the DC drain-to-source current of the transistor.
- P_{in} and P_{out} are the calibrated input and output power values.

ACPR Measurements

ACPR is the power ratio in adjacent channels to the power within the signal's main channel. ***Figure 3*** shows the FFT of the incident and reflected voltages in Figure 2, clearly illustrating the signal's main and adjacent channels.

Measuring ACPR with this system requires calculating the power in the signal's adjacent channels at the DUT's output port. This process is like calculating P_{out}, with one key difference: the average incident and reflected power must be computed for the frequency range within the adjacent channels. The calculation is performed separately for the upper and lower adjacent channels, with a 1 MHz gap between the main channel and each corresponding adjacent channel.

After obtaining the incident and reflected average power for both adjacent channels, these values undergo the same calibration process as P_{out}. The adjacent channel power is then calculated using Equation 4.

CALIBRATION

Load-pull measurements involve multiple calibration steps before data collection, with specific procedures depending on the measurement setup. This work simplifies the calibration process, requiring only knowledge of the losses in the directional couplers and certain cables to calibrate power accurately.

Power Calibration

The first step is calibrating the power to deliver the desired power level to the DUT's input port. This involves adjusting the VSG's power level and correcting the measured power to compensate for any losses from the oscilloscope channels to the DUT's ports.

This setup requires characterizing the losses of the directional couplers and cables from the oscilloscope channels to the DUT's ports in advance. This is achieved using a power meter, spectrum analyzer or VNA. With these values, when a power measurement is taken, the losses must be accounted for by adding them to the measured power values. This enables the incident and reflected power to be determined at the DUT's ports rather than at the oscilloscope channels.

Subsequently, P_{in} and P_{out} are computed using Equations 3 and 4. This simplifies the process by avoiding the more complex task of correcting the time-domain waveforms. Power calibration becomes more straightforward by focusing solely on power levels and losses in the setup.

Since load-pull measurements involve varying Γ_L presented to the DUT, the strong dependence of Γ_{in} on Γ_L[7,25] can cause the measured input power to deviate significantly from the expected value due to a highly reflective Γ_{in} at certain Γ_L values. Consequently, when computing P_{in} using Equation 3, the measured P_{in} can be significantly smaller than expected. Although Γ_{in} was not explicitly computed, initial tests suggest that increases in reflected power affecting P_{in} match the theoretical dependence of Γ_{in} on Γ_L, see ***Equation 7***. So, in addition to the initial power calibration, an input power level adjustment sequence is implemented in the MATLAB code used for the measurements to resolve this issue.

$$\Gamma_{in} = S_{11} \frac{S_{12}S_{21}\Gamma_L}{1 - S_{22}\Gamma_L} \qquad (7)$$

The sequence involves measuring P_{in} and incrementally increasing the VSG's output power level until P_{in} reaches the expected value. This adjustment is performed for each tuner position, ensuring that every measurement is conducted with a consistent input power level at the DUT's input port, regardless of the DUT's Γ_{in}.

Reflection Coefficient Calibration

The raw Γ_L value is calibrated using the method outlined by Ferrero and Pisani,[22] which involves performing open-short-load (OSL) calibrations at different reference planes within the measurement setup. The first OSL calibration is carried out at the reference plane labeled as 1 in Figure 1a. A thru standard is then connected at Reference Plane 1 to perform an OSL calibration at Reference Plane 2 that is used only during a validation step in the calibration process.

Then, after connecting the directional couplers between Planes 2 and 3, an OSL calibration is conducted at Reference Plane 3 before connecting the tuner. All reference planes are indicated in Figure 1a. This process provides the necessary values to compute the calibrated Γ_L.

Finally, before starting the measurement, some Γ_L values are measured with the thru still connected at the DUT's ports to compare the measurement from the couplers at the input port (calibrated with the second OSL) with the measurements from the couplers at the output port (calibrated with equations from Ferrero and Pisani[22]). If the calibration is performed correctly, both Γ_L values should be equal for each tuner position.

When all calibration measurements are completed, the DUT is connected in place of the thru standard, and the measurements proceed without any additional disconnections in the setup. Additionally, a thru-reflect-line (TRL) calibration[26] is necessary to de-embed the effects of the transistor's test fixture.

EXPERIMENTAL RESULTS

The signal used for the measurements is an LTE-modulated signal with an average power of 5 dBm, a center frequency of 2 GHz and a bandwidth of 20 MHz. An ATF38143 GaAs FET biased with V_{GS}=-0.56 V and V_{DS}=3 V is used. The results are shown in ***Figures 4*** through ***9***, where the load-pull contours for P_{out}, G, η_d, PAE and both upper and lower ACPR are displayed on Smith charts generated using Focus Microwave's Contour Viewer software.

These results offer a more accurate representation of the DUT's performance when designing a PA intended to operate with modulated signals in its final application and provide the designer with the optimal Γ_L values needed to achieve the desired performance.

Analyzing the P_{out} and ACPR contours in Figures 4, 8 and 9 reveal that the Γ_L values for maximum P_{out} are located on the Smith chart far from those that achieve the best performance for both the upper and lower ACPR. The same applies to the G, η_d and PAE contours, where their optimal Γ_L values differ from those that provide the best ACPR performance. This information helps the designer choose the optimal Γ_L to balance efficiency and linearity for an amplifier operating with a modulated signal, enabling analysis of the tradeoff between these factors based on a specific application.

After performing the load-pull measurement, some Γ_L values are selected to repeat the measurement using spectrum analyzers (SAs). The incident and reflected output power levels at both the main and adjacent channels are measured to validate all power-related calculations from the load-pull measurements.

The validation requires disconnecting the cables from the oscilloscope's channels 3 and 4 and connect-

ing each to a Keysight N9010A spectrum analyzer. The results are shown in ***Table 1***. P_{out} of the main channel shows minimal difference between measurement approaches, indicating that the power calculations based on the measured voltage waveforms are accurate. However, power levels in the adjacent channels differ by up to 1.7 dB, impacting ACPR (see Table 1). These discrepancies are attributed to the oscilloscope's reduced dynamic range compared to the spectrum analyzer. According to the oscilloscope's data sheet,[27] the vertical resolution is 8 bits with averaging off and 12 bits with averaging on (used only for phase calculations), resulting in a theoretical dynamic range of approximately 48 dB and 72 dB, respectively. In practice, the oscilloscope's dynamic range is also influenced by the vertical scale selected for the measurement; a lower V/div setting reduces the maximum voltage that can be measured without clipping.

Also, the directional couplers that separate the incident and reflected

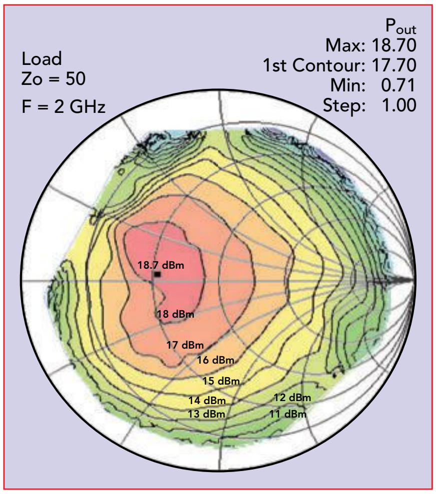

Fig. 4 Measured output power load-pull contours.

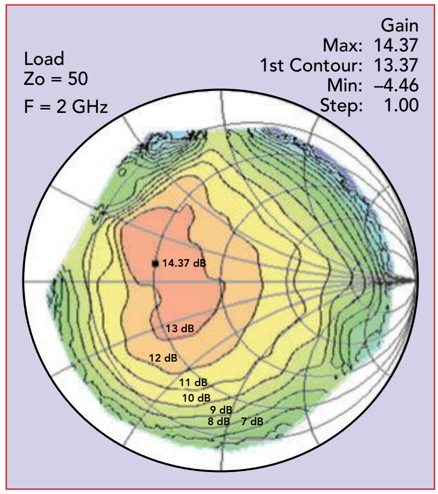

Fig. 5 Measured gain load-pull contours.

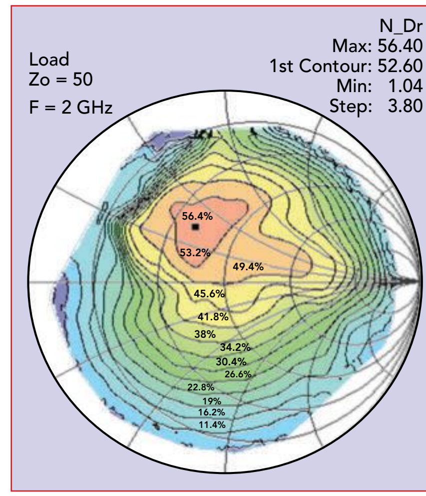

Fig. 6 Measured drain efficiency load-pull contours.

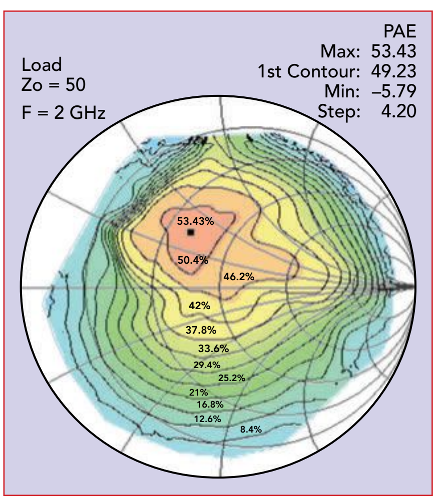

Fig. 7 Measured PAE load-pull contours.

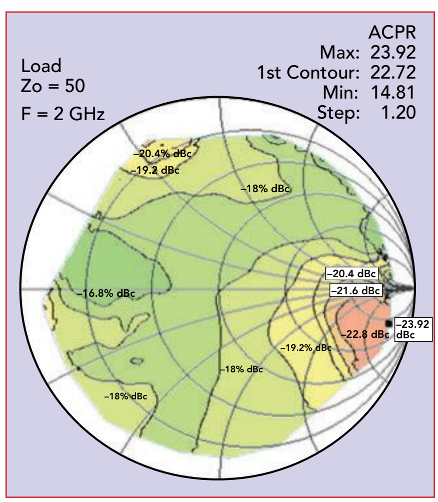

Fig. 8 Measured upper ACPR load-pull contours. ACPR values are negative and expressed in dBc.

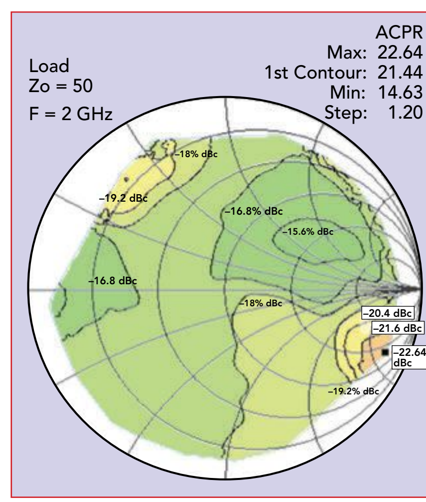

Fig. 9 Measured lower ACPR load-pull contours. ACPR values are negative and expressed in dBc.

TABLE 1

COMPARISON OF POWER MEASUREMENTS FROM AN OSCILLOSCOPE AND A SPECTRUM ANALYZER

Γ_L	P_{in} (dBm)	P_{out}(Scope) (dBm)	P_{out}(SA) (dBm)	$APCR_{lower}$(Scope) (dBc)	$APCR_{lower}$(SA) (dBc)	$APCR_{upper}$(Scope) (dBc)	$APCR_{upper}$(SA) (dBc)
0.31∠174°	4.8	18.7	18.6	-17.4	-15.8	-16.3	-15.0
0.32∠116°	5.1	17.9	17.6	-17.2	-15.6	-17.4	-15.9
0.88∠-22°	4.9	8.7	7.8	-22.6	-22.0	-23.2	-22.2
0.23∠-164°	5.1	18.0	18.0	-17.1	-15.6	-17.3	-15.9
0.16∠173°	5.1	18.2	18.2	-17.4	-15.7	-17.2	-15.7

C-Band 900 kW Crossed-Field Amplifier VXC1659

CPI Electron Device Business - Crossed-Field Amplifier

With a history of producing high quality products, we can help you with your CFA.

Contact us at ElectronDevices@cpi-edb.com or at call us at +1 978-922-6000.

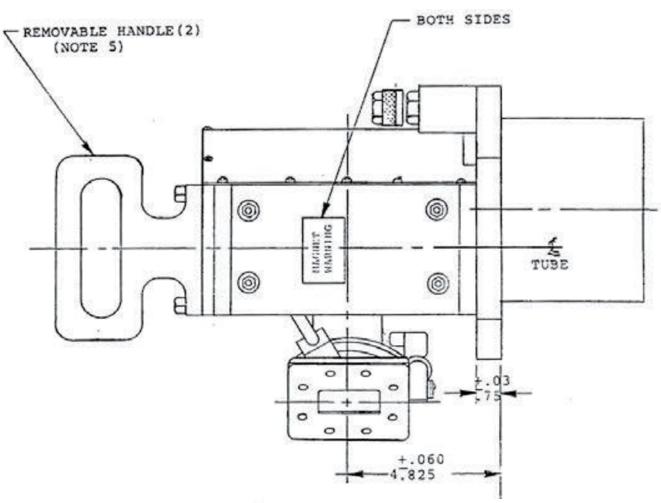

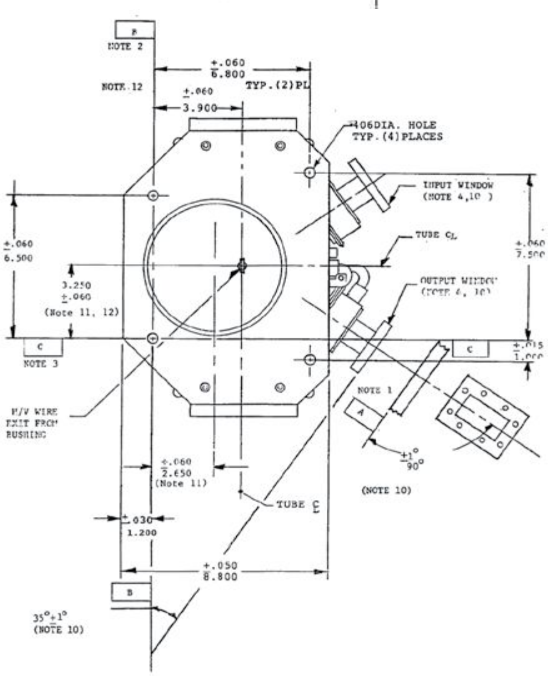

FEATURES:

- Frequency: 5.4 - 5.9 GHz
- Peak Power: 900 kW
- Duty Cycle: 0.005
- Pulsewidth: 50 µSec
- Anode voltage 30 kV
- Cold cathode
- Water cooled
- Cathode pulsed

BENEFITS:

- High peak power
- Wide bandwidth

APPLICATIONS:

- Ground based radar

CPI Electron Device Business

Beverly Microwave Division
150 Sohier Road
Beverly, Massachusetts
USA 01915

tel +1 978-922-6000
email ElectronDevices@cpi-edb.com
fax +1 978-922-8914
web www.cpi-edb.com

For more detailed information, please refer to the corresponding CPI EDB technical description if one has been published, or contact CPI EDB. Specifications may change without notice as a result of additional data or product refinement. Please contact CPI EDB before using this information for system design.

waves have a coupling factor of approximately 35 dB, consequently attenuating the measured waves by 35 dB. This makes it more challenging to accurately measure lower power levels, such as those in the adjacent channels. This technique could benefit from using directional couplers with a lower coupling factor to overcome the disadvantage of an oscilloscope's reduced dynamic range compared with equipment like a spectrum analyzer. Another option to improve dynamic range is to implement a statistical averaging technique.[28]

CONCLUSION

Load-pull measurements are performed with modulated signals using an oscilloscope, removing the need for complex equipment like an LSNA, NVNA or VNA. The proposed approach streamlines the calibration process by eliminating the need for prior tuner characterization, waveform corrections and a comb generator for phase reference. It provides accurate load-pull contours for output power, gain, drain efficiency, PAE and ACPR. Additionally, this work includes all the necessary details for setting up the measurement system and assembling the test bench. Experimental validation with an ATF38143 GaAs FET demonstrates the effectiveness of this method in optimizing the efficiency-linearity tradeoff in power amplifier design. ■

References

1. L. Angrisani, "Experimental Assessment of Modulated S-parameters Reliability in Modeling and Testing Wideband Radio Frequency Amplifiers," *IEEE Transactions on Instrumentation and Measurement*, Vol. 55, No. 5, October 2006, pp. 1474–1479.
2. S. A. K. Kahil, S. Laurent, R. Quéré, J. Sombrin, D. Floriot, V. Brunel and C. Teyssandier, "Linearity Characterization of GaN HEMT Technologies Through Innovative on-Wafer Multi-Tone Load-Pull Measurements," *11th European Microwave Integrated Circuits Conference*, October 2016.
3. J. Martin, M. Moldovan, C. Baylis, R. J. Marks, L. Cohen and J. de Graaf, "Radar Chirp Waveform Selection and Circuit Optimization Using ACPR Load-Pull Measurements," *IEEE Wireless and Microwave Technology Conference*, April 2012.
4. X. Konstantinou, J. D. Albrecht and J. Papapolymerou, "Using Active Load-Pull with Modulated Signals to Optimize Power and Linearity," *94th ARFTG Microwave Measurement Symposium*, January 2020.
5. M. Marchetti, G. Avolio, M. Squillante, A. K. Doggalli and B. Anteverta-Mw, "Wideband Load Pull Measurement Techniques: Architecture, Accuracy and Applications," *92nd ARFTG Microwave Measurement Conference*, January 2019.
6. S. Alsahali, D. Gecan, A. Alt, G. Wang, S. M. H. Syed Anera, P. Chen, S. Woodington, A. Sheikh, P. Tasker and J. Lees, "A Novel Modulated Rapid Load Pull System with Digital Pre-Distortion Capabilities," *93rd ARFTG Microwave Measurement Conference*, June 2019.
7. P. Ghanipour, S. Stapleton and J. -H. Kim, "Load–Pull Characterization Using Different Digitally Modulated Stimuli," *IEEE Microwave and Wireless Components Letters*, Vol. 17, No. 5, May 2007, pp. 400–402.
8. J. Verspecht, A. Stav, T. Nielsen and S. Kusano, "The Vector Component Analyzer: A New Way to Characterize Distortions of Modulated Signals in High-Frequency Active Devices," *IEEE Microwave Magazine*, Vol. 23, No. 12, December 2022, pp. 86–96.
9. J. Benedikt, R. Gaddi, P. Tasker, M. Goss and M. Zadeh, "High Power Time Domain Measurement System with Active Harmonic Load-Pull for High Efficiency Base Station Amplifier Design," *IEEE MTTS International Microwave Symposium Digest*, Vol. 3, June 2000, pp. 1459–1462.
10. V. Teppati, S. Pinarello, A. Ferrero and J. -E. Mueller, "An Unconventional VNA-based Time-Domain Waveform Load-Pull Test

NEW

4x4 High Accuracy Beamforming Network

24~43GHz 18~40GHz

6~18GHz 2.4~7.25GHz

- **Covering Multiple Microwave Bands.** (Such as S, C, X, Ku, K & Ka bands.)
- **Excellent Phase Accuracy, Amplitude Unbalance.**
- **Low VSWR / Low Insertion Loss / High Isolation.**
- **Good Stability & Repeatability.**

P/N	Freq. Range (GHz)	VSWR Max. (:1)	Insertion Loss* Max. (dB)	Amplitude Unbal. Max. (dB)	Amplitude Flatness Max. (dB)	Phase Accuracy Max. (Deg.)	Isolation Min. (dB)	Any Given Bandwidth within Freq. Range (MHz)	Phase Accuracy Max. (Deg.)
SA-07-4B020080	2.4~2.5	1.4	7.3	±0.5	±0.3	±4	14	100	±5
	5.18~5.83	1.5	7.7	±0.6	±0.4	±5	13		
	5.9~7.25	1.5	7.8	±0.7	±0.5	±6	13		
SA-07-4B060180	6~18	1.8	9.5	±1.1	±1.4	±12	12	100	±8
SA-07-4B180400	18~40	2.0	12.0	±1.2	±2.0	±15	10	200	±8
								400	±10
SA-07-4B240430	24~43	2.0	12.4	±1.2	±2.0	±15	10	200	±8
								400	±10

*Theoretical 6dB Included

— Typical Test Curve** —

2.4~7.25GHz 6~18GHz 18~40GHz 24~43GHz

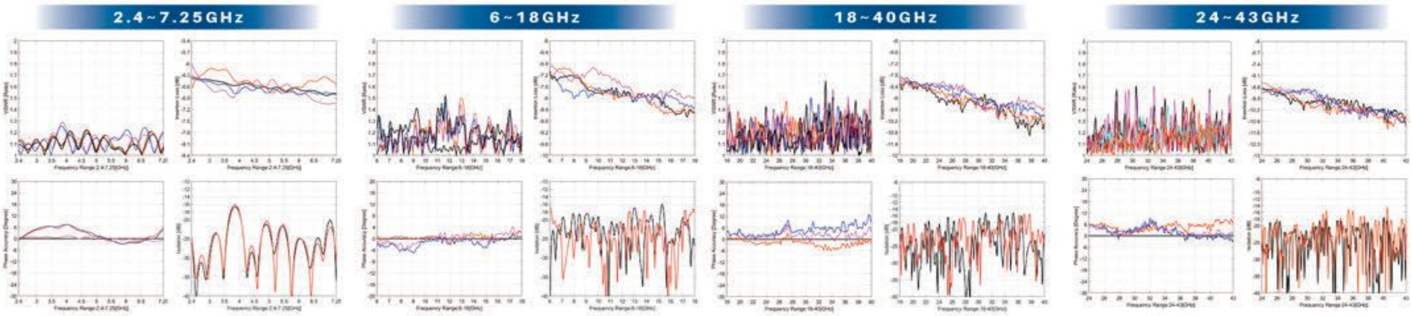

**Corresponding Channels: A1B1、A1B2、A1B3、A1B4

More Information-Scan the QR Code

MIcable Inc.

www.micable.cn sales@micable.cn +86-591-87382856

Bench," *Asia-Pacific Microwave Conference*, December 2010.

11. V. Teppati, A. Ferrero, M. Garelli and S. Bonino, "A Comprehensive Mixed-Mode Time-Domain Load- and Source-Pull Measurement System," *IEEE Transactions on Instrumentation and Measurement*, Vol. 59, No. 3, March 2010, pp. 616–622.
12. F. De Groote, J. -P. Teyssier, J. Verspecht and J. Faraj, "High Power on-Wafer Capabilities of a Time Domain Load-Pull Setup," *71st ARFTG Microwave Measurement Conference*, June 2008.
13. F. De Groote, P. Roblin, Y. -S. Ko, C. -K. Yang, S. J. Doo, M. V. Bossche and J. -P. Teyssier, "Pulsed Multi-Tone Measurements for Time Domain Load Pull Characterizations of Power Transistors," *73rd ARFTG Microwave Measurement Conference*, June 2009.
14. F. De Groote, O. Jardel, J. -P. Teyssier, T. Gasseling, J. Verspecht, V. Mallette and C. Tsironis, "On-Wafer Time Domain Load-Pull Optimization of Transistor Load Cycle with the New Multi-Harmonic MPT Tuner," *69th ARFTG Conference*, June 2007.
15. I. Volokhine, "An Extension of Existing Real-Time Load Pull Systems to Perform Voltage/Current Waveform Reconstruction," *71st ARFTG Microwave Measurement Conference*, June 2008.
16. M. Molina-Ceseña, J. A. Reynoso-Hernández, M. A. Pulido-Gaytán, J. R. Loo-Yau and M. C. Maya-Sánchez, "Experimental Investigation of Resistive-Reactive Class-J Mode Using Time-Domain Low-Frequency Active Harmonic Load-Pull Measurements," *IEEE Microwave and Wireless Components Letters*, Vol. 32, No. 1, January 2022, pp. 96–99.
17. D. F. Williams, K. A. Remley, J. M. Gering, G. S. Lyons, C. Lineberry and G. S. Aivazian, "Comparison of Large-Signal-Network-Analyzer Calibrations," *IEEE Microwave and Wireless Components Letters*, Vol. 20, No. 2, February 2010, pp. 118–120.
18. S. Gustafsson, M. Thorsell, J. Stenarson and C. Fager, "An Oscilloscope Correction Method for Vector-Corrected RF Measurements," *IEEE Transactions on Instrumentation and Measurement*, Vol. 64, No. 9, September 2015, pp. 2541–2547.
19. J. Scott, P. Blockley and A. Parker, "A New Instrument Architecture for Millimetre-Wave Time-Domain Signal Analysis," *ARFTG 63rd Conference*, June 2004.
20. M. Lindquist, P. Roblin and N. C. Miller, "New Real-Time Pulsed-RF NVNA Testbed for Isothermal Characterization of Traps in GaN HEMTS," *IEEE/MTT-S International Microwave Symposium*, June 2023.
21. M. Lindquist and P. Roblin, "Calibration of an Oscilloscope-Based NVNA for Periodic Modulated Signals," *103rd ARFTG Microwave Measurement Conference*, June 2024.
22. A. Ferrero and U. Pisani, "An Improved Calibration Technique for on Wafer Large-Signal Transistor Characterization," *IEEE Transactions on Instrumentation and Measurement*, Vol. 42, No. 2, April 1993, pp. 360–364.
23. A. Villagran-Gutierrez, J. R. Loo-Yau, E. A. Hernández-Domínguez, B. E. Figueroa-Reséndiz, P. Moreno and J. A. Reynoso-Hernández, "A Time-Domain Vector Network Analyzer Suitable to Characterize Passive and Active Devices," *IEEE MTT-S Latin America Microwave Conference*, December 2023.
24. J. Webster and H. Eren, "Measurement, Instrumentation, and Sensors Handbook: Electromagnetic, Optical, Radiation, Chemical, and Biomedical Measurement," *CRC Press*, 2017.
25. G. Gonzalez, "Microwave Transistor Amplifiers: Analysis and Design," *Prentice Hall*, 1997.
26. G. Engen and C. Hoer, "Thru-Reflect-Line: An Improved Technique for Calibrating the Dual Six-Port Automatic Network Analyzer," *IEEE Transactions on Microwave Theory and Techniques*, Vol. 27, No. 12, December 1979, pp. 987–993.
27. Infinium 90000 Series Oscilloscopes, Data Sheet, Keysight Technologies, Web: https://www.keysight.com/us/en/assets/7018-01734/data-sheets-archived/5989-7819.pdf.
28. C. Fager and K. Andersson, "Improvement of Oscilloscope Based RF Measurements by Statistical Averaging Techniques," *IEEE MTT-S International Microwave Symposium*, June 2006.

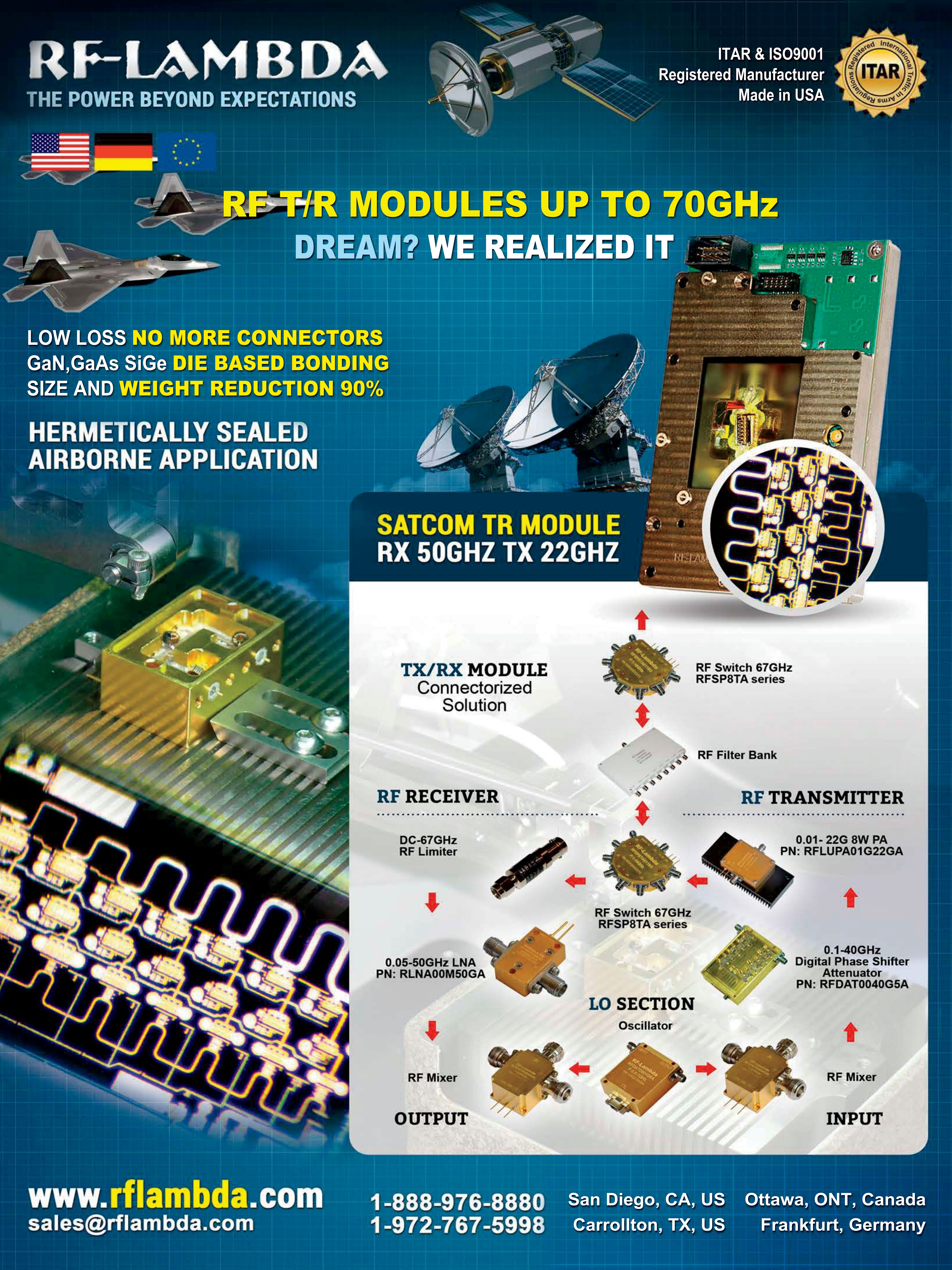

RF-LAMBDA
THE POWER BEYOND EXPECTATIONS
ITAR & ISO9001
Registered Manufacturer
Made in USA
ITAR
Registered International Traffic in Arms Regulations
RF T/R MODULES UP TO 70GHz
DREAM? WE REALIZED IT
LOW LOSS NO MORE CONNECTORS
GaN,GaAs SiGe DIE BASED BONDING
SIZE AND WEIGHT REDUCTION 90%
HERMETICALLY SEALED
AIRBORNE APPLICATION
SATCOM TR MODULE
RX 50GHZ TX 22GHZ
TX/RX MODULE
Connectorized
Solution
RF Switch 67GHz
RFSP8TA series
RF Filter Bank
RF RECEIVER
RF TRANSMITTER
DC-67GHz
RF Limiter
0.01- 22G 8W PA
PN: RFLUPA01G22GA
RF Switch 67GHz
RFSP8TA series
0.05-50GHz LNA
PN: RLNA00M50GA
0.1-40GHz
Digital Phase Shifter
Attenuator
PN: RFDAT0040G5A
LO SECTION
Oscillator
RF Mixer
RF Mixer
OUTPUT
INPUT
www.rflambda.com
sales@rflambda.com
1-888-976-8880
1-972-767-5998
San Diego, CA, US
Carrollton, TX, US
Ottawa, ONT, Canada
Frankfurt, Germany

RS103 Testing Pushes Boundaries in Military Markets

ETS-Lindgren
Cedar Park, Texas

In the world of military and aerospace electronics, compliance testing is not just a box to check; it is a matter of mission success and safety. Among the many procedures outlined in MIL-STD-461, one stands out for its rigor: RS103, the radiated susceptibility test. For systems that must withstand 200 V/m field strength, RS103 represents a formidable challenge. Within this procedure, the frequency range of 30 to 200 MHz has long been a thorn in the side of engineers and test labs.

THE PAIN POINT OF BICONICAL ANTENNAS IN HIGH-FIELD TESTING

Traditionally, the solution has been the biconical antenna, a legacy design that has served the industry for decades. Yet when pushed into high-field territory, its shortcomings become clear. Engineers face high voltage standing wave ratios (VSWR), unpredictable radiation patterns and excessive harmonic emissions. In fact, it is not unusual for harmonics to exceed the fundamental signal, undermining the integrity of the test.

Dimensional constraints add to the frustration. MIL-STD specifies that the receive biconical antenna should measure 137 centimeters overall. While this requirement does not apply to radiated susceptibility, many labs prefer to use a single antenna for both emissions and susceptibility testing. That means the balun must remain small enough to fit emissions requirements, limiting its ability to handle the power needed for RS103. The result is an antenna that cannot reliably generate 200 V/m at one meter or greater distances without being oversized and prohibitively expensive.

The inefficiency of the biconical antenna also creates standing waves in the test chamber, a dangerous condition for sensitive amplifiers and other test equipment. For facilities tasked with high-field testing, these limitations translate into risk, cost and wasted time.

SOLVING THE BICONICAL ANTENNA PROBLEM

The industry has reached a point where a new ap-

Fig. 1 **Model 3170 Intell-I-Tune™ Antenna System.**

proach is not just desirable, it is essential. To achieve the required field strength without jeopardizing amplifiers or test components, engineers need an antenna that can adapt dynamically to frequency changes, reduce standing waves, suppress harmonics and maintain a low VSWR. In short, the solution must be smarter, more efficient and more reliable than the traditional biconical antenna.

DIRECTED DIPOLE / YAGI ANTENNA APPROACH

Enter the Yagi-style antenna with tunable dipole elements, a design that reimagines low frequency testing as shown in ***Figure 1***. Unlike fixed-length antennas, which are inherently narrowband and power hungry, a tunable dipole system can adjust itself to the environment. Stepper motors, guided by precise algorithms, alter dipole lengths for each frequency and polarization. This ensures true resonance across the band and keeps VSWR below 3:1—often closer to 1.5:1—providing a clean, efficient signal path.

Harmonic emissions can be reduced by more than 25 dB, delivering a cleaner signal and eliminating the need to overdrive amplifiers. Because the antenna operates at the fundamental frequency, smaller and less costly amplifiers can be used without sacrificing compliance. This reduces system complexity and lowers overall cost.

Automation adds another layer of value. Once tuning files are stored, the antenna automatically adjusts to the correct configuration, eliminating manual intervention. This hands-free operation increases throughput, minimizes human error and ensures repeatable results. For busy test labs, the ability to streamline operations while maintaining accuracy is key.

OPTIMIZED ANTENNA TEST SOLUTION

Low frequency testing has always demanded a different approach than microwave or high frequency ranges. A tunable, automated antenna system addresses these unique needs by offering multiple configurations, maintaining low VSWR and delivering consistent performance. The result is higher throughput, improved efficiency and greater confidence in test outcomes.

TABLE 1

ELECTRICAL AND PHYSICAL TECHNICAL SPECIFICATIONS OF MODEL 3170

Technical Specifications	
Electrical	
Frequency Minimum	30 MHz
Frequency Maximum	200 MHz
Impedance (Nominal)	50 Ω
Maximum Continuous Power	2500 W
Peak Power	3500 W
Pattern Type	Directed Dipole
Polarization	Single (Vertical or Horizontal)
VSWR (Average)	1.5:1
Connectors	7/16 in. DIN for RF and DB25 for I/O Control
Physical	
Antenna Height	12.5 cm (4.9 in.)
Antenna Width	276.9 cm (109.1 in.)
Antenna Depth	101.7 cm (40.0 in.)
Antenna Weight	15.9 kg (35.0 lb.)

Such a solution is particularly valuable for government and contractor-run military EMC labs, aerospace OEMs, Tier 1 suppliers, commercial EMC facilities and industrial electronics environments. These organizations operate under intense pressure to meet compliance standards while managing costs and timelines. A smarter antenna system helps them achieve both.

INTELL-I-TUNE™ ANTENNA SYSTEM

Recognizing the need for innovation, ETS-Lindgren has introduced the Model 3170 Intell-I-Tune™ Antenna System. Designed to replace the traditional biconical antenna, the Intell-I-Tune system integrates tunable dipole technology with automated control. It delivers the performance required for RS103 testing while reducing strain on amplifiers and improving overall efficiency. ***Table 1*** shows the technical specifications, including electrical and physical characteristics.

For facilities facing the challenges of RS103, the Intell-I-Tune system represents a practical, forward-looking solution. It embodies the shift from legacy designs to smarter, adaptive technologies that meet the demands of modern military and aerospace testing.

ETS-Lindgren
Cedar Park, Texas
www.ets-lindgren.com

ProductFeature

Next-Generation VNA Extenders Covering 50 to 330 GHz

Eravant (formerly Sage Millimeter Inc.)
Torrance, Calif.

Increasing applications of mmWave technology are driving demand for higher frequency testing. With 3GPP frequency range 2 spectrum now extended up to 71 GHz, and 6G research exploring frequencies up to 175 GHz and beyond into the sub-THz range, there is a growing need for band-specific measurements such as over-the-air (OTA) characterization, antenna pattern measurement and S-parameter testing of components. The increasing development of mmWave and sub-THz application-specific integrated circuits has further intensified the demand for probe testing and on-wafer measurements. Applications such as E-Band automotive radar (76 to 81 GHz), satellite communication links from 71 to 86 GHz, wireless backhaul and fixed-wireless access in urban networks that leverage the E-Band demonstrate a growing need for mmWave band-specific testing.

Since the majority of commercially available vector network analyzers (VNAs) typically operate up to a maximum frequency of 50 GHz, frequency extension modules are essential for characterizing devices beyond the instrument's native range. A pair of VNA frequency extender transceiver modules enables full two-port S-parameter measurements. As shown schematically in ***Figure 1***, each extender transceiver (Tx/Rx) receives a local oscillator (LO) input from the VNA, which is split into two channels to drive individual receivers. The transmit path multiplies the VNA test-port signal to the target mmWave frequency, while a fixed offset between the two VNA ports generates a constant intermediate frequency (IF). The forward-coupled transmit signal provides an IF reference back to the VNA for amplitude and phase calibration, and the measurement receiver returns an IF signal representing the device under test (DUT) response. When used as a calibrated pair, these transceiver modules enable measurement of all four S-parameters across extended mmWave and sub-THz fre-

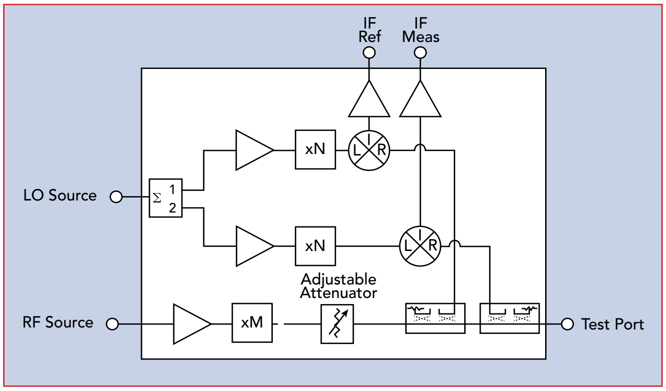

▲ Fig. 1 **Typical architecture of Tx/Rx VNA frequency extender.**

Fig. 2 **WR-10 ACCESS extender set with and without adjustable attenuators.**

quency bands.

Over the past few years, Eravant has successfully demonstrated its first-generation VNA extenders, designed with in-house discrete off-the-shelf components and covering the 20 to 330 GHz frequency range. Building on this foundation and responding to the expanding mmWave application landscape, the focus for the next generation extender line shifted toward performance optimization and manufacturing efficiency. To achieve this, Eravant developed proprietary integrated circuits that replaced various building blocks in RF assemblies with only a few integrated multifunction components. This design-for-manufacturing initiative led to the creation of the ACCESS Series VNA Extenders, as shown in *Figure 2*.

The result was a reduction in material and labor costs, streamlined assembly and a lighter supply chain load. This effort also delivered measurable technical performance improvements. The new proprietary chipsets underwent extensive qualification to ensure long-term reliability, amplitude stability and phase stability. ACCESS series extender heads maintain stable temperature over prolonged usage, which ensures long-term repeatable measurement without frequent recalibration. Furthermore, the ACCESS extenders for V-, E- and W-Bands provide up to 15 percent wider frequency coverage than their predecessors, which only cover the full waveguide bandwidth. Mechanical refinements, including a length reduction from 11.5 to 8 in. and a weight reduction from 4.4 to 2.8 lb., make these extenders ideal for space-constrained setups, such as gimbal-mounted OTA chambers and on-wafer probe testing.

Table 1 shows the complete lineup of base ACCESS series VNA extenders. The -CM-E2 versions include an optional adjustable-level attenuator that provides up to 30 dB of output power control, making it valuable for testing input-power-sensitive devices such as LNAs and power amplifiers. Each extender module includes 1 in. and 2.5 in. waveguide straight sections featuring Eravant's Proxi-Flange™ contactless interface. By incorporating this flange section, setup and calibration time for two-port calibrations, such as short-open-load-thru and thru-reflect-line, can be reduced significantly because there is no need

TABLE 1

ACCESS VNA EXTENDER, BASE VERSION LINEUP

Model	RF Port	Frequency (GHz)	Dynamic Range (dB)	Output Power (dBm)
STO-1520313-C-E2 STO-1520313-CM-E2	WR-15	45 to 80	120	13
STO-1220313-C-E2 STO-1220313-CM-E2	WR-12	55 to 95	120	13
STO-1020307-C-E2 STO-1020307-CM-E2	WR-10	67 to 116	120	7
STO-08203N05-C-E2 STO-08203N05-CM-E2	WR-08	90 to 140	100	-5
STO-06203N05-C-E2 STO-06203N05-CM-E2	WR-06	110 to 170	100	-5
STO-05203N05-C-E2 STO-05203N05-CM-E2	WR-05	140 to 220	90	-5
STO-03203N12-C-E2 STO-03203N12-CM-E2	WR-03	220 to 330	90	-12

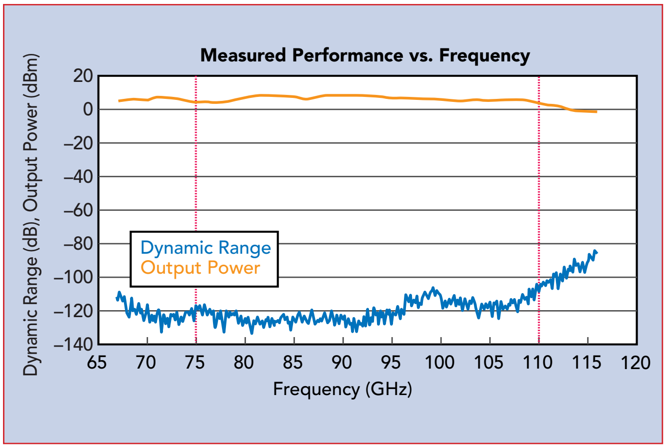

Fig. 3 **ACCESS VNA Extender's measured dynamic range and output power.**

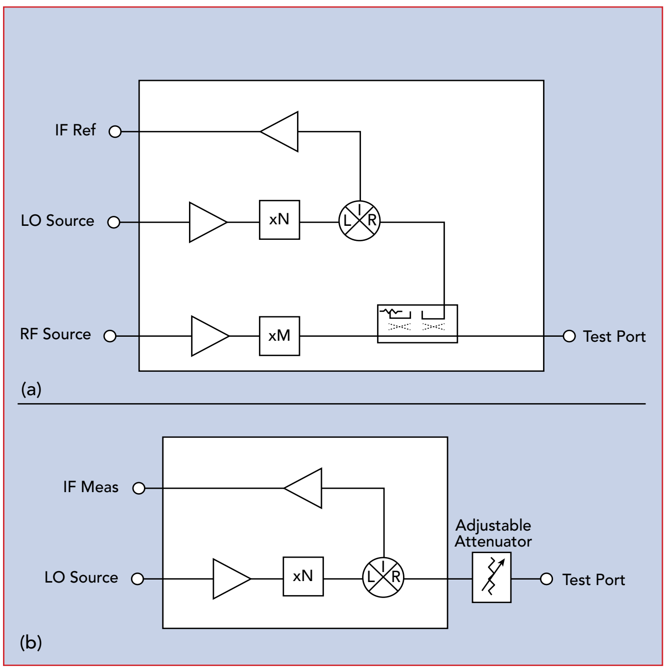

Fig. 4 **Miniature extender architecture, Tx/Ref (a) and Rx (b).**

to manually tighten waveguide screws and worry about flange misalignment. This feature also improves measurement repeatability and reliability as the screwless measurements prevent the risk of cross-threading and mechanical wear that could potentially compromise calibration accuracy at mmWave and sub-THz frequencies. Each extender ships with a test report including measurements like test port output power, dynamic range and calibration certificate, ensuring full specification compliance. These reports are stored in a USB memory which can be accessed via the USB-C port provided on the rear panel of the extender head. Performance of the WR-10 ACCESS VNA extender over 67 to 116 GHz is shown in *Figure 3*.

Compact form-factor of the ACCESS series extenders can be further tailored for OTA testing applications, where one-directional measurement, such as gain and radiation pattern characterization, does not require full-duplex extender heads. A miniaturized set consisting of a transmit reference (Tx/Ref) module and a receive (Rx) module can be developed simply by reducing the number of components in the current ACCESS extender RF chain, as illustrated in *Figure 4*. This further reduction in size and weight enables easier integration on gimbals while preserving the gimbal's payload capacity for the DUT, which makes this configuration ideal for open-bed mmWave compact antenna test range (CATR) setups. *Figure 5* shows the VNA extender setup measuring 110 to 170 GHz using open-bed CATR.

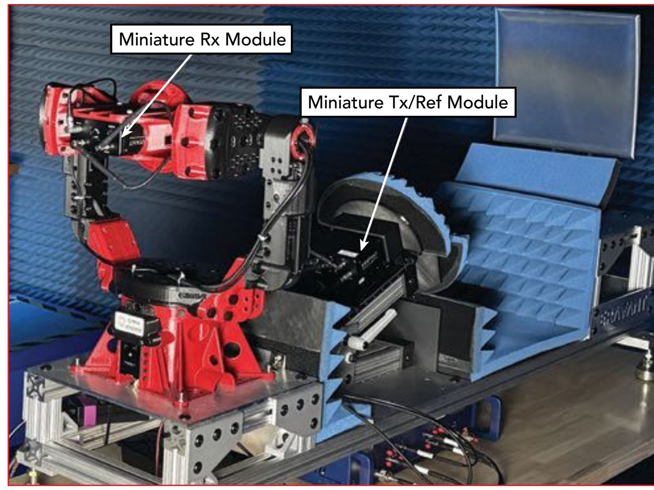

Fig. 5 **VNA extender setup using open-bed CATR.**

While passive component testing generally requires only moderate output power, many advanced applications demand VNA extenders with higher test port power to overcome signal loss and enable accurate characterization. High-output extenders are useful for applications such as on-wafer measurements, OTA antenna testing and sub-THz material characterization, where path losses and setup attenuation dictate stronger test port output power in order to maintain sufficient drive power and dynamic range. In the future, current base ACCESS extenders can be upgraded with high test port output power by adding a power amplification stage on the transmit path.

The Next Generation ACCESS Series VNA Extenders feature a compact, high performance and thermally stable architecture designed with cost efficiency in mind. This initiative aims to reduce the traditional barriers to entry in mmWave developments. As demand for higher frequency characterization continues to expand across 6G, automotive radar, satellite communications and other emerging applications, Eravant's ACCESS platform reflects the company's mission to make mmWave technology more accessible, empowering engineers and innovators to advance the next generation of high frequency systems.

Eravant (formerly Sage Millimeter Inc.)
Torrance, Calif.
www.eravant.com

VENDORVIEW

Enabling Spectrum Dominance with Phase Coherent Receivers

Signal Hound
Battle Ground, Wash.

The electromagnetic spectrum has become a highly congested environment, creating challenges for various mission-critical operations. Government, military and even critical infrastructure protection depend on clear insight into what signals are present, how they behave and how to respond effectively. Traditional spectrum monitoring provides part of this picture, but it often lacks the precision needed to act decisively in dynamic and cluttered RF environments.

This is where the value of phase coherent receivers (PCRs) becomes apparent. By aligning multiple receiver channels to a common local oscillator (LO) or reference clock, PCRs preserve stable phase relationships across signals. This coherence unlocks a set of capabilities that extend far beyond simple detection. PCRs enable electromagnetic spectrum awareness and spectrum dominance applications, empowering operators to detect hidden signals, manage interference and maintain control of the spectrum.

SPECTRUM AWARENESS

Spectrum awareness is the foundation of electromagnetic operations. It refers to the ability to detect, identify and characterize signals across a region of interest. A PCR, such as Signal Hound's new PCR4200, enhances this awareness, building a clear picture of the spectrum in several key ways.

Multi-Signal Characterization

Standard receivers measure power and frequency. A PCR adds the ability to analyze relative phase, allowing operators to differentiate overlapping signals, spot subtle modulations and separate friendly transmissions from interference or malicious activity.

Reliable Coherent I/Q Capture

PCRs deliver calibrated I/Q data that is phase-aligned across channels. This makes the data useful for post-process analysis, machine learning or forensic investigations, because signals can be correlated with high confidence across different antennas or monitoring nodes. ***Figure 1*** shows Signal Hound's proprietary Spike software displaying I/Q versus time, as well as a spectrum plot, channel power, FM versus time, waterfall chart and AM versus time.

Detection of Low Probability of Intercept (LPI) Signals

LPI waveforms, burst transmissions and frequency-hopping signals are increasingly common in both commercial and military systems. PCRs, with their high sweep speeds and coherent capture, provide the fidelity needed to detect these fleeting signals and tie them to broader RF patterns.

Creating Multi-Node Coherent Networks for RF Monitoring

On a local scale, PCRs can be daisy-chained across a

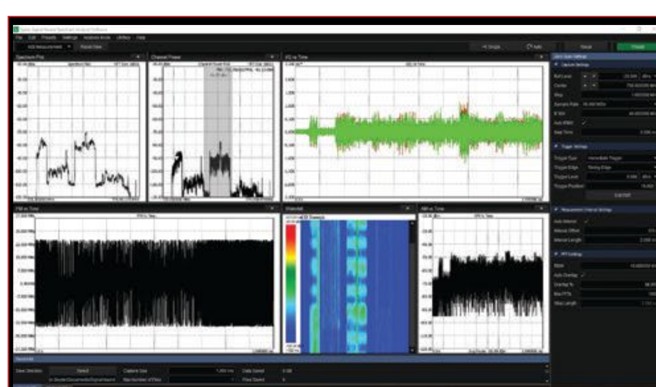

Fig. 1 **Signal Hound's proprietary Spike software display.**

Fig. 2 **Signal Hound's new PCR4200 phase coherent receiver.**

building or campus to create a coherent monitoring grid. This enables continuous spectrum awareness for facilities where sensitive information or operations must be protected. For instance, up to four Signal Hound PCR4200 PCRs can be connected, enabling up to 16 phase coherent channels. This type of broad, coherent monitoring grid means unauthorized signals, rogue base stations or hidden transmitters can be identified by their RF footprints, even if they attempt to blend into normal background activity.

SPECTRUM DOMINANCE

Once awareness is achieved, the next step is spectrum dominance, the ability to shape or control the electromagnetic environment to support friendly operations and deny advantages to adversaries. Phase coherence is central to many advanced dominance techniques. *Figure 2* shows Signal Hound's PCR4200 phase coherent receiver.

Adaptive Electronic Warfare Countermeasures

PCRs provide the phase-accurate data needed to inform adaptive jamming or deception systems. Instead of blanket interference, which risks disrupting friendly signals, PCR-enabled systems can surgically target hostile transmissions while preserving the rest of the spectrum.

Beamforming and Null Steering

By maintaining stable phase relationships, PCRs enable transmitters or transceivers to perform advanced beamforming — directing energy where it is needed and creating nulls where protection is required. This ensures communications or radar systems remain functional even in dense interference environments.

Cognitive Spectrum Operations

The future of spectrum control lies in cognitive electromagnetic spectrum operations, where AI and machine learning dynamically allocate spectrum resources and adapt to new threats in real-time. PCRs provide coherent, high-fidelity data that these algorithms require to make accurate decisions quickly.

Distributed Awareness and Control

Multiple PCRs, synchronized via GPS or high-stability clocks, can be deployed across wide areas. These distributed networks deliver a coherent, wide-angle view of the RF environment, supporting collaborative operations and real-time spectrum management.

SIGNAL HOUND'S PCR4200 PHASE COHERENT RECEIVER

Signal Hound recently launched the PCR4200, a new versatile, four-channel receiver that operates from 45 MHz to 20 GHz and streams 40 MHz of bandwidth per channel over 10 GbE SFP+. It can sweep independently tuned channels at up to 200 GHz per second to capture any signal of interest within the bandwidth. Each channel on the PCR4200 may be configured as a phase coherent channel using the high performance shared LO or independently tuned using that channel's dedicated LO. Other features include a built-in 30 MHz to 20 GHz vector signal generator to simplify system alignment and calibration, and an internal GPS to provide precise time, frequency and location.

This receiver expands its functional capacities with the included PCR Series API, allowing the device to integrate with multiple third-party software applications. At just 16 lbs. and measuring 12 × 11.5 × 3 in., this innovative new product offers a combination of precision and power in a portable form factor that is equally suited to the benchtop, lab or out in the field. *Figure 3* shows an example of the PCR4200 phase coherent receiver connected to a PC and using the Spike software.

Fig. 3 **PCR4200 connected to a PC and using Spike software.**

WHY PCRS ARE ESSENTIAL FOR THE FUTURE

The electromagnetic spectrum is a contested and strategic resource. PCRs transform spectrum monitoring into actionable data analysis. They empower operators to see deeper into the spectrum, detect signals that evade conventional monitoring and act decisively to maintain visibility and control. As the spectrum becomes more contested, PCR-enabled spectrum awareness and dominance will define the future of secure operations, from protecting facilities to ensuring mission success in the most demanding environments.

Versatility, performance and precision; the PCR4200 delivers fast sweep speeds, dynamic range and ultra-low phase noise to ensure sweeps, data and accuracy are of the highest quality. Independently configurable channels, flexibility in diverse signal environments and deep data analysis in a multi-channel monitoring configuration make the PCR4200 an ideal companion across a diverse range of scenarios.

Signal Hound
Battle Ground, Wash.
https://signalhound.com/

Radiation-Hardened Space-Based Power Systems

Designing a power system to support today's sensitive RF systems is a complex challenge, particularly in space-based applications. These systems are integral to satellite communications, remote sensing and navigation and demand an environment free from electromagnetic interference and noise. These specifications add further complexity to power system design.

The need to provide clean and stable power poses one of the primary challenges. Power supplies inherently generate parasitic noise and ripple, which can couple into RF circuits, degrading their signal integrity and overall performance. In the vacuum of space, conventional grounding and shielding techniques are less effective, necessitating solutions such as differential signaling, advanced filtering and meticulous circuit layout to contain stray emissions.

A further obstacle is the harsh space environment, where power systems must withstand extreme temperatures, radiation and the absence of convection cooling. Components face threats such as radiation-induced upsets, latch-ups and long-term degradation, requiring the use of radiation-hardened parts and system redundancy for resilience. Weight and efficiency are also crucial, so spacecraft have strict mass and power limitations.

Infineon has over 50 years of experience with rad-hard RF and power systems. Its family of rad-hard R9 MOSFETs uses a superjunction design architecture and patented hermetic ceramic packaging, making it more resilient to radiation effects while maintaining efficiency. More recently, Infineon released the first internally fabricated, rad-hard GaN transistor to obtain DLA certification. Combining the inherently radiation-resistant qualities of GaN with Infineon's circuit design, they are paving the way for more efficient and reliable power systems in space.

International Rectifier HiRel Products, Inc., an Infineon Technologies Company
Andover, Mass.
www.infineon.com/products/high-reliability/space

Sub-1 GHz Wideband Power Amplifier

Demand for long-range, portable wireless communication is growing across markets such as public safety radios, smart utility metering, RFID logistics and telematics. Designers face mounting pressure from these industries to support multiple regional bands, extend battery life and minimize form factors.

Qorvo's QPA9510 is a new RF power amplifier (PA) that aims to meet these new demands. The QPA9510 delivers wideband coverage from 100 to 1000 MHz with an efficiency of 55 percent, enabling a longer runtime in battery-powered radios and IoT devices. The amplifier provides +36 dBm output power and 34 dB gain for link budgets in space-constrained systems.

The QPA9510 is designed for use as the final RF amplifier in Global System for Mobile Communications (GSM) hand-held equipment in the 900 MHz band and other applications in the ultra-high frequency (UHF) bands. By replacing multiple discrete PAs with one device, the QPA9510 reduces SKU count, simplifies board design and accelerates time to market for next-generation sub-1 GHz systems.

An analog on-board power controller provides over 70 dB range of gain adjustment for simplified system calibration and tuning. This control also allows for power down with a voltage equal to the logic "Low" to set the device in standby mode. The QPA9510 is tunable over any sub-bands in the operating range to optimize performance. The amplifiers sit in a 3 mm x 3 mm compact quad-flat no-lead (QFN) package.

When combined with Qorvo's low noise amplifiers, digital step attenuators and RF switches, the QPA9510 enables complete RF front-end solutions for transmit-and-receive chains in linear communication systems.

VENDORVIEW
Qorvo
Greensboro, N.C.
www.qorvo.com

MAKING WAVES

Apollo MxFE's Feature Spotlight: Fast Frequency Hopping

This advanced digital feature allows the carrier to be changed in the fastest time possible. Feature background, hopping methods, performance and resources are covered.

Analog Devices
www.analog.com

Cadence Product Free Trials

Cadence invites you to try one of their innovative solutions to see how it can help you accelerate your time to market.

Cadence
www.cadence.com

Outstanding OIP2 from a Small Dual MMIC Amplifier

Explore a tiny, wideband push-pull amplifier solution that runs from high frequency to the lower ultra-high frequency range, achieving an OIP2 of nearly +100 dBm along the way, with the Mini-Circuits' PHA2-13HLN+ dual matched pair at the centerpiece.

Mini-Circuits
www.minicircuits.com

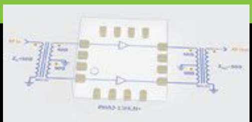

The AI-Powered Future of People Sensing

What if your environment could sense how you move, feel and function? Read this blog post and learn how Algorized and Qorvo are delivering that reality with UWB-powered, privacy-first, people sensing AI.

Qorvo
www.qorvo.com

StrataWorks' RF Design Tool for Custom RF Filters

Bring your RF designs from concept to production faster with StrataWorks' RF design tool that lets you design, simulate and order custom RF filters from 10 to 60 GHz.

Nuvotronics
www.nuvotronics.com

New Blog Post: AESA Radar Breaks into Commercial Markets

Once reserved for defense, AESA technology now drives commercial radar innovations with unmatched speed, precision and adaptability. Check out the blog post titled, "Active Electronically Scanned Array Radar is Breaking Through Defense into Commercial Markets" to learn more.

RFMW
www.rfmwblog.com

NEW PRODUCTS

COMPONENTS

35 GHz Cavity Bandpass Filter

VENDORVIEW

3H's CC35000-X2500-8KK is a high performance 35 GHz cavity bandpass filter with a low insertion loss of 1.5 dB in a 2500 MHz passband. 3H's cavity filter offerings provide the lowest loss, highest Q in both military and commercial applications such as radar, weather monitoring, airborne navigation and military surveillance.

3H Communication Systems
www.3hcommunicationsystems.com

Multi-hole Directional Couplers

Series 136, high directivity, and Series 137, very high directivity, are offered in all waveguide sizes within 33.0 to 500 GHz. The standard coupling values are 3, 10 and 20 dB, other values, for example 6, 30, 40, 50 and 60 dB, can be supplied.

Flann Microwave
www.flann.com

Double Balanced Mixer

VENDORVIEW

The MM1-1886LM is a passive double balanced MMIC mixer. It features excellent 8.5 dB conversion loss, superior isolations and spurious performance across a broad 18 to 86 GHz RF/LO bandwidth. Low LO drive requirement allows operation at as low as +7 dBm inputs. The MM1-1886L is available as a wire bondable chip or a connectorized package.

Marki Microwave
www.markimicrowave.com

Surface-Mount SP4T Switch

VENDORVIEW

Mini-Circuits' model M4SWA4-34DR+ single-pole, four-throw (SP4T) absorptive GaAs MMIC switch covers DC to 30 GHz with input IP3 of +33 dBm. It features an internal driver and holds typical insertion loss to 0.9 dB at 10 MHz and 3.3 dB at 30 GHz. Isolation between switch ports is typically 76 dB at 10 MHz and 42 dB at 30 GHz. The switch is supplied in a 4 × 4 mm 24-lead QFN-style package.

Mini-Circuits
www.minicircuits.com

Coaxial Circulator

The new 3A5BAF S-Band coaxial circulator from Renaissance Electronics, an AEM company, delivers superior performance in demanding satcom links. Operating from 2.5 to 3.5 GHz, it features low insertion loss and high isolation in a compact size while handling up to 5 kW peak and 500W CW across a -20°C to +70°C range. Renaissance can customize performance, power and environmental specifications to your needs. Get the edge in your RF designs.

Renaissance Electronics
www.aeminc.com/RF

CABLES & CONNECTORS

High Speed Multi-pin Cable Assemblies

VENDORVIEW

The MIcable 40/50 GHz high speed multi-pin cable assemblies are designed with blind-mate, high precision contacts. It features a stable and reliable structure with a pin pitch of 4 mm, offering high density and excellent mechanical strength. The assembly also delivers superior electrical performance, including low VSWR, low insertion loss, high delay matching accuracy and excellent amplitude-phase consistency. It is ideally suited for applications such as high speed data testing, semiconductor design and testing and automated test and measurement.

MIcable Inc.
www.micable.cn

AMPLIFIERS

K-Band Amplifier

VENDORVIEW

Spanning 18 to 27 GHz, amplifier model SBP-1832736850-KF42-EP delivers 68 dB gain and +50 dBm saturated output power with WR-42 waveguide and 2.92 mm (F) interface. Other port configurations, such as 2.92 mm (M) connectors and WR-42 waveguides for either the input or output port, are also available under different model numbers.

Eravant
www.eravant.com

New Space COTS Amplifier

ERZIA's New Space COTS amplifier line has been specifically developed to address the stringent requirements of New Space applications. Each amplifier maintains the same high RF performance as ERZIA's COTS equivalent, ensuring robustness against vibration, acceleration, shock, thermal cycling and other environmental stresses encountered in space environments. In addition, several design enhancements have been implemented.

ERZIA
www.erzia.com

25 dBm Solid-State Amplifier

VENDORVIEW

Exodus LNA80004 is a 50 to 6000 MHz solid-state Class A linear amplifier delivering 25 dBm P1dB with 30 dB gain and ±2.0 dB flatness. Designed for EMI/RFI, CW/Pulse, lab and communication applications, it features built-in protection and a universal AC supply in a rugged, compact benchtop chassis.

Exodus Advanced Communications
www.exoduscomm.com

Low Noise Amplifier

VENDORVIEW

Quantic PMI Model PLN-25-812-10-LCA is an 8 to 12 GHz low noise amplifier that provides 25 dB of gain while maintaining a gain flatness of ±1 dB. The amplifier requires +12 to +15 VDC and the maximum current draw is 75 mA. The unit is supplied with removable SMA female connectors in Quantic PMI's standard PE2 housing measuring 1.08 x 0.71 × 0.26 in. COTS Availability!

Quantic PMI
www.quanticpmi.com

NewProducts

Ku-Band Power Amplifier (PA)

VENDORVIEW

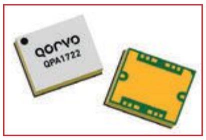

Now available at RFMW, Qorvo's QPA1722 GaN PA delivers 10 W saturated output power and 35% PAE across 17.7 to 20.2 GHz, making it ideal for high performance satcom uplinks and Ku-Band radar systems. With 5 W of linear power at -25 dBc IMD3 and 26 dB gain, it simplifies gain staging while maintaining signal integrity. Housed in a 6 × 5 mm SMT package, it supports SWaP-C goals for both defense and commercial platforms.

RFMW
www.rfmw.com

Broadband High Linear PA

Model ABP0100-10-1729 is a single stage E-PHEMT technology-based high linearity medium power amplifier (PA) module operating in the frequency range from 100 to 1000 MHz. It offers 17 dB of linear gain and +29 dBm minimum output power at 1 dB gain compression point. The output third order intercept point is about +44 dBm. The unit can operate with a single DC power supply and it has built-in voltage regulator. The package size of the amplifier is 1.2 × 1.0 × 0.4 in.

Wenteq
www.wenteq.com

SOURCES

Smart Frequency Synthesizer

Z-Communications, Inc. released the SSG4522ALX, a new smart PLL frequency synthesizer delivering wideband tuning from 45 MHz to 22.6 GHz with 0.1 Hz resolution and +18 dBm RF output, providing the precision and stability required in advanced radar, satcom, defense, test instrumentation and field signal generation systems. The SSG4522ALX measures 4.25 × 2.25 × 0.5 in., allowing integration into both lab-grade and portable architectures.

Z-Communications
www.zcomm.com

ANTENNAS

Compact 8 GHz UWB Patch Antenna

Johanson Technology's P/N7987A-T45A0200001E is an 8 GHz (Channel 9) mini surface-mount ceramic patch antenna designed for directional UWB systems. It operates from 7887 to 8087 MHz, providing stable and efficient performance for a wide range of UWB applications. Target applications include keyless entry, angle-of-arrival, ranging, radar and autonomous mobile robots (AMR beacons) in both consumer and industrial environments.

Johanson Technology
www.johansontechnology.com

Conical Horn Antenna

VENDORVIEW

URF's new 18 to 40 GHz dual polarized quad-ridged conical horn antenna is engineered for RF testing and measurement applications. This high performance wideband antenna delivers exceptional port isolation (≥ 30 dB) and a low VSWR (≤ 2.2:1). Achieve 16 dBi typical gain and 20 dB minimum cross-polarization, making it the ideal microwave component for precision system integration. Now live in stock at $4,500 each.

URF
www.urfinc.com

TEST & MEASUREMENT

2-Port 6.5 GHz VNA

VENDORVIEW

The SC5065 is a 2-port 6.5 GHz VNA that features excellent dynamic range, fast measurement speed and a high output power, in a compact package with the maximum standard software feature set. VNAs and ACMs are delivered with factory calibration certificates containing no data. The add-on option for ISO17025/Z540-1 Accredited, Traceable Calibration Certificate and Uncertainties is available, specification needed when ordered.

Copper Mountain Technologies
www.coppermountaintech.com

Spectrum Analyzers

The HAROGIC PXR Series is not only a rugged spectrum analyzer with IP68 standard design and benchtop-grade RF performance, but also an all-in-one AI platform open platform that deeply integrates the open API and cutting-edge AI computing power of NVIDIA.

HAROGIC Technologies
www.harogic.com

Switch Matrix

Ikalogic launched the CS8216, a high performance 2×16 RF switch matrix designed for automated RF and microwave test environments. The CS8216 is the first product in the new CS8000 modular RF switching platform, enabling flexible routing, fast switching and simplified multi-port test setup configuration. Engineered for demanding applications in 5G/6G research, multi-port RF device characterization, wireless module validation and production test automation, the CS8216 offers excellent RF performance combined with a modern software-driven control interface.

IKALOGIC S.A.S
www.ikalogic.com

Reviewed by Katerina Galitskaya

Bookend

Relativistic Field Theory for Microwave Engineers
Matthew A. Morgan

Electromagnetics and relativity are deeply interconnected, yet this connection is often overlooked in engineering education. "Relativistic Field Theory for Microwave Engineers" by Matthew A. Morgan bridges this gap, offering a fresh perspective on electromagnetics through the lens of special relativity. The book challenges conventional thinking and provides an accessible introduction to a topic that has remained largely confined to theoretical physics.

The author starts with an engaging reflection on his own journey, questioning why relativity is rarely applied in practical engineering despite its fundamental role in electromagnetics. He methodically builds the case that magnetic fields themselves are a relativistic effect, arising from the motion of electric charges. This perspective is not new, but the presentation's aim toward engineers rather than physicists makes it particularly insightful.

The book takes readers through a structured exploration of how relativistic principles are naturally derived from Maxwell's equations. Unlike traditional approaches that leave relativity to high-energy physics, Morgan argues that it is already at play in everyday electromagnetic phenomena.

One of the book's notable choices is the use of SI units instead of the more traditional Gaussian-CGS system. While some might find this unconventional, the author makes a compelling case that staying within the familiar SI framework helps engineers grasp the concepts more intuitively. An appendix is provided for those who prefer Gaussian notation, ensuring that the book remains accessible to a broad audience.

Overall, this book is a must-read for engineers seeking to deepen their understanding of electromagnetics beyond the standard view. It challenges the reader to rethink fundamental concepts and provides a refreshing new perspective on a topic that deserves more attention in applied engineering. The book is a valuable read for both experienced engineers and fresh graduates who want to broaden their understanding of the relativistic field theory.

ISBN : 9781685690670
Copyright: 2024
Pages: 352
To order this book, contact:
Artech House
us.artechhouse.com

AdvertisingIndex

Sales Representatives

Eastern and Central Time Zones
Carl Sheffres
Group Director
(New England, New York, Eastern Canada)
Tel: (781) 619-1949
csheffres@mwjournal.com

Michael Hallman
Associate Publisher
(NJ, Mid-Atlantic, Southeast, Midwest, TX)
Tel: (301) 371-8830
Cell: (781) 363-0338
mhallman@mwjournal.com

Pacific and Mountain Time Zones
Brian Landy
Western Reg. Sales Mgr.
(CA, AZ, OR, WA, ID, NV, UT, NM, CO, WY, MT, ND, SD, NE & Western Canada)
Tel: (831) 426-4143
Cell: (831) 713-9085
blandy@mwjournal.com

International Sales
Michael O'Kane
Tel: +44 (0) 1875 825 700
Cell: +44 (0) 7961 038 245
mokane@horizonhouse.com

Germany, Austria, and Switzerland (German-speaking)
Victoria and Norbert Hufmann
Tel: +49 911 9397 6442
victoria@hufmann.info
norbert@hufmann.info

Korea
Jaeho Chinn
JES MEDIA, INC.
Tel: +82 2 481-3411
inter11@jesmedia.com

China
Shanghai
Linda Li
ACT International
Tel: +86 136 7154 0807
lindal@actintl.com.hk

Shenzhen
Linda Li
ACT International
Tel: +86 136 7154 0807
lindal@actintl.com.hk

Beijing
Cecily Bian
ACT International
Tel: +86 135 5262 1310
cecilyb@actintl.com.hk

Hong Kong
Floyd Chun
ACT International
Tel: +86 137 2429 8335
floydc@actintl.com.hk

Taiwan, Singapore
Simon Lee
ACT International
Tel: +852 2838 6298
simonlee@actintl.com.hk

Japan
Katsuhiro Ishii
Ace Media Service Inc.
Tel: +81 3 5691 3335
amskatsu@dream.com

Submitting ad material?
Visit: www.adshuttle.com/mwj
(866) 774-5784
outside the U.S. call
+1-414-566-6940

Ed Kiessling
(781) 619-1963
ekiessling@mwjournal.com

Corporate Headquarters: 685 Canton Street, Norwood, MA 02062 • Tel: (781) 769-9750

NEW

CBN SERIES

Phase Stable Flex Cables

For Precision Measurement Applications

Mini-Circuits' new CBN-series of phase-stable flexible cables is ideal for a wide range of precision applications from DC to 26.5 GHz, including test labs, high-speed data systems and precision measurements. CBN-series models provide exceptional phase and amplitude stability (±6˚, ±0.08 dB) in bend radii as small as 50 mm. 90 dB shielding effectiveness and 74% velocity of propagation ensure outstanding transmission efficiency for outstanding measurement integrity and consistency. These high-performance cables are available from stock in lengths from 1 to 5 ft., with custom lengths available on request.

Key Features

- DC to 26.5 GHz
- Ultra-flexible, 50 mm min. bend radius
- Superior phase & amplitude stability
- (±6.0˚, ±0.8 dB max. @ 26.6 GHz)
- Low loss & high velocity of propagation
- 1 to 15 ft. lengths in stock

LEARN MORE

Mini-Circuits®

FABS and LABS

Flann Microwave: Unlocking the Power of Waveguide

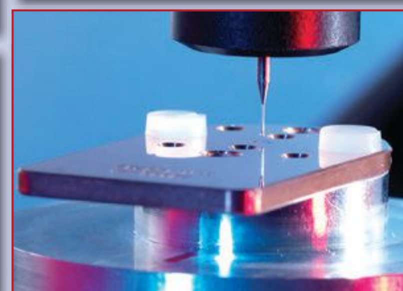

Flann Microwave is celebrating 70 years of providing precision microwave components to the communications, security, radar, satellite, standards and research industries. Flann was founded in 1956 by engineers Fleming and Mann, and was based in Kingston-upon-Thames until moving 15 years later to its current location in Bodmin, U.K. From this location, Flann has grown into a trusted, recognizable brand across the microwave industry.

Flann Microwave manufactures passive waveguide components, subassemblies, calibration kits and instrumentation from 1 GHz to 1.1 THz. Flann has a robust manufacturing site with capabilities for design, analysis, machining, assembly, plating, electroforming and testing. Key instruments include HFFS modeling software, heat transfer analysis software, CNC mills, optical measurement systems and VNAs up to 220 GHz. Flann is capable of high volume production or custom-level production to suit all customer needs.

Flann serves a number of markets, including satcom and spaceflight, test and measurement, telecom, radar, automotive, research and academia, security, mining and aerospace and defense. Flann started serving the space market with hi-rel, TVAC-compliant components over 10 years ago, and supplies major customers including JPL, Airbus, RAL Space and more. Flann has components on LEO, MEO and GEO satellites and continues to serve the space industry through bespoke designs. Along with their spaceflight products, Flann manufactures metrology-grade calibration kits using their in-house micro-machining and fabrication plant, and other waveguide manufacturers utilize Flann metrology components to calibrate and verify their own manufacturing processes. The Flann team has been working with the IEEE Standards working group since it was formed in 2008, and the interface drawing of the standard was produced by Flann mechanical engineers. As the telecom industry grows 5G, introduces 6G and begins to think about 7G, Flann is staying ahead of customer needs by introducing products into the THz frequency range. Flann takes pride in its ability to anticipate industry needs and provide custom and COTS products at critical moments.

In addition to the commercial sector, Flann has served the military market since its founding in 1956 and continues to do so with both components and full subassemblies. Recently, a U.K. Defense Prime contractor required an antenna for a very high-power directed energy application, capable of bringing moving targets to a controlled stop at a safe distance without collateral damage. Flann used their in-house electromagnetic, physical and multi-physics finite element analysis tools to model and design the product, successfully built and tested. Flann serves the military and defense markets through custom products designed and tested for harsh environments.

Flann continues to build on its legacy products and introduce new products to the market, including a new line of variable attenuators and new 33 to 330 GHz switches for load-pull systems and on-wafer testing for OEM systems, spaceflight and other critical applications. As the RF, microwave and mmWave industry forges ahead, Flann Microwave will continue to make a big impact with leading waveguide technologies.

Flann Microwave
https://flann.com/

Editor's Note: This is the first of a two-part article on advanced coaxial filter design. Part 1 discusses the design and analysis of the filter building blocks, and Part 2, to be published next month, discusses their use in advanced filter design.

Part 1 discusses the properties of filter building blocks containing strongly coupled posts that offer new possibilities for advanced coaxial (combline) filter designs. Equivalent circuits based on the individual resonances of the posts cannot be used to reliably describe the behavior of these structures because of the strong coupling between the posts. Instead, sets of electromagnetic (EM) resonances that satisfy the boundary conditions are used. The resulting equivalent circuits are either fully transversal or contain locally transversal sub-circuits, depending on the strength of the coupling between the cascaded blocks. The validity of similarity transformations that result in topologies with unusually strong coupling coefficients is questionable, even though they yield the correct frequency response. Such coupling matrices obscure the physics of the problem and fail to predict the correct behavior of filtering structures. However, topologies that match the post layout can be used to optimize a filter in connection with a full-wave solver or measurement.

In Part 2, examples of dual-post and triple-post units are used to illustrate the key findings. The basic knowledge of the real functionality of these special resonator configurations allows their consideration in advanced filter implementations using well-established classical design methods, without limitation by the design approach. This is demonstrated with an example of a second-order inline filter providing one transmission zero by using a combination of single and transverse dual-post resonators. This fundamental understanding of the special properties provides the prerequisite for a variety of novel filter solutions.

Properties of Building Blocks Comprising Strongly Interacting Posts and Their Consideration in Advanced Coaxial Filter Designs: Part 1

Smain Amari
Royal Military College, Kingston, Canada

Mustafa Bakr
University of Oxford, Oxford, U.K., University of Leeds, Leeds, U.K.

Uwe Rosenberg
Mician Global Engineering GbR, Bremen, Germany

Advanced filter design aims to realize tailored filter functions that satisfy rejection demands with the lowest possible filter order while accommodating low passband insertion loss and reasonable implementation expense. Filtering functions with transmission zeros (TZs) whose frequency locations are chosen to meet rejection requirements are exploited. Cross (bypass) coupling is the most used mechanism to implement TZs in microwave filters.[1] TZs may also be realized with extracted poles. Since such special implementations are not relevant to the introduction of the basic properties of close-post arrangements, they are not further mentioned.

Placing a TZ at a given frequency with respect to the passband often imposes specific relations between the coupling coefficients, especially their relative signs. Building blocks are characterized by the maximum number of TZs they can generate and the relative signs of the required coupling coefficients for the generation of the TZs at the corresponding locations.

Most filter designs consider (combinations of) basic building blocks for the implementation of TZs, like doublets, triplets and quadruplets, since they enable the individual control of dedicated TZs in an overall (higher-order) filter design (see ***Figure 1***). For the implementation of TZs, they rely on combinations of couplings with inductive (positive) and capacitive

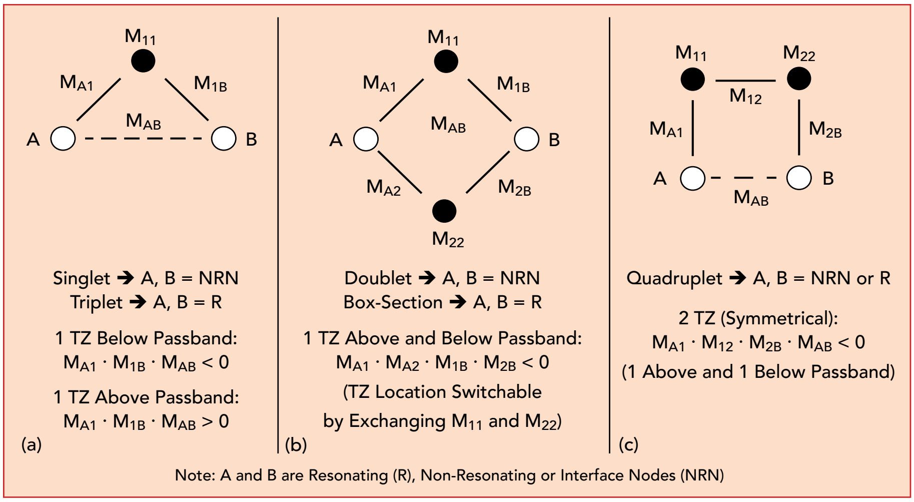

Fig. 1 Basic building blocks and prerequisites (coupling signs) for the realization of TZs: singlet [A, B = NRN] or triplet [A, B = R] (a), doublet [A, B, = NRN] or box-section [A, B = R] (b) and quadruplet [A, B = NRN or R] (c).

(negative) natures.

Classical coaxial filter designs are based on sequentially arranged l/4 resonators (posts) within a housing. Note that the resonators may be shorter than l/4 depending on capacitive loading at the top (e.g., gap toward the top wall). The coupling between adjacent resonators is generally of an inductive nature due to the dominant magnetic field components at the bottom of the housing, while there are also electric field components at the top (open end) of the resonators. Thus, a partial wall between adjacent resonators may be used to control dedicated couplings; i.e., a partial wall at the top yields an increased inductive coupling, where a partial wall at the bottom suppresses the dominant inductive coupling and yields a weak capacitive coupling between adjacent resonators.

For stronger capacitive coupling, special probe designs are usually considered that are supported in the separation wall between adjacent resonators.[2,3] The implementation of such coupling designs is more elaborate and sensitive, especially in the case of strong couplings requiring small distances between resonators and probes. This may also degrade the power handling capability of the filter. Consequently, solutions that avoid any probe couplings for the implementation of needed negative couplings are preferred. This can be done principally by using transformation properties, such as phase reversal, of certain resonator implementations as introduced for waveguide cavity filters.[4]

A building block, which contains two strongly coupled identical posts, was introduced by Bastioli et al.[5] and Machiarella et al.[6] Only the odd mode of the block was used in the design of the passband; the even mode resonated far away from (below) the passband and was considered spurious. The odd mode nature of this configuration was used to implement TZs below and above the passband.

The same idea was used in a triple-post building block.[7-9] This configuration exhibits two close resonances, which are used in the passband; the third resonance that is located far away (below) the passband is considered spurious. TZs below and above the passband can be implemented as the results show.

While closely placed posts for filter applications were first reported almost three decades ago by Rosenberg et.al.,[10] they have been used in different and interesting ways in recent literature.[5-9] A common feature of the dual-post and triple-post building blocks analyzed in these references is the presence of strong coupling between at least two posts. Consequently, the number of passband resonances provided by each building block is one less than the number of posts. This observation suggests that associating a resonance with each post, as is the case in some coupling schemes, should be viewed with suspicion.

A transversal network, which is also known as the admittance representation in the theory of linear systems, and its narrow band limit, which is commonly known as the transversal coupling matrix, use the eigen-resonances of the complete structure with all the perturbations present as a basis. Note that the meaning of 'narrow band' is related to the validity in view of the dedicated physical implementation and passband; there are also special broadband resonator filter designs relying on this representation, but it is only valid for the realizable characteristics close to the passband.

Although it provides a general and universal representation of coupled resonator filters, the transversal coupling matrix is not convenient for initial designs. Instead, similarity transformations (rotations), which preserve the symmetry of the coupling matrix and its frequency response, are then used to generate new coupling schemes with a topology that matches the layout of the individual physical and localized "resonators."

Such transformations, which are perfectly valid at the coupling matrix level, are questionable for real structures with strong couplings between resonators whose EM fields share the same volume, mainly because of the violation of the boundary conditions. It is important not to lose sight of the fact that the actual filter is described by vector quantities, the components of the EM field, that obey a set of coupled partial differential equations, Maxwell's equations, with associated boundary conditions. The coupling matrix represents a system that obeys a set of coupled first-order ordinary differential equations with no knowledge of the boundary conditions. The concept of equivalence between the two must be viewed with care and suspicion, especially when strong coupling coefficients are present.

The following section discusses the concept of similarity transformations and the implications of boundary conditions. This is fol-

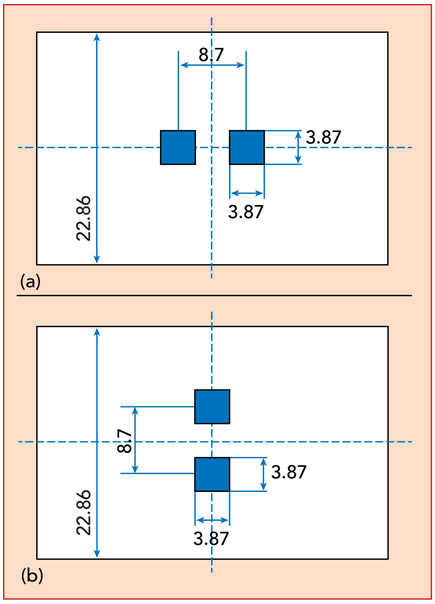

Fig. 2 **Dimensions (mm) of dual-post configurations for analyses of basic behavior: inline (a) and transverse (b). The housing height = 22.86 mm and the post height = 22.00 mm.**

lowed by an analysis of dual-post and triple-post resonators to understand their properties. The use of these building blocks in filter designs is then addressed in Part 2 of this article.

Understanding of the characteristics of close-post resonators allows the application of classical, well-established filter design methods without limitations, even when combining different types of resonators. This is demonstrated in Part 2 of this article by way of an example of a second-order inline filter design providing one TZ by using the combination of single and transverse dual-post resonators. The dimensions obtained by a pre-design with a classical design approach yield already accurate performance results. In addition, examples of novel building blocks and third- and fourth-order filters are also introduced to confirm the results of the standard design methods.

BOUNDARY CONDITIONS AND SIMILARITY TRANSFORMATIONS

Consider the structures shown in ***Figure 2***. They consist of two closely placed posts inside a metallic enclosure. Assume that the structures are lossless and homogeneous. The posts are identical with a gap between their tops and the metallic cover. The eigen-resonances of the structures can be straightforwardly determined by using a modern full-wave solver.

The field distributions of the two lowest eigen-resonances of the transverse dual-post structure (see Figure 2b) are shown in ***Figures 3*** and ***4*** (EM calculations and design analyses conducted with Mician µWaveWizard™).[11] The EM fields of the resonances are not concentrated around either of the two posts.

These two resonances are not coupled to each other as required by the orthogonality of the solutions of Maxwell's equations in a given volume. Because of the symmetry of the structure, we denote the even mode by $\varphi_e(\vec{\tau})$ and the odd mode by $\varphi_o(\vec{\tau})$. The quantity $\varphi_{e,o}(\vec{\tau})$ can be taken as a component of the electric field, magnetic field or a relevant modal EM quantity depending on the coordinate system. These two functions are eigenfunctions of a linear operator, $\mathcal{L}$, along with the associated boundary conditions. If the eigenvalues are $\lambda e = \omega_e^2$ and $\lambda o = \omega_0^2$, then $\mathcal{L}\varphi_e$ and $\mathcal{L}\varphi_0$ are determined by ***Equations 1a*** and ***1b***:

$$\mathcal{L}\varphi_e = \omega_e^2\varphi_e \qquad (1a)$$

$$\mathcal{L}\varphi_o = \omega_o^2\varphi_o \qquad (1b)$$

If the input and output ports that couple to both resonances are added to the structure, we get the equivalent circuit shown in Figure 1b when the resonances $\varphi_e(\vec{\tau})$ and $\varphi_o(\vec{\tau})$ are used as a basis. It is a doublet.

Now consider the question of representing the circuit by using localized "resonances" that are associated with each of the posts individually. The following two functions are defined in ***Equations 2a*** and ***2b***:

$$\varphi_1 = \frac{1}{\sqrt{2}}(\varphi_e + \varphi_o) \qquad (2a)$$

$$\varphi_2 = \frac{1}{\sqrt{2}}(\varphi_e - \varphi_o) \qquad (2a)$$

When the structure is represented in the new basis (φ_1,φ_2), it results in the coupling scheme shown in ***Figure 5***.

The transformation described by Equations 2a and 2b is a similarity transformation; in this case, it is rotated by 45 degrees. The first im-

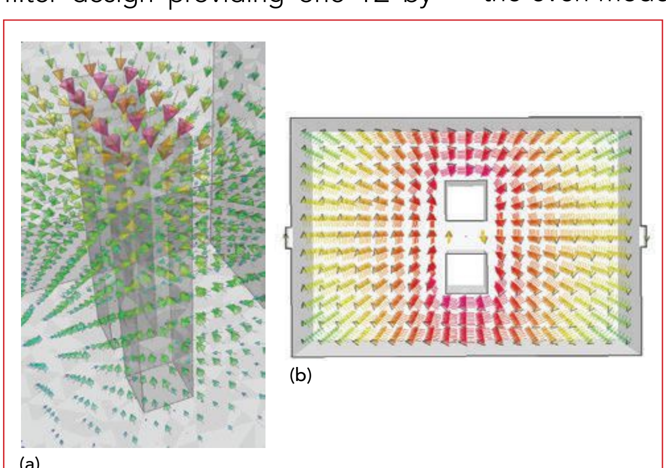

Fig. 3 **EM field patterns of the dual-post fundamental mode (resonant frequency = 2.095 GHz): zoom of E-fields (a) and H-fields cut at half housing height (b).**

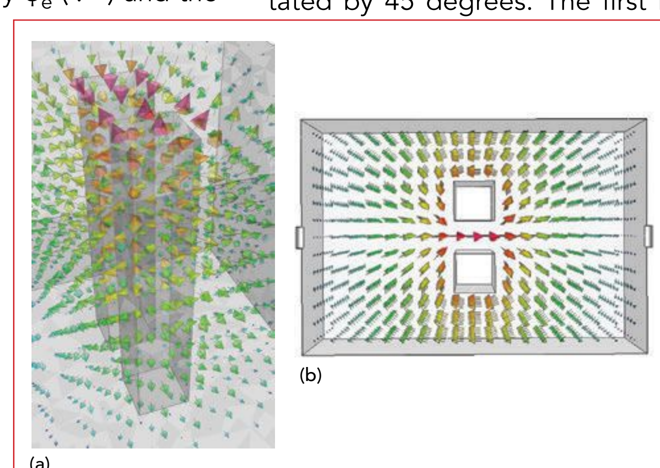

Fig. 4 **EM field patterns of the dual-post second mode (resonant frequency = 2.781 GHz): zoom of E-fields (a) and H-fields cut at half housing height (b).**

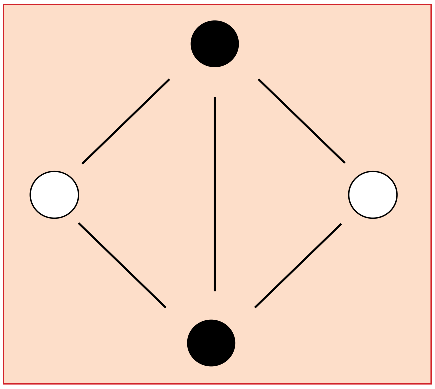

Fig. 5 Dual-post coupling scheme with φ_1 and φ_2 in Equations (2a and b) used as a basis.

portant point to address is whether the quantities φ_1 and φ_2 are eigen-resonances. For this to be the case, they must satisfy the eigen-problem in Equation 1, yielding ***Equations 3a*** and ***3b***:

$$\varphi_1 = \frac{1}{\sqrt{2}}(\mathcal{L}\varphi_e + \mathcal{L}\varphi_o) = \frac{1}{\sqrt{2}}(\omega_e^2\varphi_e + \omega_o^2\varphi_o) \quad (3a)$$

$$\varphi_2 = \frac{1}{\sqrt{2}}(\mathcal{L}\varphi_e - \mathcal{L}\varphi_o) = \frac{1}{\sqrt{2}}(\omega_e^2\varphi_e - \omega_o^2\varphi_o) \quad (3b)$$

To get more insight into this transformation, the sum and difference in ***Equations 4a*** and ***4b*** are introduced:

$$S = \omega_e^2 + \omega_o^2 \quad (4a)$$

$$D = \omega_e^2 - \omega_o^2 \quad (4b)$$

Combining Equations 3 and 4 yields ***Equations 5a*** and ***5b***:

$$\mathcal{L}\varphi_1 = \frac{S}{2}\left(\varphi_1 + \frac{D}{S}\varphi_2\right) \quad (5a)$$

$$\mathcal{L}\varphi_2 = \frac{S}{2}\left(\varphi_2 + \frac{D}{S}\varphi_1\right) \quad (5b)$$

It is evident that these two functions are not eigenfunctions unless D/S = 0, or equivalently, that the two original modes are degenerate, i.e., $\omega_e=\omega_o$. However, if D/S, which is nothing other than the coupling coefficient between the two posts, is small enough to be neglected, the two functions are approximately eigenfunctions, and the eigenfunctions are approximately degenerate. This is the case for narrow band coupled resonator filters.

When D/S is large, as in strongly coupled resonators, the error in treating φ_1 and φ_2 as eigenfunctions (resonances) may be large enough to render a coupling matrix based on these non-physical local resonances unreliable, especially when these share the same volume because of the orthogonality properties of solutions to Maxwell's equations.

The elements of the resulting coupling matrix will not be independent because of the boundary conditions. Paths going through such "resonances" are not allowed to transport energy independently. Predictions based on coupling schemes that use these localized "resonances" are not always reliable.

An interesting by-product of this analysis is the appearance of a coupling coefficient. Indeed, Equations 5a and 5b show that the relative amplitudes of the functions φ_1 and φ_2 are related by ***Equation 6***:

$$k = \frac{D}{S} = \frac{\omega_e^2 - \omega_0^2}{\omega_e^2 + \omega_0^2} \quad (6)$$

An identical expression for the coupling coefficient between two resonators was given by Awai.[12] The advantage of the derivation in this article is its generality since it applies to any two-state system that is linear and invariant under time reversal, so that the eigenvalues are the squares of the angular frequencies.

When the "resonators" share the same volume, it is important to use those solutions that satisfy the boundary conditions in predicting the behavior of the filter, especially when strong inter-resonator coupling is present, as in the case of strongly coupled dual and triple posts. These are the only separate paths that the energy can follow between the input and the output and contain all the relevant physics of the problem, assuming that all other resonances are far enough from the frequency range of interest.

Certain properties of the filter that are determined by the signals following these different paths are obscured by similarity transformations. For example, it is known that the TZ of a doublet, or a box-section, can be shifted from one side of the passband to the other by changing the signs of the diagonal elements of the coupling matrix.[13] Although similarity transformations preserve the response of the filter, they do not preserve the TZ-shifting property. Instead, similarity transformations result in coupling schemes that obscure this important feature that is exploited in moving the TZ from one side of the passband to the other.

At this point, one might wonder why the coupling matrix whose topology matches the layout of the localized "resonators" is used successfully in designing these filters even when strong inter-resonator coupling is present.[7-9] Here, it is important to understand that this is the case only for optimization-based design methods that rely on the frequency response of the filter (or dedicated subsection) that is obtained from a full-wave solver.

The full-wave simulator guarantees that the boundary conditions are all satisfied. As long as the structure is capable of implementing a response in the range of the coupling matrix whose elements are assumed reliably extracted from the full-wave solution, the process should be successful. However, yielding the desired response does not mean that the coupling matrix represents the local physics of the problem accurately.

All matrices that are related by similarity transformations yield the same response, but this does not mean they represent the local physics of the problem equally well. The coupling matrix that is based on localized resonators is 'helped' by the fact that not all coupling coefficients are strong, meaning that parts of filters are adequately represented by localized resonances.

However, this coupling matrix cannot correctly represent the physics of individual sections that contain strong couplings, such as dual-post and triple-post units. Consequently, the classic design technique that is based on isolated pairs of localized resonators, which provides a more rigorous test of the localized resonator concept, will fail in the case of strong coupling coefficients between "resonators." This failure, which is familiar to filter designers, was also reported by Macchiarella et al.[6]

The important conclusions of this analysis are the following:

a) The physics of the structure is accurately represented by those resonances that satisfy all the boundary conditions.

b) Similarity transformations do not define new valid local "resonances" because of the violation of the boundary conditions when they result in strong inter-resonator coupling. Coupling matrices with such strong coupling coefficients do not correctly describe the characteristics of those sections of the filter that contain resonators that share the same volume, although they produce the correct overall frequency response (by construction).

c) Similarity transformations define approximate resonances which are valid representations for filters with narrow bandwidths or weak inter-resonator coupling, where the resonances that satisfy the boundary conditions are approximately degenerate.

d) The frequency response of the filter as obtained from a full-wave solver or measurement can be used in connection with a coupling matrix whose topology matches the layout of the localized "resonators" to optimize the filter even when strong coupling coefficients are present. The classic design approach that is based on pairs of localized "resonators" will fail when strong inter-resonator coupling coefficients are present.[6]

These ideas are next applied to cases of strongly coupled dual and triple posts.

PROPERTIES OF DUAL-POST UNITS

Transversal Dual-Post Unit

A top view of the analyzed structure is shown in Figure 2b. Assume that the coupling between the unit and the input and output is weak enough for the modal field distributions not to be significantly affected. This is the case for narrow-bandwidth filters. With this assumption, the coupling scheme is a classic doublet (see Figure 1b) where the even and odd resonances of the dual-post units are taken as Resonances 1 and 2. We use the odd resonance in the passband and call the even out-of-band resonance, Resonance 2, spurious. The other choice is naturally possible.

A straightforward analysis of the coupling scheme in Figure 1b shows that a TZ appears at the normalized frequency expressed in ***Equation 7***:

$$\omega_z = -\frac{M_{11} + pM_{22}}{1 + p}, \qquad p = \frac{M_{s1}M_{1L}}{M_{s2}M_{2L}} \tag{7}$$

Introducing the normalized resonant frequencies of the even and odd modes, $\omega_{od} = -M_{11}$ and $\omega_{sp} = \omega_e = -M_{22}$, Equation 7 can be rewritten in the form shown in ***Equation 8***:

$$\omega_z = -\frac{\omega_{od} + p\omega_{sp}}{1 + p}, \qquad p = \frac{M_{s1}M_{1L}}{M_{s2}M_{2L}} \tag{8}$$

From this equation, the distances from the TZ to the two resonances are determined by ***Equations 9a***, ***9b*** and ***9c***:

$$\omega_z - \omega_{sp} = \frac{1}{1+P}(\omega_{od} + \omega_{sp}) \tag{9a}$$

$$\omega_z - \omega_{od} = \frac{1}{1+P}(\omega_{od} + \omega_{sp}) \tag{9b}$$

$$\frac{|\omega_z - \omega_{od}|}{|\omega_z - \omega_{sp}|} = |p| \tag{9c}$$

From these equations, assuming that the odd mode resonates above the even mode, i.e., $\omega_{od} - \omega_{sp} > 0$, we establish the following results:

1. $0 < p < 1$. The TZ is located between the two resonances and is closer to the odd resonance than the spurious even resonance.
2. $p = 1$. The TZ is located at the average of the two resonances.
3. $p > 1$. The TZ is located between the two resonances and is closer to the spurious even resonance.
4. $0 > p > -1$. The TZ is located above the two resonances.
5. $p = -1$. The TZ is located at infinity. This is an all-pole response.
6. $p < -1$. The TZ is located below the two resonances.

From the field distributions of the two modes of the dual-post unit (see Figures 3 and 4, respectively), note that the coupling to the odd mode is weaker than the coupling to the even mode. In fact, the odd mode is not excited at all when the input and output ports are placed at the horizontal symmetry plane between the two posts (see Figure 2b). This gives the freedom needed to adjust the parameter, p, in Equation 7. More specifically, there are two cases:

1. Input and output ports on the same side of the symmetry plane of the dual-post unit. The coupling coefficients are such that $0 < p < 1$. The TZ is between the odd and the even resonances but is closer to the odd resonance, i.e., below the passband. Its distance to the passband is reduced by moving the input and output ports closer to the symmetry plane of the dual-post unit.
2. Input and output ports on opposite sides of the symmetry plane of the dual-post unit. The coupling coefficients are such that $-1 < p < 0$. The TZ is located above the passband. Its distance to the passband is reduced by moving the input and output ports closer to the symmetry plane of the dual-post unit.

In both cases, the TZ can be placed arbitrarily close to the passband regardless of the value of the resonant frequency of the spurious even mode.

Inline Dual-Post Unit

The coupling scheme of the dual-post configuration with a 90-degree alignment (see Figure 2a) is still a doublet. In this case, the input and output form an inline configuration with the two posts of the unit. The EM field distribution of the resonances is similar to that of Figures 3 and 4 but rotated by 90 degrees. Consequently, the field distributions of the two resonances at the outer sides of the posts along a line joining the two posts are very similar except for a phase reversal for the odd mode.

This means that the coupling coefficients to the two modes, mainly

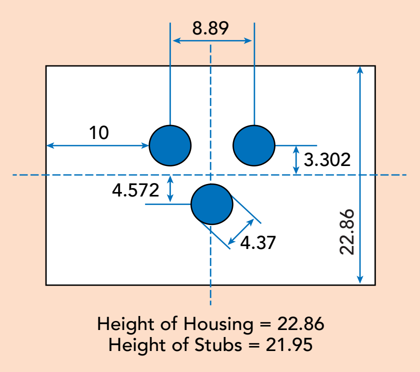

Fig. 6 **Dimensions (mm) of triangular post configuration for eigenmode analyses (footprint and housing height according to Bastioli et al.,[7] Figure 12).**

through the evanescent TE_{10} mode in the uniform waveguide section, are approximately equal, but with one of them negative. This corresponds to p = -1. As a result, this configuration generates a TZ that is far away from the passband or even at infinity. Note that a TZ might be generated if the higher-order modes carry enough energy around the resonant frequency of the odd mode.

PROPERTIES OF A TRIPLE-POST UNIT

Consider a unit formed by a pair of strongly coupled posts and an additional post that is not necessarily as strongly coupled to the pair. The structure generates three resonances, two that are close to each other, which contribute two resonances in the passband; the third one is far away from the passband and is called spurious. The pair of posts is placed in the longitudinal direction (see ***Figure 6***).

First, the EM field distributions of the three resonances are determined (see ***Figures 7*** through ***9***). These resonances are orthogonal to one another (not coupled). It is obvious that none of these resonances are localized around any of the posts, although the EM fields of the third one are approximately concentrated near the individual post. Consequently, a good model of the structure is the transversal coupling scheme shown in ***Figure 10***. Assume that the spurious resonance, taken as Resonance 3 (see Figure 7), is far below the passband.

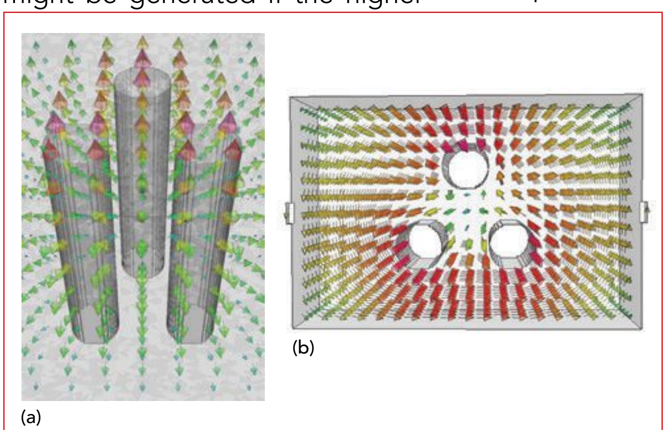

Fig. 7 **EM field patterns of the fundamental mode – all three posts (resonant frequency: 2.057 GHz): zoom of E-fields (a) and H-fields cut at half housing height (b).**

From the field distributions, there are two even modes and one odd mode. The symmetry is with respect to the axis going through the individual post and the symmetry plane of the dual-post unit. This means that one coupling coefficient to the odd mode (either to the input or the output) can be assumed negative, with the remaining ones all positive.

This unit generates up to two TZs at finite frequencies. To generate only one TZ, constraints must be imposed on its coupling coefficients. The generated TZ location is determined by ***Equations 10a***, ***10b*** and ***10c***:

$$\omega_z = \frac{\omega_1 + p\omega_2}{1+p} + \delta\left(\frac{1}{\omega_{sp}}\right), \quad |\omega_{sp}| \gg 1 \qquad (10a)$$

with

$$p = \frac{M_{s1}M_{1L}}{M_{s2}M_{2L}}, \omega_1 = -M_{11}, \omega_2 = -M_{22}, \omega_{sp} = -M_{33} \qquad (10b)$$

and

$$M_{s1}M_{1L} + M_{s2}M_{2L} + M_{s3}M_{3L} = 0 \qquad (10c)$$

Equation 10c is the constraint needed to generate only one TZ at a finite frequency. The notation in Equation 10a is used to indicate that the effect of the spurious resonance on the location of the TZ decreases at least as the reciprocal of ω_{sp}.

The important point to note from this equation is that the position of the TZ is mainly determined by the two resonances that contribute to the passband. In other words, the position of the TZ is not

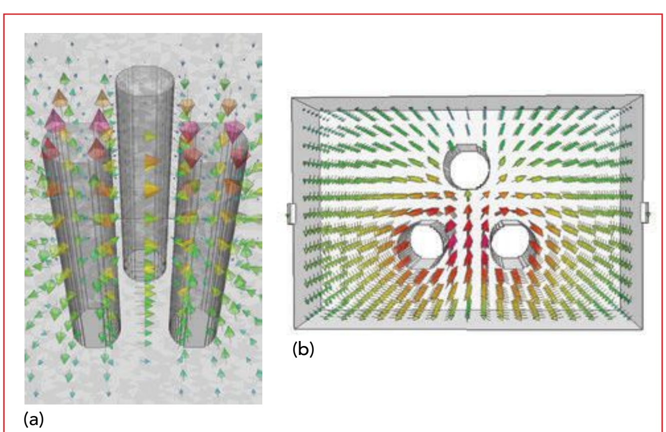

Fig. 8 **EM field patterns of second (odd) resonant mode dedicated to both inline stubs (resonant frequency: 2.663 GHz): zoom of E-fields (a) and H-fields cut at half housing height (b).**

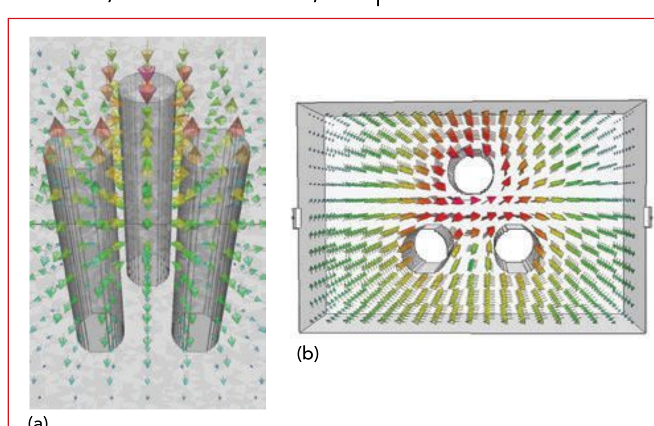

Fig. 9 **Fig. 9 EM field patterns of third (even) resonant mode dedicated to all three stubs (resonant frequency: 2.706 GHz): zoom of E-fields (a) and H-fields cut at half housing height (b).**

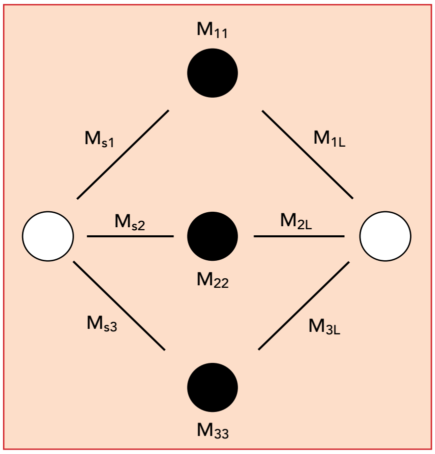

Fig. 10 **Transversal coupling scheme of triple-post configuration.**

very sensitive to the location of the spurious resonances if it is not too close to the passband. This is contrary to the transverse dual-post unit, where the location of the TZ is directly related to the frequency of the spurious resonance, as shown by Equation 8.

The parameter, p, in Equation 10b is negative because one of the coupling coefficients is negative. This means that the TZ is located either below the passband or above, depending on the relative strengths of the coupling to the two resonances.

From Equation 10a, note that the position of the TZ can be shifted from one side of the passband to the other by simply changing the signs of ω_1 and ω_2. This TZ-shifting property is not exact since it affects the shape of the response, but it becomes more accurate as the spurious resonance moves away from the passband. The position of the TZ is indeed moved to the other side of the passband under this transformation, as shown on actual designs in Part 2 of this article.

ROLE OF THE SPURIOUS RESONANCE

The even (spurious) mode of the transverse dual-post unit is, in principle, necessary for the generation of the TZ. For the triple-post unit, the dominant even (spurious) mode is not necessary for the design of the filter. It is the price one pays for generating the odd mode with the required phase reversal by using this structure. It is best to

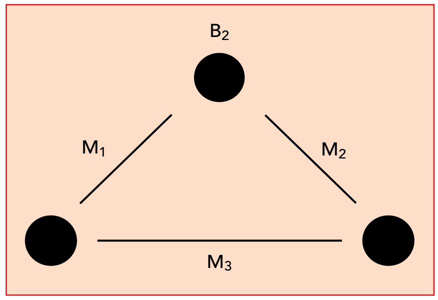

Fig. 11 **Triple-post represented by localized "resonances."**

place it as far away from the passband as possible, while considering other resonator design aspects like unloaded Q. Although its effect on the passband may not be significant, it is important to have a way of taking it into account.

One approach would be to use a model that is based on the non-physical resonances localized around each post by viewing the filter as a dual-band filter.[7-9] The triple-post unit is then represented by a triplet with unrealistic coupling coefficients (see Figure 2 in Zeng et al.[9]). Although the corresponding coupling matrix can be used to optimize the filter from a full-wave analysis, it obscures the physics of the problem. It does not correctly represent the behavior of the sections with strong coupling.

The elements of the coupling matrix corresponding to the topology in ***Figure 11*** are no longer independent because of the boundary conditions. Several elements are affected by the same quantity, for example, the location of a TZ generated by the triple-post unit as given by Zeng et al.[9] in ***Equation 11***:

$$\omega_z = \frac{M_1 M_2}{M_3} - B_2 \qquad (11)$$

An examination of the results given by Zeng et al.[9] in their Figure 2 shows that B_2 changes from 2.1214 to 1.2912 when the normalized location of the spurious resonance changes from -11.69 to -3.09. At the same time, Figure 4 in the same reference shows that the location of the TZ has barely moved. Note that ω_p in Equations 10a through c is not exactly equal to the spurious resonance of the fourth-order filter in this example, but the difference between the two is not sizable.

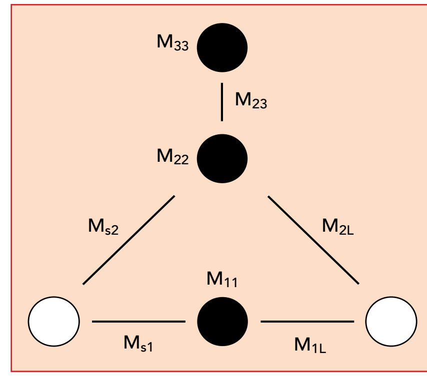

Fig. 12 **Alternative coupling scheme of a triple-post unit (after Zeng et al.[9]).**

An examination of Equation 11 shows that this is possible only if the coupling coefficients and B_2 all depend on the spurious resonance. Unfortunately, the nature of this dependence is completely lost after the series of similarity transformations. On the other hand, Equation 10a clearly shows that the location of the TZ is indeed not sensitive to the frequency of the spurious resonance when it is sufficiently far from the passband.

Another proposed coupling scheme for the triple-post unit is shown in ***Figure 12*** (also shown as part of Zeng et al.[9] in their Figure 7). A straightforward analysis of this circuit shows that when only one transmission zero is generated, then its TZ is given by ***Equations 12a*** and ***12b***:

$$\omega_z = -M_{33} + \frac{M_{23}^2}{M_{22} - M_{11}} \qquad (12a)$$

$$M_{s1} M_{1L} + M_{s2} M_{2L} = 0 \qquad (12b)$$

Here, Resonator 1 is the odd resonance of the dual-post unit, Resonator 2 is the even mode and Resonator 3 is the single post. This model predicts that the TZ is completely determined by the single post (M_{33}) when the spurious resonance, $-M_{22}$, is far away from the passband. In the same limit, the structure produces only one return loss pole, instead of the desired two, because of a zero-pole cancellation. Naturally, this result cannot be correct since the location of the TZ depends on the in-band eigenresonances, as given by Equation 10a in this limit. This is another manifestation of using "resonances" that do not satisfy the boundary conditions, despite the fact that the corresponding coupling schemes are admittedly intuitive. Energy cannot flow through anything other than solutions to Maxwell's equations that satisfy the boundary conditions.

From a practical point of view, arguably the strongest reason for not including the spurious resonance in the model, especially for design purposes, is the impossibility of controlling it. Unfortunately, this is not the case. If we were able to control it, we would simply not couple to it and eliminate it.

The spurious resonance plays a marginal role in the passband and only a small role in determining the location of the TZ of a triple-post unit. It should not be treated on par with the resonances that directly determine the passband performance of the filter. In this work, we adjust the elements of the model that are based on the physical resonances that contribute to the passband to compensate for the effect of the spurious resonances on the passband and its vicinity. This approach has been used successfully for decades in waveguide technology.

CONCLUSION

The investigations of building blocks with strongly coupled posts have shown that the individual posts are not pivotal to the design of filters containing these structures. Because of the strong coupling between posts that share the same volume, resonances localized around the post are not physical. Instead, the resonances of the complete block and their properties must be examined to identify those features that are relevant to the design of filters that contain one or more of such structures.

Similarity transformations yield coupling matrices that conserve the frequency response of the entire filter but not necessarily the dominant "internal" physics of these structures because of the strong coupling and the boundary conditions. Nevertheless, coupling matrices based on localized resonances can be and have been successfully used to optimize the filter in connection with the full-wave response of the entire filter or subsections that consider these structures with adjacent single-post resonators.

However, classic design methods based on pairs of resonators will most likely fail when applied to such coupling matrices. Using resonances that satisfy the boundary conditions and contribute to the passband is essential to understanding how these structures work and how to use them in interesting and innovative designs. These filters can be designed by following well-established methods if they are based on an equivalent circuit (coupling matrix) that contains only those physical resonances that contribute to the passband.

Knowledge of the real functionality is a prerequisite for the systematic application of standard design methods for a convenient geometrical pre-design of the desired filter configuration, considering also different kinds of resonators without general design limitations.

In Part 2 of this article, the usual basic considerations for the pre-design of a second-order filter with one TZ are introduced for an implementation using dual- and single-post resonators. The analysis results of the initial configuration, obtained by the application of this classical design approach, provide almost the desired filter characteristic response without any EM-optimization/tuning. The effect of spurious resonance is then addressed by a final adjustment of the filter dimensions in connection with the equivalent circuit and a field solver. ■

References

1. R. J. Cameron, C. M. Kudsia and R. R. Mansour, "Microwave Filters for Communication Systems," *Wiley*, Hoboken, NJ, USA, 2007.
2. J. Brian Thomas, "Cross-Coupling in Coaxial Cavity Filters—A Tutorial Overview," *IEEE Transactions on Microwave Theory and Techniques*, Vol. 51, No. 4, April 2003, pp. 1368–1376.
3. S. Li, X. Wang, Y. Li and J. Wang, "Design of Compact Coaxial Cavity Bandpass Filter with High Selectivity," *IEEE MTT-S International Microwave Biomedical Conference*, May 2019.
4. U. Rosenberg, "New `Planar' Waveguide Cavity Elliptic Function Filters," *25th European Microwave Conference*, September 1995.
5. S. Bastioli and R. V. Snyder, "Evanescent Mode Filters Using Strongly Coupled Resonator Pairs," *IEEE MTT-S International Microwave Symposium*, June 2013.
6. G. Macchiarella, S. Bastioli and R. V. Snyder, "Design of In-Line Filters with Transmission Zeros Using Strongly Coupled Resonators Pairs," *IEEE Transactions on Microwave Theory and Techniques*, Vol. 66, No. 8, August 2018, pp. 3836-3846.
7. S. Bastioli, R. V. Snyder and G. Macchiarella, "Design of In-Line Filters with Strongly Coupled Resonator Triplet," *IEEE Trans. Microwave Theory and Techniques*, Vol. 66, No. 12, December 2018, pp. 5585–5592.
8. Y. Zeng, Y. Yang and M. Yu, "Flexible Design of Generalized Strongly Coupled Resonator Triplet Filters by Regulating Redundant Resonant Modes," *IEEE MTT-S International Microwave Symposium*, June 2021.
9. Y. Zeng, Y. Yang, M. Yu and S. Bastioli, "Synthesis of Generalized Strongly Coupled Resonator Triplet Filters by Regulating Redundant Resonant Modes," IEEE Transactions on Microwave Theory and Techniques, Vol. 70, No. 1, January 2022, pp. 864-875.
10. U. Rosenberg, W. Hägele and K. Beis, "Line Resonator," European Patent Office EP0632518A1, June 11, 1993. Web: https://patents.google.com/patent/EP0632518A1/en).
11. µWaveWizard, Mician GmbH, Bremen, Germany.
12. I. Awai, "Meaning of Resonator's Coupling Coefficient in Bandpass Filter Design," *Electronics and Communications in Japan, Part 2: Electronics*, Vol. 89, No. 6, June 2006.
13. U. Rosenberg and S. Amari, "Novel Design Possibilities for Dual-Mode Filters Without Intracavity Couplings," *IEEE Microwave and Wireless Component Letters*, Vol. 12, No. 8, December 2002, pp. 296-298.